KANSAS GEOLOGICAL SURVEY
OPEN-FILE REPORT 99-59

Electrofacies Model and Sequence Stratigraphy of the Lower Morrowan, Southwestern Kansas, Case Study of Arroyo and Gentzler Fields

by

Abdulrahman M.I. Alissa

KANSAS GEOLOGICAL SURVEY
1930 Constant Avenue
University of Kansas
Lawrence, KS 66047

ELECTROFACIES MODEL AND SEQUENCE STRATIGRAPHY OF THE LOWER MORROWAN, SOUTHWESTERN KANSAS, CASE STUDY OF ARROYO AND GENTZLER FIELDS

By

Abdulrahman M. I. Alissa
B.Sc., King Abdul Aziz University, 1992
P.G.D., Royal Holloway University of London, 1996

Submitted to the Department of Geology and the
Faculty of the graduate school of the University
of Kansas in partial fulfillment of the requirement
of the degree of Master of Science

Professor in Charge

Committee Member

For the Department

ACKNOWLEDGMENTS

Above all, I would like to praise God for his wisdom and strength in guiding my work and giving me insight and internal power to finish this task that he laid before me.

I would like to dedicate this thesis in memory of my beloved Aunt Alanoud and to the soul of his majesty King Khalid Alsaud. This thesis was completed in honor of my Father, Mother, and Uncle who provided both emotional and financial assistance.

I wish to express my deep appreciation and thanks to Dr. Timothy Carr for his unlimited support for without it, this research would never have been completed. I would also like to thank both Drs. Anthony Walton and Douglas Walker for their revisions and suggestions for my thesis.

I would like to thank both the Saudi Government represented by King Abdul Aziz University for their scholarship and the Kansas Geological Survey for providing my research assistant position, geological data, and computer-support.

I wish to acknowledge Professor John Doveton and Mr. Bill Guy for their scientific contributions and ideas for petrophysical ideas regarding my electrofacies model.

Special thanks to Kristie Luchtel for her encouragement, ultimate support, and helpful suggestions, without her assistance, this research would not have been exciting or finished in a timely manner.

I would also like to thank the following people from the Kansas Geological Survey: Drs. Lynn Watney, Scott Beaty, David Collins, David Newell, and Evan Franseen for their scientific contributions.

Finally, I would like to thank my brother Abdulaziz for supporting me while I was preparing for my master's defense.

TABLE OF CONTENT

LIST OF FIGURES

LIST OF TABLE

LIST OF APPENDIX

ABSTRACT

Wireline logs and cores from Arroyo (T29S / R41W, Stanton County) and Gentzler (T33S / R38W, Stevens County) fields were used to construct a sequence-stratigraphic framework for the lower Morrow successions in the Hugoton Embayment, southwestern Kansas. Core analysis defined twenty-one separate lithofacies in the lower Morrow representing upper estuarine to offshore depositional environments. Core data and wireline log responses were combined to construct an electrofacies model. Distinctive wireline-log responses define five electrofacies, related to depositional environment. Crossplots, RHOmaa-Umaa and Nphi-Dphi versus photoelectric index, were used to determine lithology and distinguish facies in the absence of core data.

The upper estuarine electrofacies Ae is confined to the deeper part of valleys incised in the pre-Pennsylvanian unconformity. Laterally, the incised valley fill of electrofacies Ae is bounded by electrofacies Ee, which is interpreted as interfluve paleosol deposits. Lower estuarine and upper shoreface facies form electrofacies Be. Electrofacies Ce typifies lower shoreface to offshore facies. Electrofacies De defines the open marine deposits of the middle Morrow limestone.

In the Arroyo Field, a surface of subaerial exposure (SB) and a transgressive surface (TS) were identified from core in the Fritz 16-1, and inferred from the spectral gamma ray in the Arnold 1-1. In addition, two maximum flooding surfaces (MFS) and a transgressive surface of erosion (TSE) were inferred. At Arroyo Field,

the incised valley-fill deposits (electrofacies Ae, and Be) constitute the initial Pennsylvanian transgressive systems tract (TST). A maximum flooding surface (MFS) separates the TST from the overlying offshore to lower shoreface facies of the highstand system tract (electrofacies Ce). Overlying the offshore and lower shoreface deposits (electrofacies Ce), the middle Morrow limestone (electrofacies De) is separated from the lower Morrow sequence by a transgressive surface of erosion (TSE). The middle Morrow limestone (electrofacies De) and the overlying upper Morrow offshore facies (electrofacies Ce) represent the transgressive and highstand systems tracts of an overlying sequence. In the Arroyo Field, the lower Morrow successions represent a simple incised-valley fill deposit consisting of one sequence of estuarine and marine deposits.

Facies interpretations and the electrofacies model developed at Arroyo Field were used to construct a sequence-stratigraphic framework for the lower Morrow at Gentzler Field. Lower Morrow successions at Gentzler Field represent more open-marine environments. Lithofacies and electrofacies are arranged into three sequences composed of lower estuarine and upper shoreface deposits (electrofacies Be) and offshore to lower shoreface facies (electrofacies Ce).

The proposed sequence-stratigraphic framework for the lower Morrow departs from previous simple layer-cake models. Prior models do not accurately represent the complex stratigraphy of the lower Morrow in the Hugoton Embayment.

1.0 INTRODUCTION

This investigation proposes a sequence-stratigraphic framework for two oil and gas fields in the lower Morrow (Lower Kearny Formation) in the western Hugoton embayment, southwestern Kansas. The study area focused on the Arroyo and Gentzler fields of Stanton and Stevens counties respectively. Gentzler field is located approximately 50 kilometer to the southeast of Arroyo field (Figure 1.1).

The major goals of this study are: 1) describe the lithofacies from core using objective criteria (e.g. grain size, sedimentary structures, and ichnofauna); 2) interpret the depositional environments of the lower Morrow in the Arroyo and Gentzler Fields; 3) integrate the lithological and wireline-log data to construct an electrofacies model in order to discriminate facies geometries in the lower Morrow where no cores are available; and 4) develop a sequence-stratigraphic framework for the lower Morrow in southwestern Kansas that relates facies genetically.

Geologic Setting

The Hugoton Embayment is an asymmetrical basin located in western Kansas and eastern Colorado that has an overall northwest-southeast trend into the Anadarko basin, Oklahoma (Rader, 1987; Youle, 1992). This embayment is considered to be an extension of the Anadarko basin and referred to as the Anadarko or Dodge City Shelf (Merriam, 1963; Rader, 1987). The embayment began to develop in the late Cambrian time and received its thickest accumulation of sediment during the late

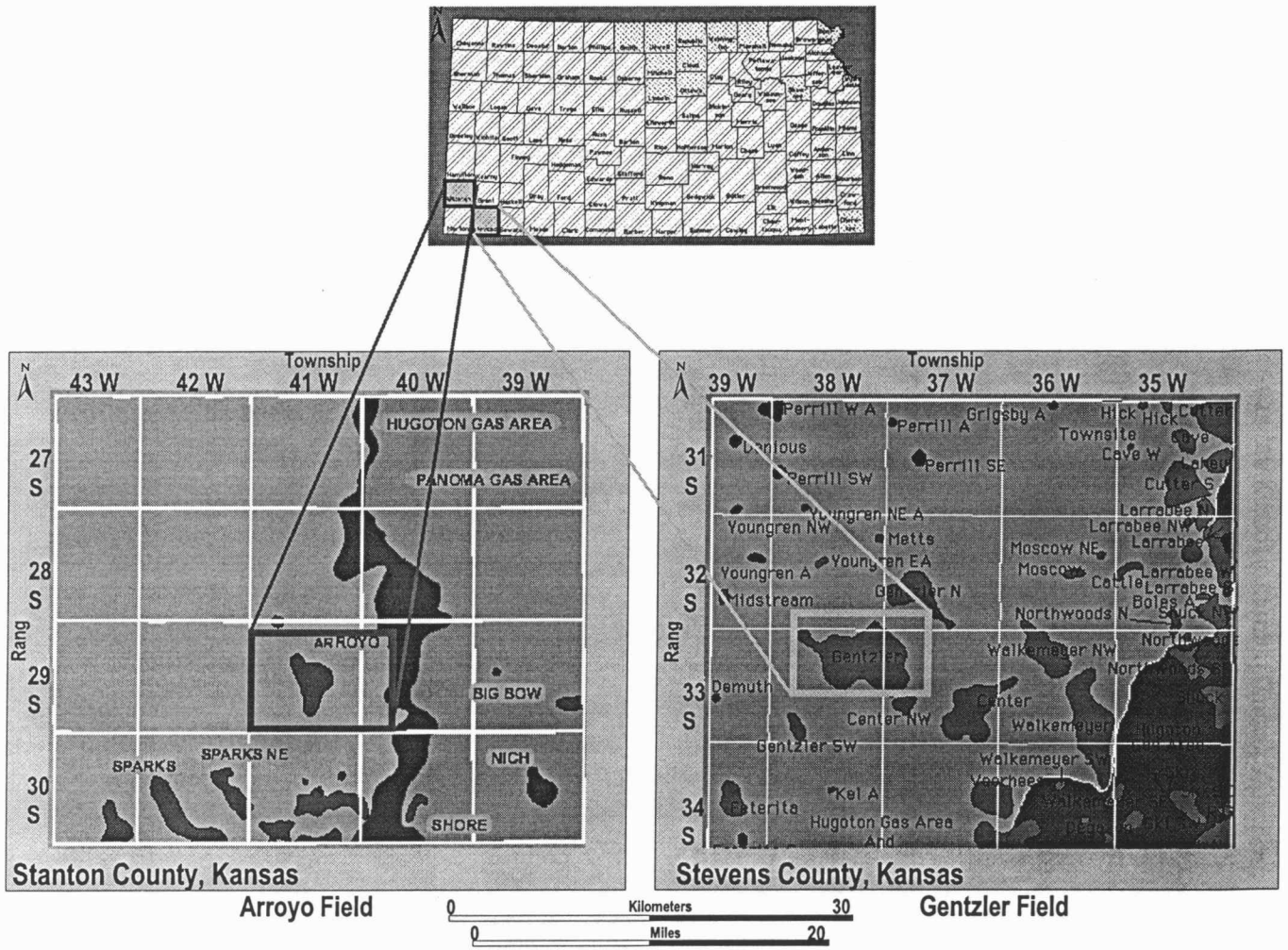

Figure 1.1 Location map for the Arroyo and Gentzler Fields (Modified from Digital Petroleum Altas, http://www.kgs.ukans.edu/PRS/petroIndex.html).

Mississippian, Pennsylvanian, and Early Permian. By the Mesozoic time, this embayment was tectonically inactive (Merriam, 1963).

Tectonic activity in the Mid-continent was at a minimum at the beginning of the Mississippian; however, by the Osagian, rapid subsidence began in the Anadarko Basin and Hugoton Embayment as a result of the collision of North American and the South American (Craig and Varnes, 1979). Differential uplift also began to occur in Kansas along major structural features such as the Nemaha uplift and the Central Kansas uplift (Brown, 1995). Throughout the Mississippian, several uplift and subsidence events occurred with the continued differential downwarping induced sea-level fluctuations. The paleotopographic highs that surrounded the Hugoton Embayment included the Transcontinental Arch to the north, the Central Kansas Uplift and Pratt Anticline to the east, the Amarillo-Wichita Uplift to the south, the Keyes Dome and Sierra-Apishapa-Grande Uplift to the southwest, and the Las Animas Arch to the west (Figure 1.2; Merriam, 1963). During late Mississippian time (Meremecian), the craton was uplifted and extensive erosion occurred on the shelf as the seas withdrew from the Hugoton Embayment (Frezon and Dixon, 1975). During the Chesteran, the Hugoton Embayment began receiving siliciclastic sediments from the Apishapa Uplift and Las Animas Arch, which served as sediment source areas from the west, and from the Central Kansas Uplift (Rader, 1987; Montgomery and Morrison, in press).

In the Early Pennsylvanian Morrowan, sea-level is thought to have been at a eustatic lowstand and later became more erratic with seven glacially

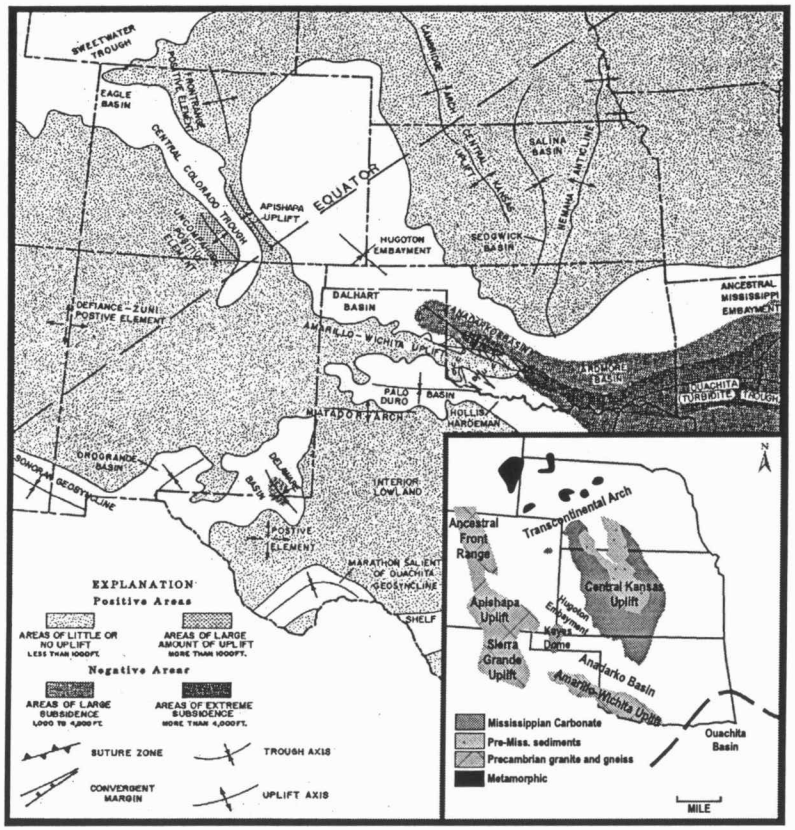

Figure1.2 Paleogeography and structural features during Morrowan time (modified from Mekee and Crosby,1975). Equator position from Habicht (1979). Plate boundaries from Kulth and Coney (1981). Source area From Rader (1988)

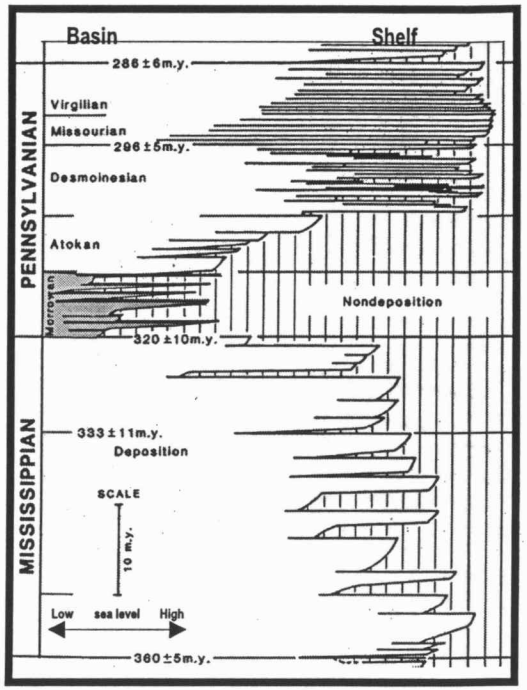

Figure 1.3 Coastal onlap curve for Mississippian and Pennsylvanian (modified from Ross and Ross, 1988). Morrowan is highlighted.

Induced eustatic sea-level fluctuations (Figure 1.3; Ross and Ross, 1985). Bounding erosional surfaces mark these high-frequency events. Even though a majority of the craton was exposed, the Hugoton Embayment remained a downwarped area that continued to receive siliciclastic sediments shed from the west by the Ancestral Front Range (Las Animas Arch) and the Apishapa Uplift and to a lesser degree from the Central Kansas Uplift to the east (Figure 1.2; DeVoto, 1980; Clark, 1987; Youle, 1992).

Stratigraphy

The Kearny Formation (Morrowan Stage, Lower Pennsylvanian Series) of southwestern Kansas contains strata that lie immediately below the Gray Group (Thirteen-Finger Limestone) and above the Mississippian Shore Airport Formation (Chester Formation) (Youle, 1992). The Kearny Formation is informally subdivided into the lower and upper Morrow. The lower Morrow lies above the pre-Pennsylvanian unconformity with the Mississippian carbonates (Figure 1.4).

Zeller (1968) indicated that lower Morrow rocks are present in Kansas only in the subsurface of the Hugoton embayment. These strata thicken to approximately 600 feet thick in the south and consist of conglomerates, sandstones, shales, thin limestones, and coal. Youle (1992) showed that the Kearny Formation thins toward the north, northeast and the east in the Hugoton Embayment and pinches out toward the Central Kansas Uplift. Wheeler et al., (1990), classified rocks of the lower Morrow into twelve facies that are assembled into four depositional units.

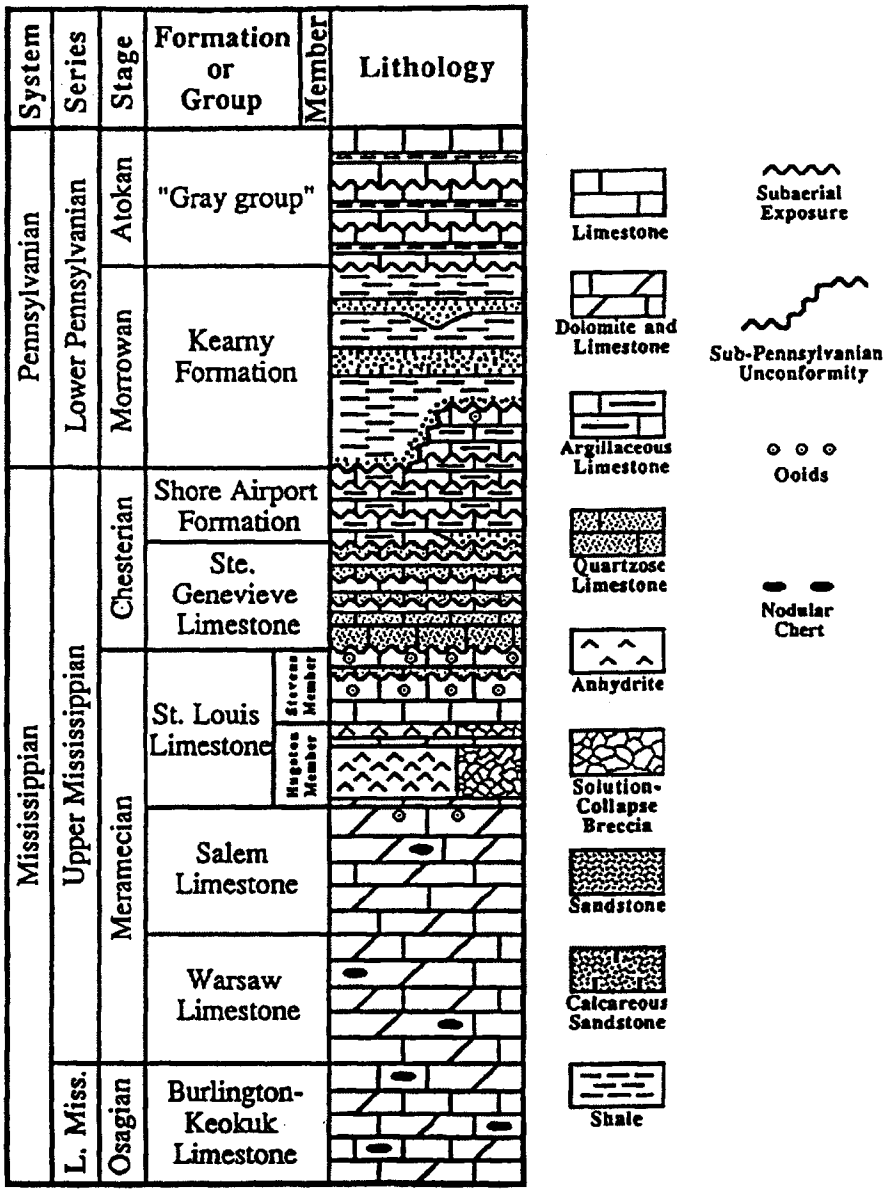

Figure 1.4 Upper Mississippian to Lower Pennsylvanian lithostratiraphic column in the Hugoton embayment, southwestern Kansas (modifeded from Abegg, 1994).

Lower Morrow rocks were thought to be composed of delta front, carbonate platforms or shoreface deposits which underwent periodic subaerial exposure due to relative drops in sealevel.

Within the study area, the lower Morrow rocks were deposited within incised valleys (Cheyenne, Kiowa, and Lincoln Counties, Colorado, and Stanton and Clark Counties, Kansas; Germinario, 1996 and Bartberger, 1996). Sonnenberg (1985) was the first to identify the lower Morrow sandstone in southeast Colorado as a valley-fill deposit. Seismic modeling, wireline correlation and core description in the Minneola Field (Ford and Clark counties, southwestern Kansas) showed that the lower Morrow sand was deposited in an incised valley (Clark, 1987). This study also suggested that the lower Morrow in the Arroyo Field is composed of fluvial deposits that might have been reworked by marine processes. To the south in Stevens County, the lower Morrow is represented by retogradational, open marine siliciclastic successions..

Methods of Study

Four cores were described to establish the lithofacies and deduce the depositional environments for the lower Morrow in the study areas. Core descriptions (Kendrick 1-23, Fritz 1-16, Gaskill 2A, Nell A-1) and geologist reports were integrated with modern log suites that included gamma ray, spontaneous potential, density (Dphi), compensated neutron (Nphi), sonic, and photoelectric (PEF) wireline-logs in order to develop an electrofacies model. The electrofacies model was used to establish and map the depositional environments in areas without core

control. The depositional model, based on core and wireline data, was used to build a sequence-stratigraphic framework for the lower Morrow in the Arroyo and Gentzler Fields. Lower Morrowan sandstone bodies were classified into depositional facies within the frameworks developed by Reading (1996), Dalrymple et al. (1992), Zaltin et al. (1994), Allen and Posamentier (1993) and Nichols (1991). These classifications consist of segments that are categorized by the presence and absence of sedimentary structures and lithological features. Although these classification schemes have primarily been used on outcrops, this study applied them to the subsurface.

2.0 CORE DESCRIPTIONS

J. M. Huber Kendrick 23-1

Eighty-five feet of siliciclastic-dominated lower Morrowan strata was recovered as three cores from J. M. Huber Kendrick 23-1 in Stanton County, Kansas (Table 2.1).

Core No.	Top (ft)	Bottom (ft)	Recovered (ft)	Sandstone (ft)	Shale (ft)
1	5370	5397	27	27	0
2	5397	5424	27	23.5	3.5
3	5424	5454	30	29	1

Table 2.1—Cored intervals from J. M. Huber Kendrick 23-1, section 23, T29S, R41W, Stanton County, Kansas.

The three cored intervals were subdivided into 11 lithofacies based on grain-size, and sedimentary and biological structures present (Table 2.2; figures 2.1a, b). Each lithofacies is described and its depositional environment interpreted. In general, I interpret the composite core interval to represent a transition from brackish-water at the base to open marine water at the top.

Facies A

Facies A (5459–5445.4 ft) is restricted to the base of the core. It is represented by a 4.4 m (14.5-ft) of gray, very fine- to fine-grained, well-sorted, glauconitic, pyritic, homogeneous quartz sandstone. Faint, low-angle cross bedding, subhorizontal-planar beds, pyrite nodules, and stylolitic structures are common

Facies	Lithofacies Description	Sedimentary Structures	Depositional Environment
A	Non-fossiliferous, massive, well-sorted, poorly defined planar cross-bedding, fine-grained sandstone.	Faint cross–bedding and subhorizontal bedding.	Brackish
B	Very, coarse- to fine-grained sandstone with mud drapes.	Mud drapes, climbing ripples, and laminations	Tidally influenced brackish
C	Burrowed, fine-grained siltstone and sandstone interbedded with black fissile shale.	Wavy, lenticular and flaser bedding.	Lagoon
D	Mud-supported conglomerate interbedded with pebbly, moderately sorted, sandstone.	Massive and graded bedding.	Tidal inlet floor.
E	Bioturbated, pebbly, medium-grained sandstone; interbedded with pebbly mud-supported conglomerate	Massive and graded bedding.	Tidal channel margin or abundant tidal inlet.
F	Bioclastic, low-angle cross-bedded medium- to coarse-grained sandstone.	Low-angle cross-bedding, erosive surfaces and graded bedding.	Active inlet fill
G	Bioturbated, bioclastic, pebbly, medium- to coarse-grained sandstone.	Horizontal bedding and laminations.	Low-energy, protected setting behind spit platform
H	Bioclastic, slightly bioturbated, moderately-sorted, pebbly medium-grained sandstone; interbedded with pebbly conglomeratic medium-grained sandstone.	Massive, graded bedding and cross-bedding.	Inlet floor
I	Bioclastic, massive, moderately- to well-sorted, medium-grained sandstone.	Massive and discontinuous laminations.	Upper shoreface
J	Bioclastic, heavily calcite cemented, low-angle cross-bedded, well-sorted coarse-grained sandstone.	Low-angle cross-bedding and laminations.	Upper shoreface

Table 2.2 Summary of lithofacies and interpreted depositional environments for the J. M. Huber, Kendrick 23-1.

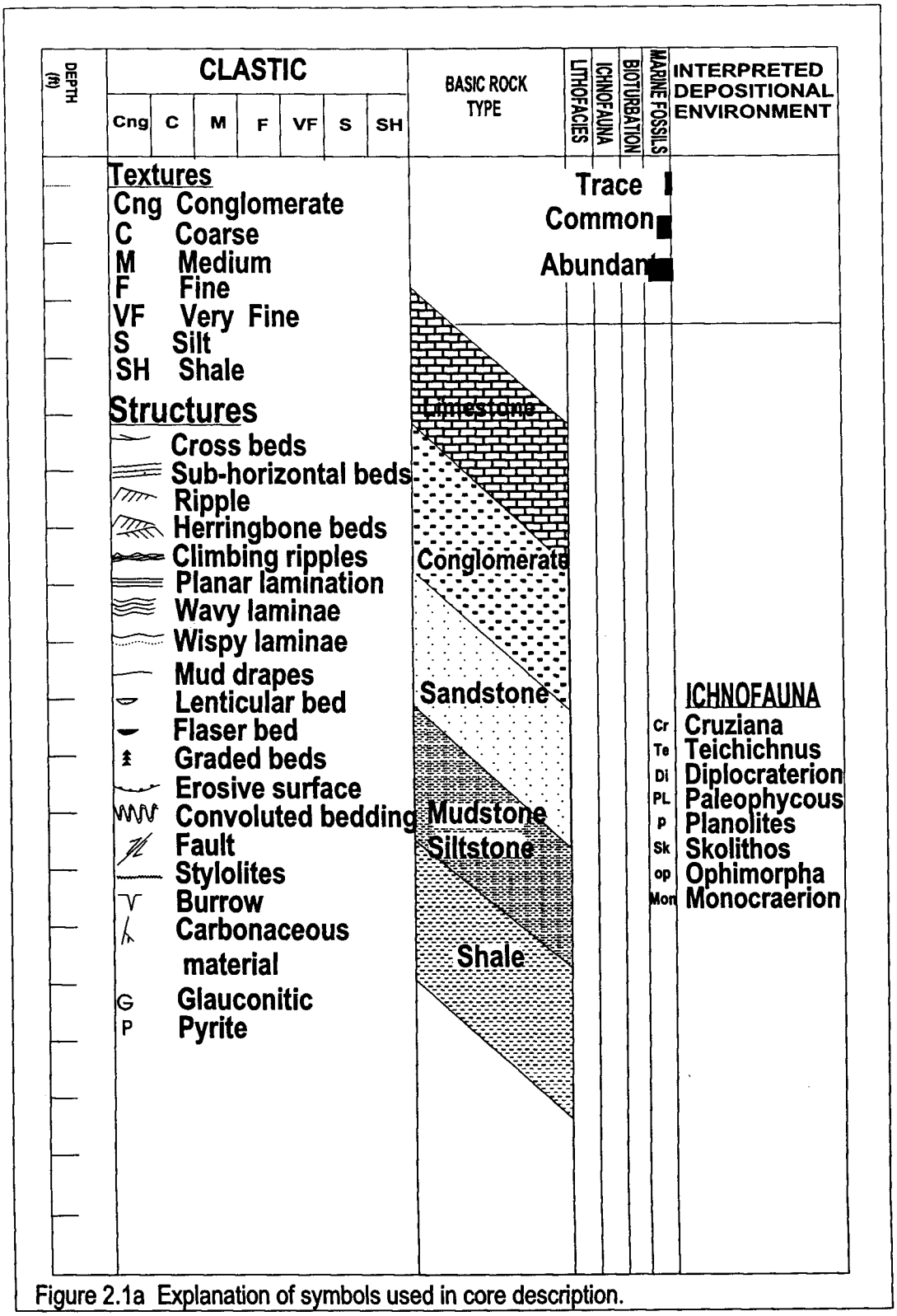

Figure 2.1a Explanation of symbols used in core description.

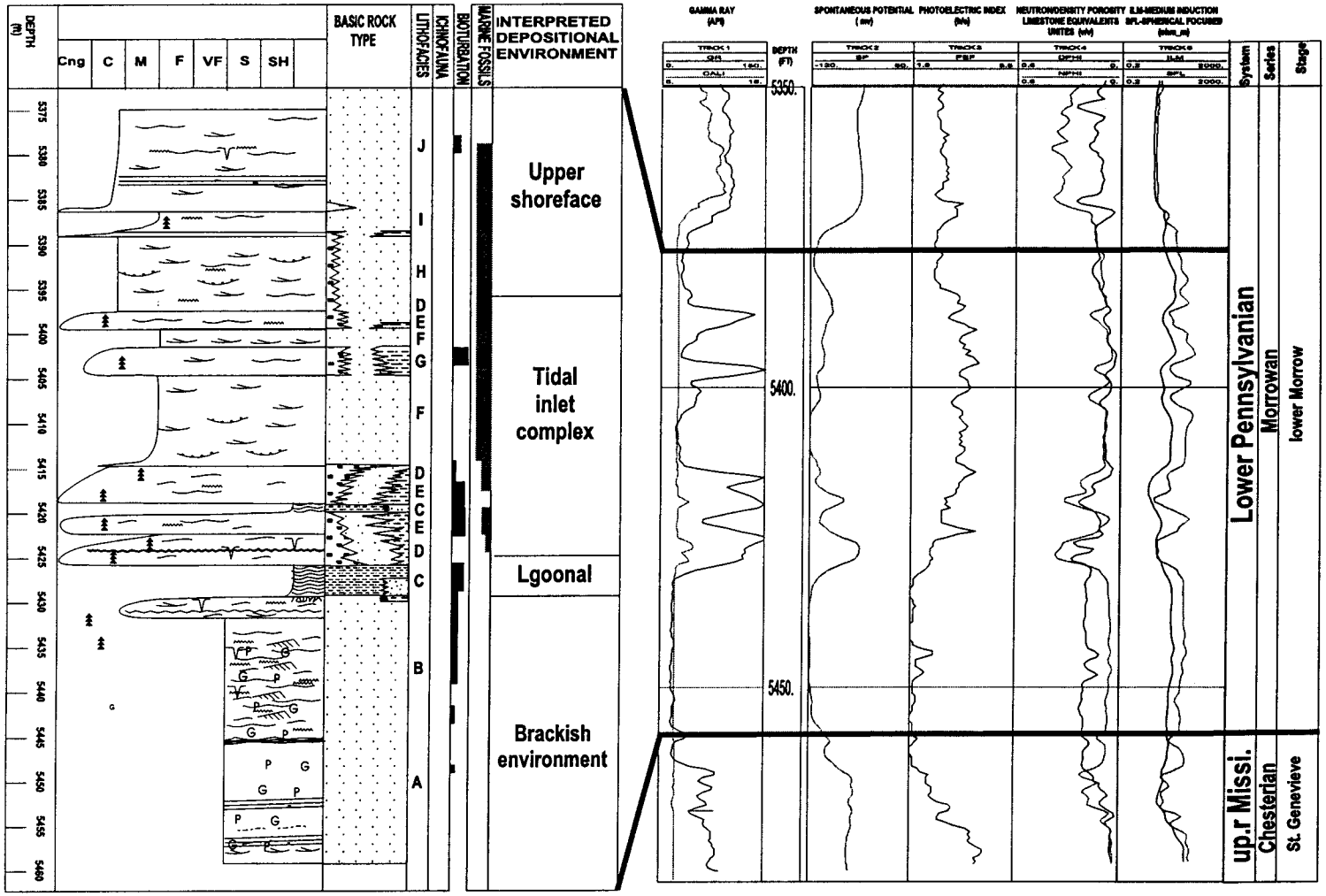

Figure 2.1 b Core description and wireline log of the J. H. Huber Kendrick 23-1 (sec. 23, T 29s, R41 W, Stanton County, Kansas)

features in facies A (figures 2.2a, b). High-angle cross-bedded pyritic sandstone beds are locally present, as are faint discontinuous to continuous shale laminae, which are associated with stylolitic structures. Bedding structures are highlighted by variation in pyrite concentrations (Figure 2.2b).

The base of facies A consists of a structureless, massive, glauconitic, pyritic, fine-grained sandstone that grades upward into a low-angle cross-bedded and subhorizontal planar-bedded sandstone. Locally, facies A is interbedded with a light-gray, massive, glauconitic and pyritic, calcite-cemented, fine-grained quartz sandstone that has sharp contact with beds both above and below. Bioturbation, other than that of *Palaeophycous*, was not observed in facies A. Facies A is gradationally overlain by facies B (Figure 2.2c). The basal contact of facies A was not recovered in the core interval.

The homogeneity and well-sorted nature of facies A, together with the absence of mud drapes, lithoclasts and bioclasts, indicate a high-energy environment and significant reworking. The presence of high-angle cross stratification, and lack of bioturbation suggest a rapid sedimentation rate. The absence of marine bioclasts, hummocky cross stratification or bioturbation suggests that facies A was not deposited in a fully marine setting. A gradational transition up-section from low-angle cross bedding into subhorizontal planar bedding indicates that the current energy was changing from a lower flow regime to an upper flow regime.

The presence of glauconite and pyrite, in conjunction with the absence of siderite, indicates a marine influence. Berner (1971) found that dissolved sulfate is

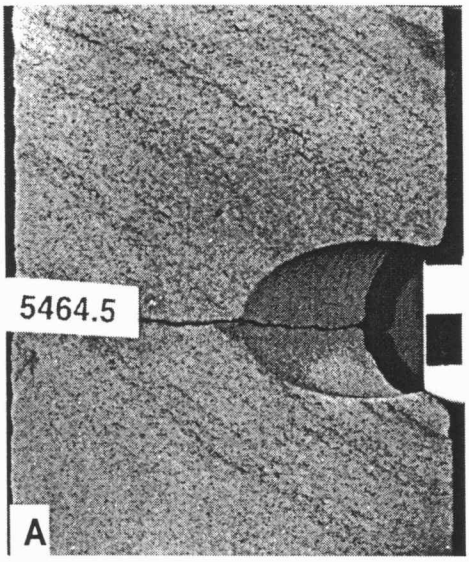

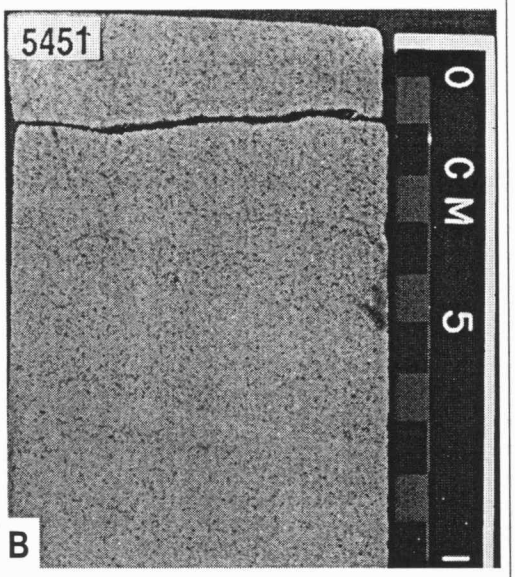

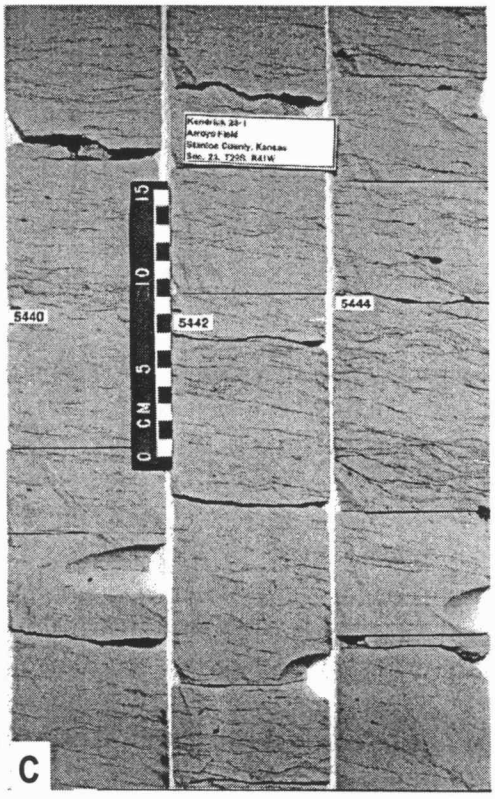

Facies B

Facies A

Figure 2.2 Facies A a) High-angle cross-bedding; b) Sub-horizontal-bedding
Note: bedding structures are recognized by variations in pyrite concentrations;
c) Photo shows gradual contact (arrow) between Facies A and B.

abundant in marine waters. Sulfur-reducing environments, commonly restricted to marine and brackish-water conditions, are thought to contribute to the formation of pyrite (Horne et al., 1978). In a nonmarine setting, the availability of dissolved sulfate is recognized as the limiting factor in pyrite formation. Sulfate has been shown to be anywhere from 100 to 230 times more abundant in marine water than in freshwater (Stumm and Morgan, 1970; Berner and Raiswell, 1984). There is a smaller amount of sulfate than of sulfide to be reduced in a freshwater environment, which results in the formation of diagenetic siderite instead of pyrite. A brackish-water environment contains more dissolved sulfate than a freshwater environment, but it contains much less dissolved sulfate than a marine environment (Casagrande et al., 1977). Martens and Goldhaber (1978) and Postma (1982), correlate diagenetic pyrite concentrations in both brackish and freshwater environments with fluctuations in marine conditions at the time of deposit. Berner et al. (1979), propose that the ratio of FeS_2 to FeS could be used as a paleosalinity indicator.

Low diversity of the ichnofauna taxon *Palaeophycous* suggests that facies A was deposited in a stressful brackish-water environment (Frey and Howard, 1975, 1980, 1985; Ekdale et al., 1987; Wightman et al., 1987). The low diversity of ichnofauna reflects the limited number of benthic species that have evolved the physiological specialization necessary to live in brackish-water (Barnes, 1984). Facies A is much different from other marine facies encountered in this core (particularly facies F, I, and J) regarding grain size, nature of sorting, type of cement,

sedimentary structures, rock constituents, size and type of lithoclasts and bioclasts, and diversity and size of ichnofauna.

Lithostratigraphic cross-sections and isopach map of electrofacies Ae (Figure 5.5 and Appendix A) show that facies A is restricted to the valley wall and has axial geometry that trends northwest to southeast. Clark (1987) studied similar facies in the Minneola Pool area (T30S, R25W, Clark County, Southwestern Kansas). She suggested that the facies was probably deposited in a fluvial system that was later reworked by marine processes. The same facies in the Minneola area was described and mapped by Youle (1992), who suggested that the facies was part of a valley-fill system incised into underlying Mississippian limestone. The character visible in core and stratigraphic geometry, imply that facies A accumulated in a paleovalley under brackish-water conditions.

Facies B

Facies B (5445.6–5432 ft) is a light-gray, glauconitic, pyritic, fine- to coarse-grained quartz sandstone (Figure 2.1b). Mud drapes, ripple marks, low-angle cross bedding, shale stringers and laminae, reactivation surfaces, pyrite nodules and stylolitic structures are present throughout the facies. Commonly, ripple marks are associated with stylolitic structures. Climbing ripples are locally present (Figure 2.3a). Herringbone structures, while difficult to discern in the core are locally present (Figure 2.3b). The abundance of ripple marks and mud drapes varies throughout the facies. Bioclasts are scarce to absent, and the degrees of bioturbation and trace fossil

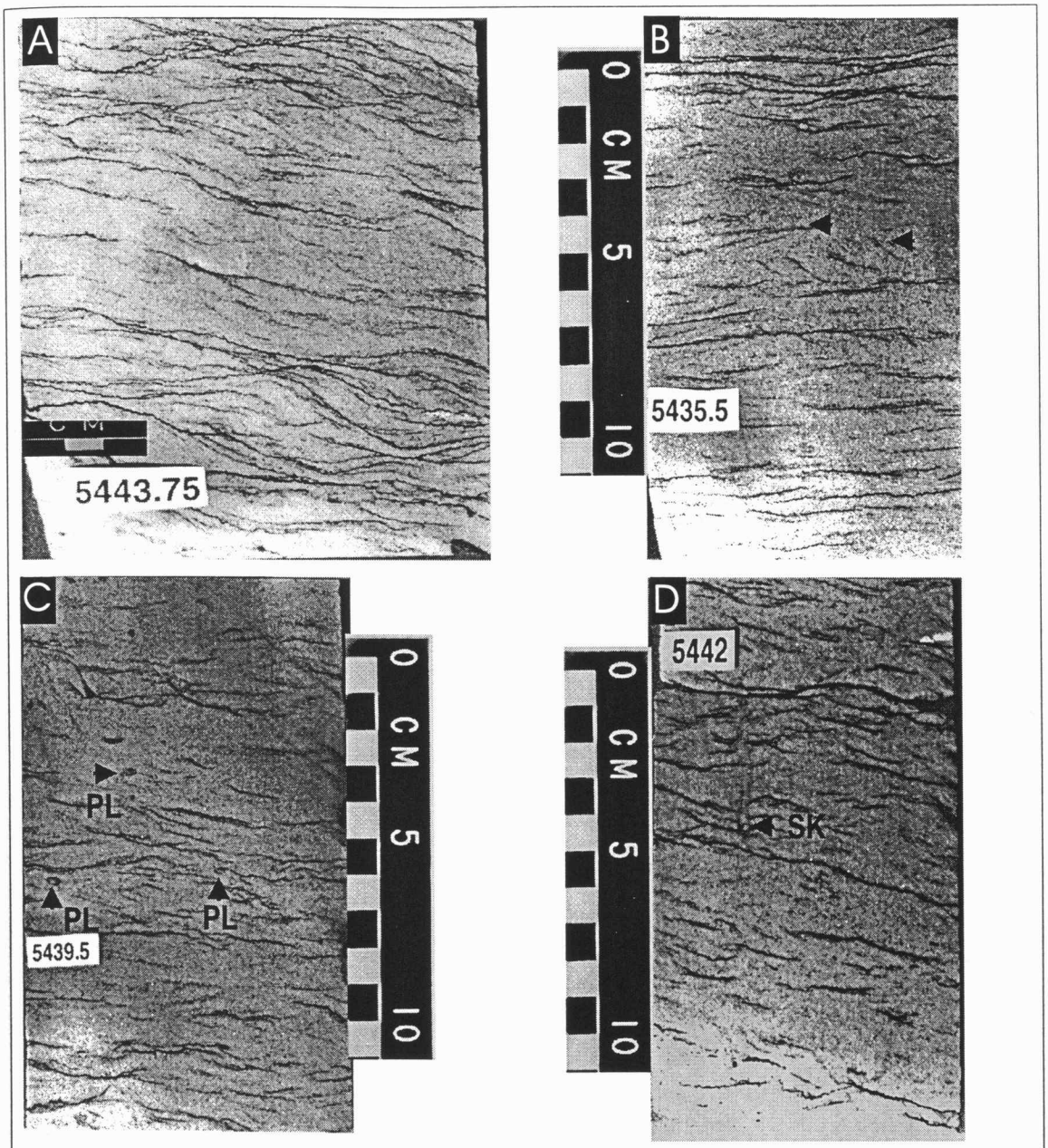

Figure 2.3 Facies B. a) climbing ripple marks and mud drapes; b) poorly developed herringbone structures and ripple marks; c) fine-grained sandstone with *Palaeophycus* (PL); d) fine-grained sandstone with *Skolithos* (SK).

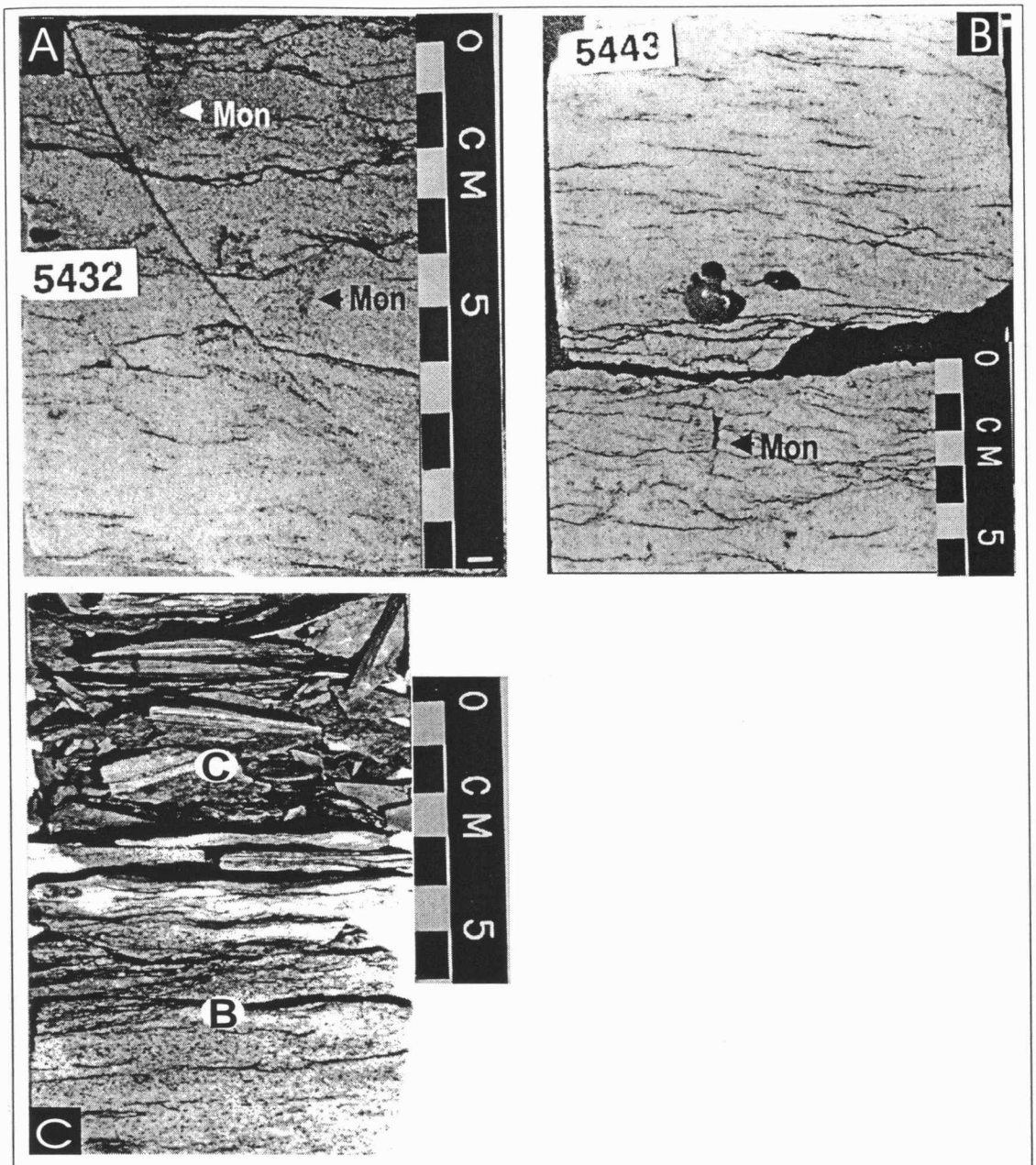

Figure 2.4 a), b) fine-grained sandstone of facies B with *Monocraterion (*Mon*);*
c) gradual transition from Facies B to Facies C. Note: the soft-sediment deformation within Facies B.

diversity are low. *Palaeophycous*, *Skolithos*, and *Monocraerion* are the ichnofauna taxa observed within facies B (figures 2.3c, d, 2.4a, b).

Near the top of facies B (5432–5431.8 ft), there is a sharp transition from well-sorted, fine-grained sandstone to moderately sorted, coarse-grained glauconitic quartz sandstone. Observed within the coarse-grained interval are fining-upward beds, high-angle cross stratification, ripple marks, burrows and locally erosive bases. The uppermost 10 cm of facies B show soft-sediment deformation (Figure 2.4c). Several coarse quartz grains are coated with pyrite. The ichnofauna is dominated by *Monocraerion*. The coarse-grained glauconitic sandstone displays a gradational transition upward into a slightly bioturbated, very fine-grained, silty sandstone interbedded with fissile shale characteristic of facies C (figures 2.2c and 2.4c). Facies B has gradational contacts with both the underlying facies A and the overlying facies C.

The presence in facies B of mud drapes, ripple marks, glauconite, pyrite, and climbing ripples, along with the absence of subaerial exposure, bioclasts, coal seams, and oxidized shale, suggest a subtidal environmental. Mud drapes, mud laminae, reactivation surfaces, and poorly developed herringbone cross stratification indicate tidal influence (Dalrymple, 1992). Climbing ripples suggest a significant introduction of sediment during high flow conditions (Jopling and Walker, 1968; McKee, 1965). I interpret the localized, coarse-grained sandstone near the top of facies B to be the result of traction deposition resulting from a single high-energy event, such as a storm

or a flood. However, this interval might have been deposited as a ravinement surface during transgression.

The presence of *Palaeophycous*, *Skolithos*, and *Monocraerion* species is indicative of the *Skolithos* ichnofacies (Pemberton and Frey, 1982). This assemblage is composed of simple dwelling structures produced by suspension feeders, and suggests a high-energy setting with stressful brackish-water conditions (Wightman et al., 1987; Beynon et al., 1988; Barnes, 1984). Wheeler et al. (1990) attributed similar facies (their facies 6) as deposited in a fluvial or estuarine setting. I interpret facies B to have been deposited in a wave- and tide-influenced brackish-water environment.

Facies C

Facies C (5423–5425.7 and 5416.3–5416.8 ft) is characterized by a light-gray, burrowed, fine-grained sandstone or silty sandstone interbedded with black, fissile shale. Starved ripples, discontinuous silty sand laminae, planar, lenticular, and wavy beds, wavy and planar laminations, and burrows are present within the silty, fine-grained sandstone (figures 2.5a, b). *Cruziana*, *Teichichnus*, *Diplocraterion*, and *Planolites* species are the ichnofauna observed within facies C (figures 2.6a, b). Facies C has either a gradational contact with facies B or a sharp erosional contact with facies D and E (figures 2.7a, b).

The interbedded sandstone and mudstone interval of facies C represents a quiet water setting with alternation between a slow current depositing sand as ripple or lamina, and a very slow current depositing mud (Tillman and Martinson, 1984; Strobl, 1988; Reading, 1996). Lenticular and wavy beds, wavy and planar

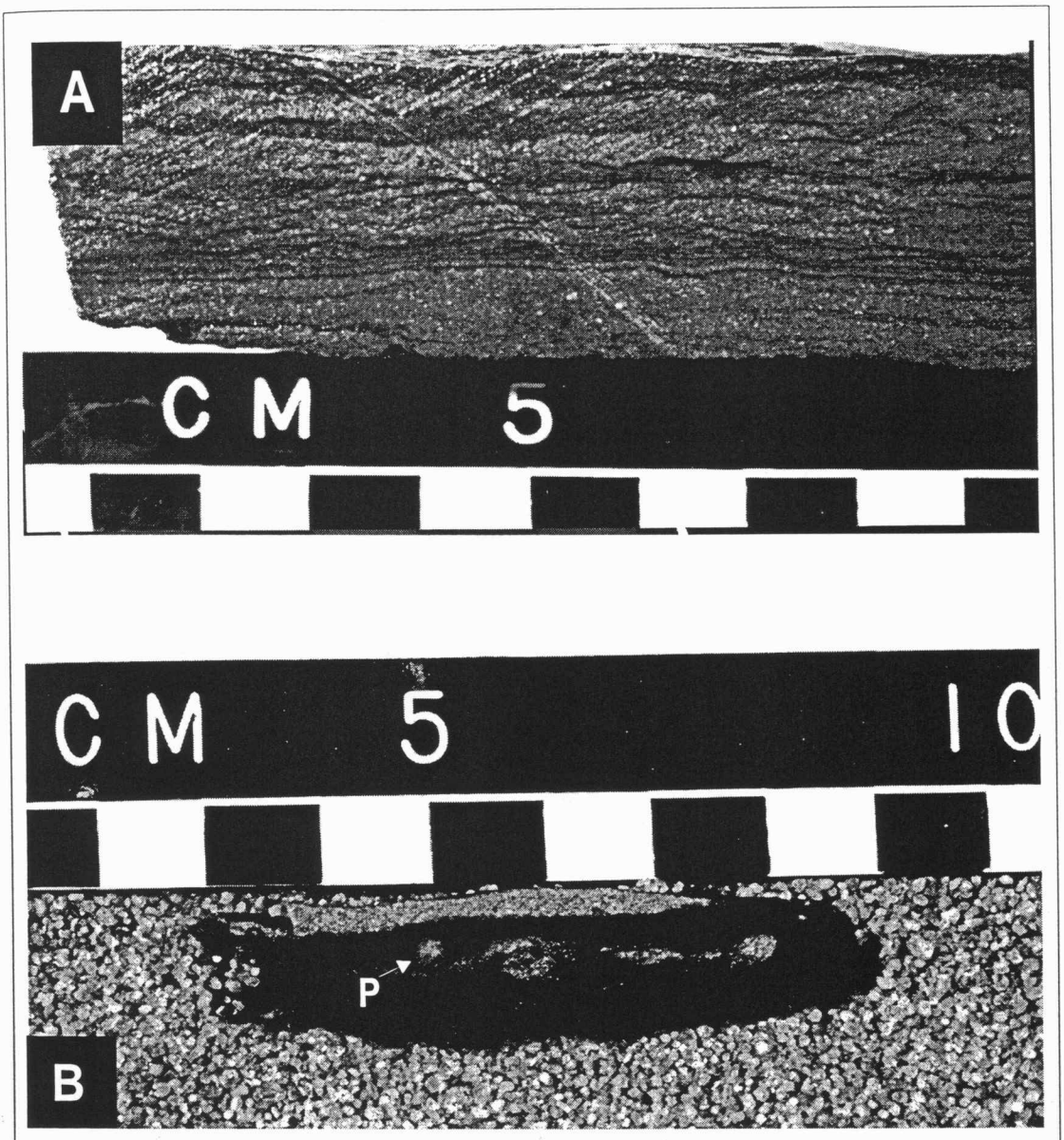

Figure 2.5 Characteristic lithologies of Facies C. a) interbedded of silty fine-grained sandstone and mudstone; b) Lenticular and wavy fine-grained sandstone beds, and *Planolites* burrows (P).

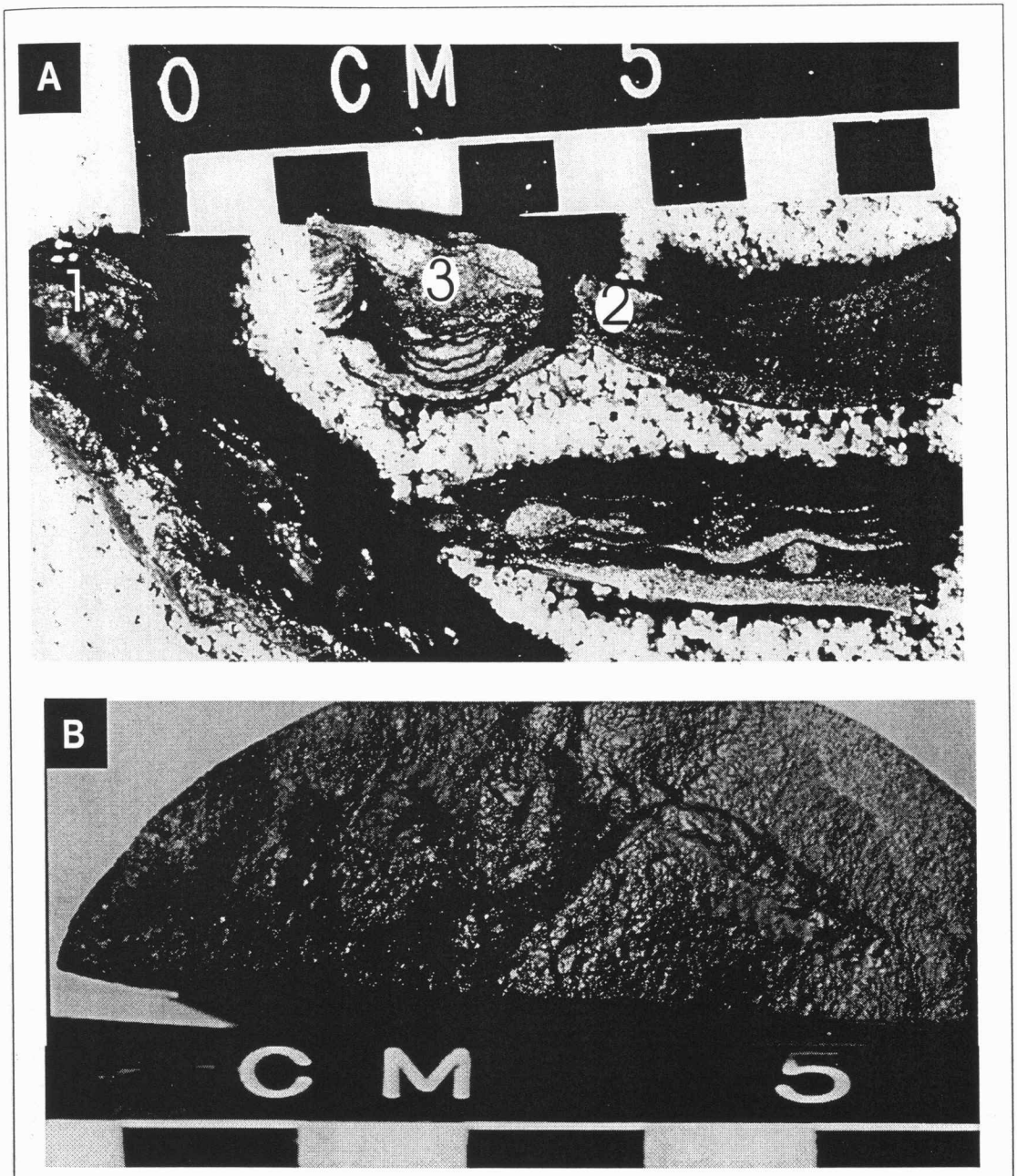

Figure 2.6 Trace fossils observed in Facies C. a) 1- *Diplocraterion*; 2- *Teichichnus*. View is parallel to the burrow axis, 3- *Teichichnus,* View is perpendicular to the burrow axis; b) *Cruziana*. View is parallel to the bedding plain.

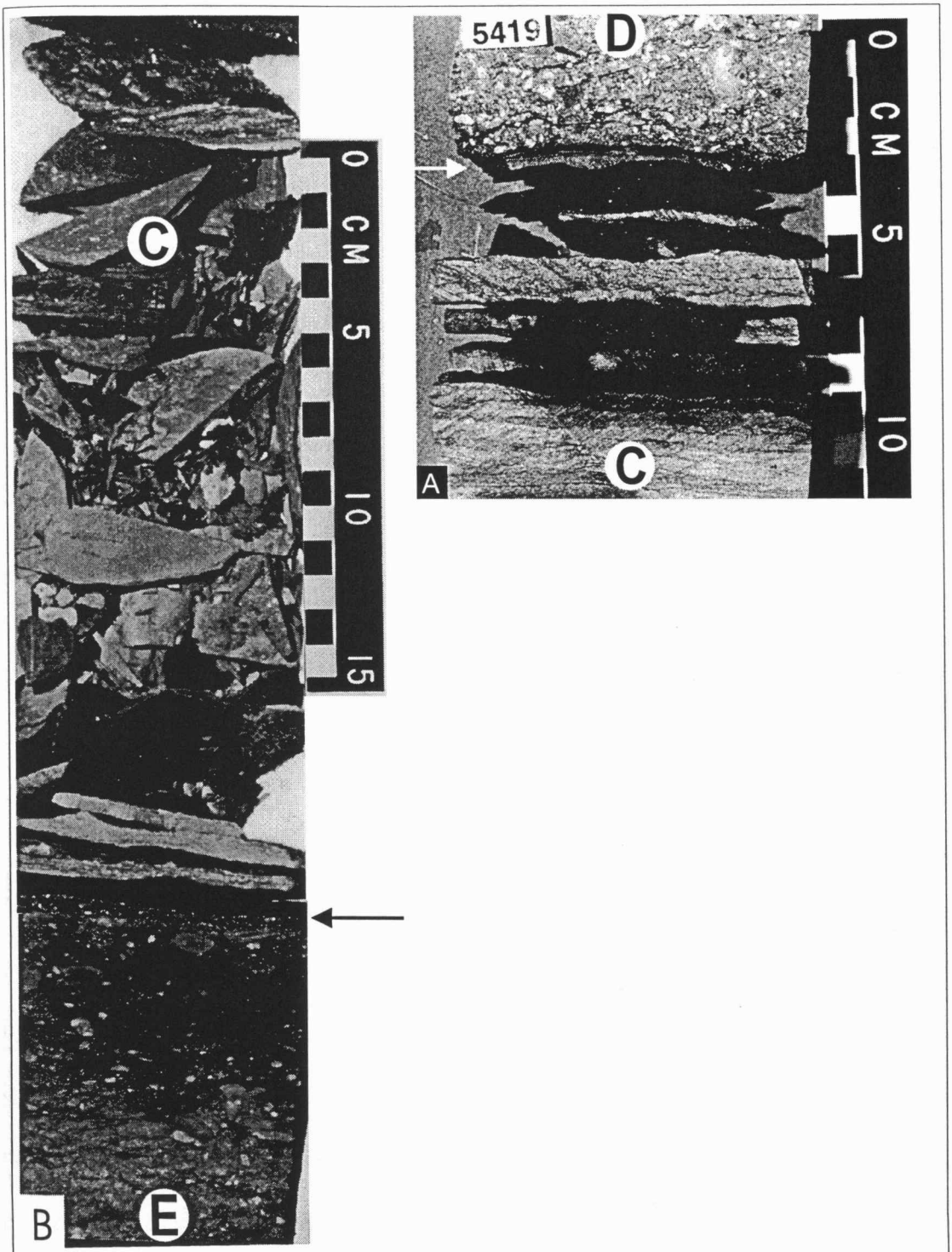

Figure 2.7 a) Photo shows a sharp contact between Facies C and D (arrow);
b) Photo shows a sharp contact between Facies C and E (arrow).

laminations, starved ripples, and discontinuous silty sand laminae are common features of tidal environments (Davis, 1983; Nio and Yang, 1991; Dalrymple, 1992). There is a low diversity of trace fossils, including a mixture of feeding structures formed by deposit feeders and dwelling structures constructed by suspension feeders. The assemblage may represent a depauperate *Cruziana* ichnofauna that developed under low-energy, stressful, brackish-water conditions (Beynon et al., 1988; Barnes, 1984; Pemberton et al., 1992). I interpret facies C as having been deposited in a low-energy environment, such as a back barrier lagoon, or in a mid-estuarine environment.

Facies D

Facies D (5427.8–5422.8 and 5416.3–5415.8 ft) is represented by a light-gray, mud-supported, calcite-cemented conglomerate interbedded with pebbly, moderately sorted, coarse-grained quartz sandstone (4–10 cm thick). The conglomerate matrix is composed of a fine- to medium-grained sandstone that locally has a series of fining-upward beds (figures 2.8a, b). The conglomerate clasts are polymictic (Figure 2.8a). Lithoclasts are composed of rounded to subrounded sand and mud clasts that show either fissile laminations or concentric structures (Figure 2.8a). Bivalves and brachiopods are the main bioclasts. Bioclasts are rare to absent at the base, but become more abundant upward. *Skolithos* burrows are found only within the sandy intervals (Figure 2.8c). Locally, facies D fines upward into a light-gray, pyritic, calcite-cemented, pebbly, coarse-grained sandstone (Figure 2.8b). Mud drapes, a

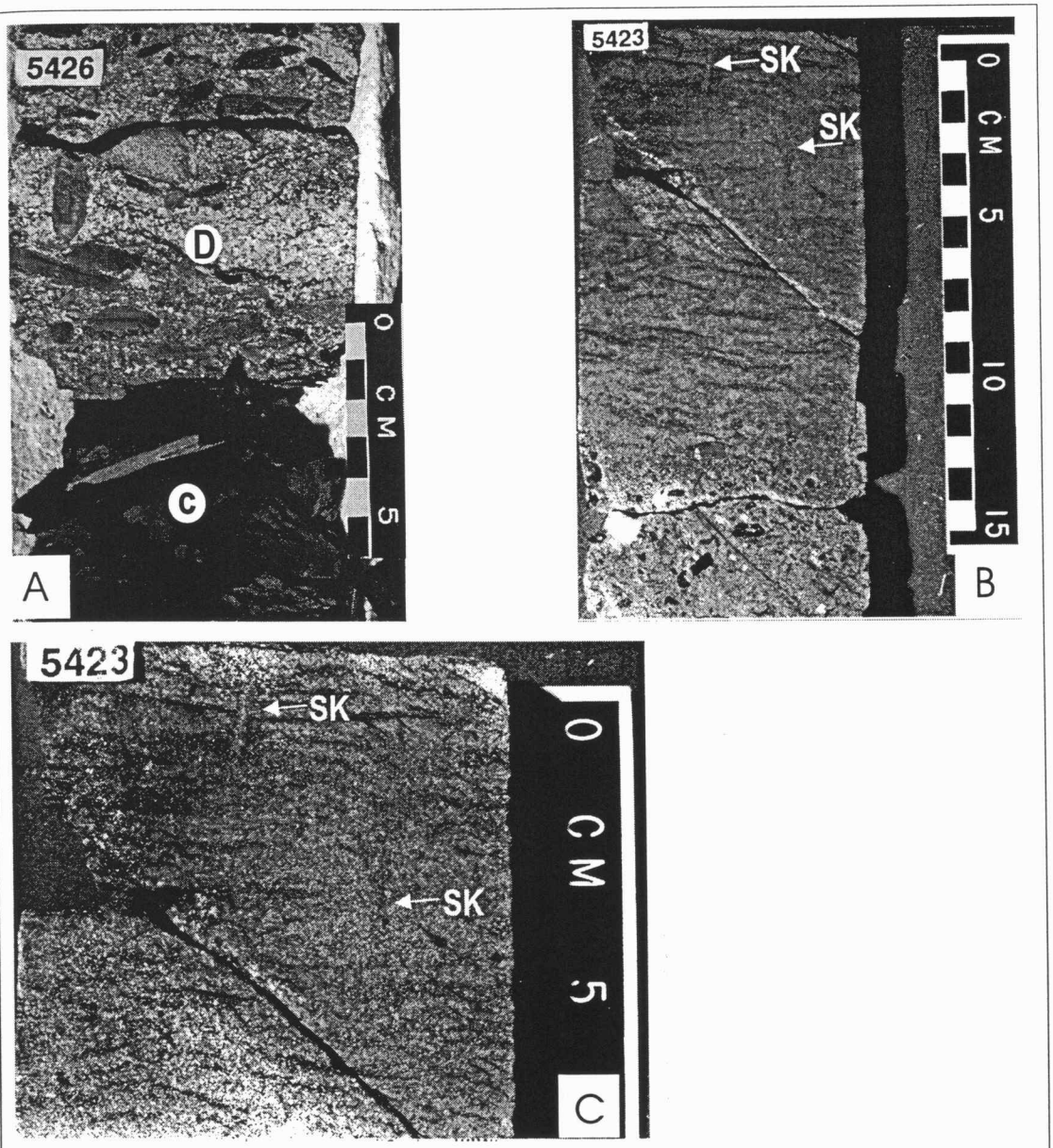

Figure 2.8) Facies D. a) Clast-supported conglomerate of facies D. Note: the roundness and the internal structures of the clasts; b) Serious of fining upward sand beds and conglomeratic intervals; Note: the diversity of the clasts, discontinuous laminae and mud drapes; c) Close-up photo shows the *Skolithos (SK)* burrows within the sand intervals.

series of fining-upward intervals, bioclasts, and *Skolithos* burrows are common within sand-rich intervals (Figure 2.8c). Facies D has sharp erosional contacts with the underlying facies C (Figure 2.8a), underlying facies E and the overlying facies E (Figure 2.9b) and a gradual contact with the overlying facies F (Figure 2.9a).

The presence of marine bioclasts in facies D is an indication of an increasingly marine setting. The lack of imbrication of the lithoclasts and the bioturbation in the lower part of facies D indicate rapid bedload deposition (Raddysh, 1988). Local presence of fining-upward beds in facies D suggests periodic deceleration of flow (Reinson et al., 1988). The gradational transition upward into medium-grained sandstone with biogenic sedimentary structures and mud drapes near the top of the facies indicates that depositional rates decrease up-section and suggests shoaling and tidal influences. This interpretation is consistent with the grain sizes and the internal structures of the lithoclasts, which are similar to those observed in facies C. The low diversity of ichnofauna (notably *Skolithos*) within the sandy intervals suggests high-energy, stressful, brackish-water conditions (Beynon et al., 1988; Barnes, 1984; Pemberton et al., 1992). The coarse-grained sand, shells, and pebbles were interpreted as a lag in the deeper portion of an active inlet channel, where the velocity of the current was greatest during tidal and wave exchange. I interpret facies D as having been deposited as the inlet floor of a tidal channel in the mid- to lower estuarine environment.

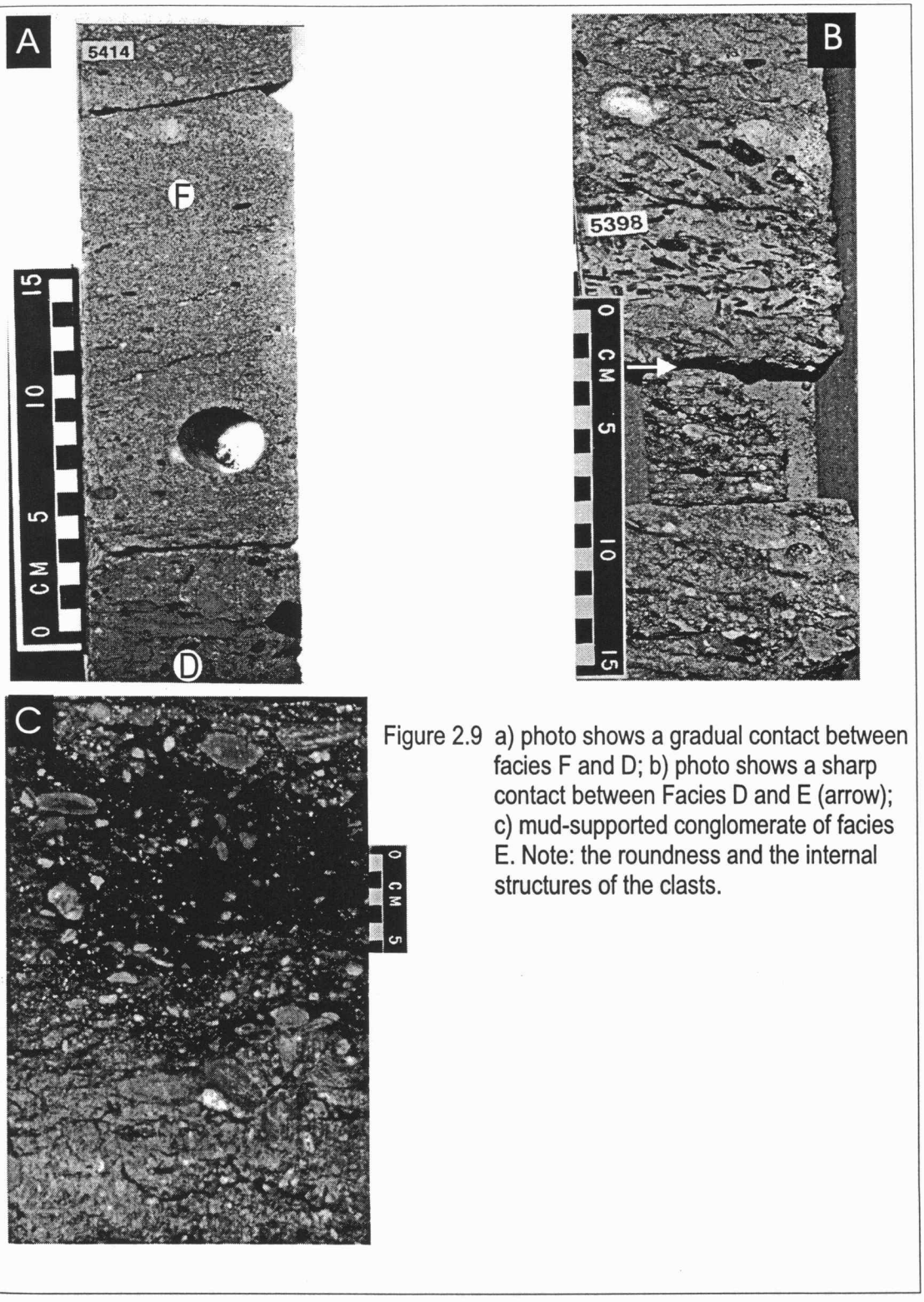

Figure 2.9 a) photo shows a gradual contact between facies F and D; b) photo shows a sharp contact between Facies D and E (arrow); c) mud-supported conglomerate of facies E. Note: the roundness and the internal structures of the clasts.

Facies E

Facies E (5420.8–5416.3, 5404.1–5403, and 5399–5397 ft) is a light to dark gray, bioturbated, bioclastic, glauconitic, pyritic, poorly sorted, pebbly, medium-grained sandstone interbedded with pebbly, polymictic, mud-supported conglomerate (Figure 2.9c). Facies E contains shale stringers, lithoclasts, and bioclasts, as well as a series of beds that fines upward. The sandstone and conglomerate beds are locally interbedded with shale and dark gray silty laminae associated with stylolitic structures (Figure 2.9c). The lithoclasts consist of rounded to subrounded mud and sand clasts (1–4 cm in diameter) that show fissile laminations or concentric structures. Bivalves, crinoids, and coral (1–2 cm in diameter) are the predominant bioclasts. Facies E has either gradual or sharp contacts with facies G and a sharp contact with facies F and H (Figure 2.11a).

Facies E and D are similar, but differ in the degree of bioturbation, clast size, grain size, and mud–sand content. Facies E contains smaller clasts, and more mud and sand than facies D. The presence of marine bioclasts in facies E is indicative of marine influence. Mud and silty laminae, along with moderate bioturbation, indicate either low sedimentation rates or relatively quiet-water depositional conditions (Strobl, 1988). The fining-upward beds are the products of either the activity of organisms or the periodic waning of the current's energy. The internal structures of the lithoclasts suggest that they were likely transported from an adjacent lagoon (facies C). This interpretation is supported by the erosional relationship of facies E with the facies C, which is associated with lagoon environment. On the basis of its

stratigraphic position and internal sedimentary structures, I interpret facies E as having been deposited in a protected setting adjacent to a tidal channel margin. However, Facies E may also have been deposited prior to abandonment of a tidal channel.

Facies F

Facies F (5415.3–5404.1 and 5401–5398 ft) consists of gray, bioclastic, calcite-cemented, medium- to coarse-grained quartz sandstone. Sedimentary structures that characterize facies F include low-angle planar cross-bedding, subhorizontal bedding, a series of fining-upward intervals, and stylolitic structures (Figure 2.10). Locally present are erosive bases floored with bioclasts and lithoclasts ranging from 1 to 2 cm in length (Figure 2.10b). Crinoids and bivalves are the main bioclast constituents. Lithoclasts consist mainly of sand and mud clasts. Facies F has a gradual contact with the underlying facies D (Figure 2.9a), and a sharp contact with the overlying facies E and facies G (Figure 2.11a).

The abundant marine bioclasts and associated calcite cement suggest a strong marine influence. The degree of sorting and roundness, the low-angle cross-bedding, and the absence of fine-grained facies and mud drapes suggest a high-energy, wave-dominated depositional environment. Large-scale foresets may indicate migration of subaqueous megaripples. The local presence of fining-upward beds and erosive surfaces floored with bioclasts suggests periodic high-energy events. The gradual transition from coarse-grained massive lag deposits (facies C) to medium-grained, moderately sorted, cross-bedded sandstone suggests an active channel fill (Moslow

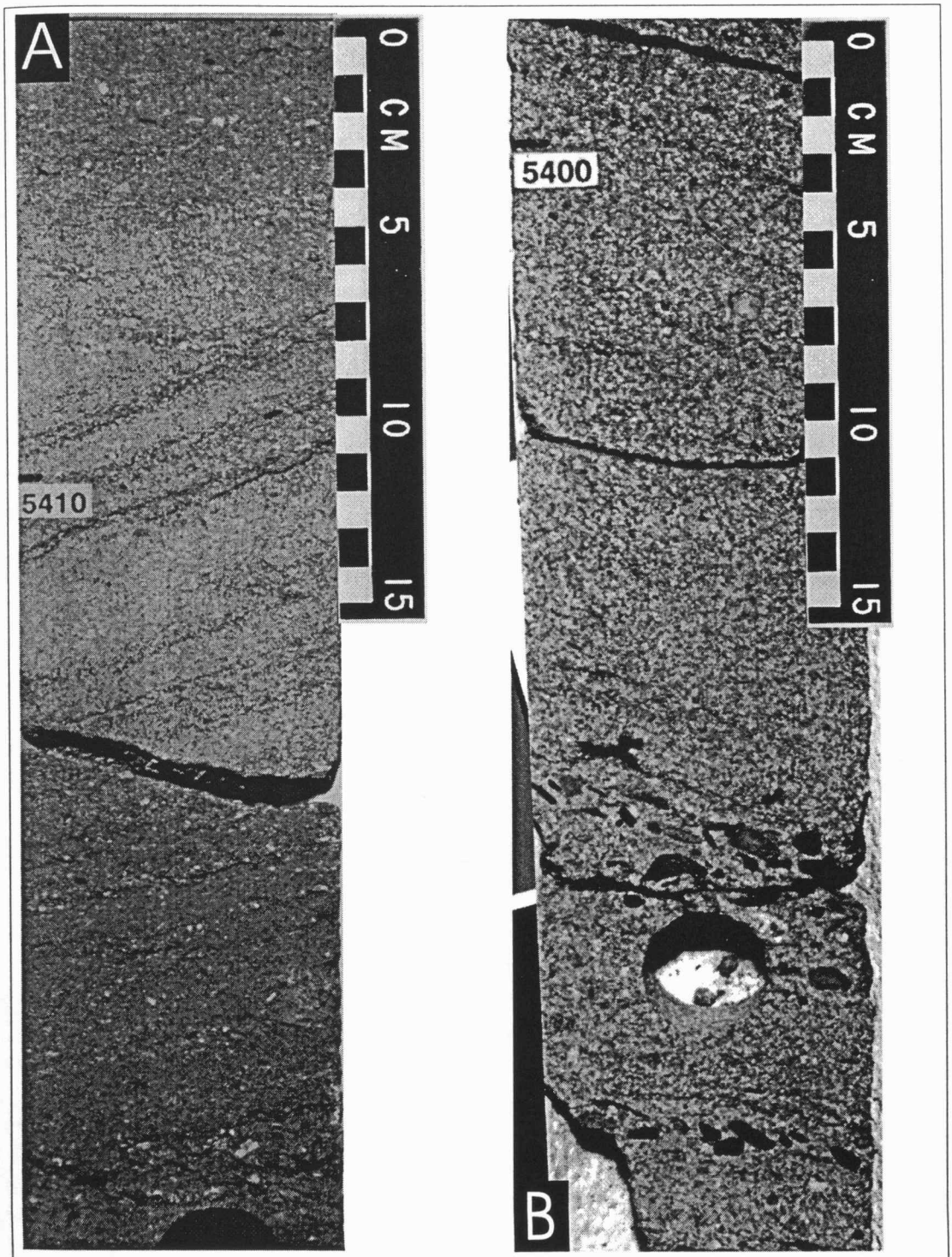

Figure 2.10 a, b) Facies F, showing low-angle cross bedding. Note: the erosive surfaces and the pebbles that floor the foreset in the lower part of the photo b.

and Tye, 1985). Wheeler et al. (1990) attributed similar facies (their facies 5) to have been deposited in an upper shoreface environment. On the basis of its stratigraphic position and internal sedimentary structures, I interpret facies F as having been deposited in a high-energy, wave-dominated, marginal marine setting, such as an estuary mouth.

Facies G

Facies G (5403–5401 ft) is represented by a dark gray, bioclastic, moderately bioturbated, pebbly, medium- to coarse-grained, calcite-cemented quartz sandstone. Series of normally graded beds, mud clasts ranging from 1 to 2 cm in length, low-angle cross bedding, and planar bedding are present throughout (Figure 2.11b). Scattered irregular shale stringers and flaser beds are observed. Bivalves and crinoids are the main bioclastic constituents (Figure 2.11b). Facies G has a gradational contact with the underlying facies E and a sharp contact with the overlying facies F (Figure 2.11a).

The presence of crinoid and bivalve fossil fragments suggests a marine influence. The degree of sorting and bioturbation and the presence of irregular shale lamina and flaser bedding suggest biogenic activity and a relatively low-energy condition. The preservation of the low-angle cross bedding suggests a period of high-energy prior to the bioturbation events. On the basis of its stratigraphic position and internal sedimentary structures, I interpret facies G to represent an abandoned tidal-inlet channel fill.

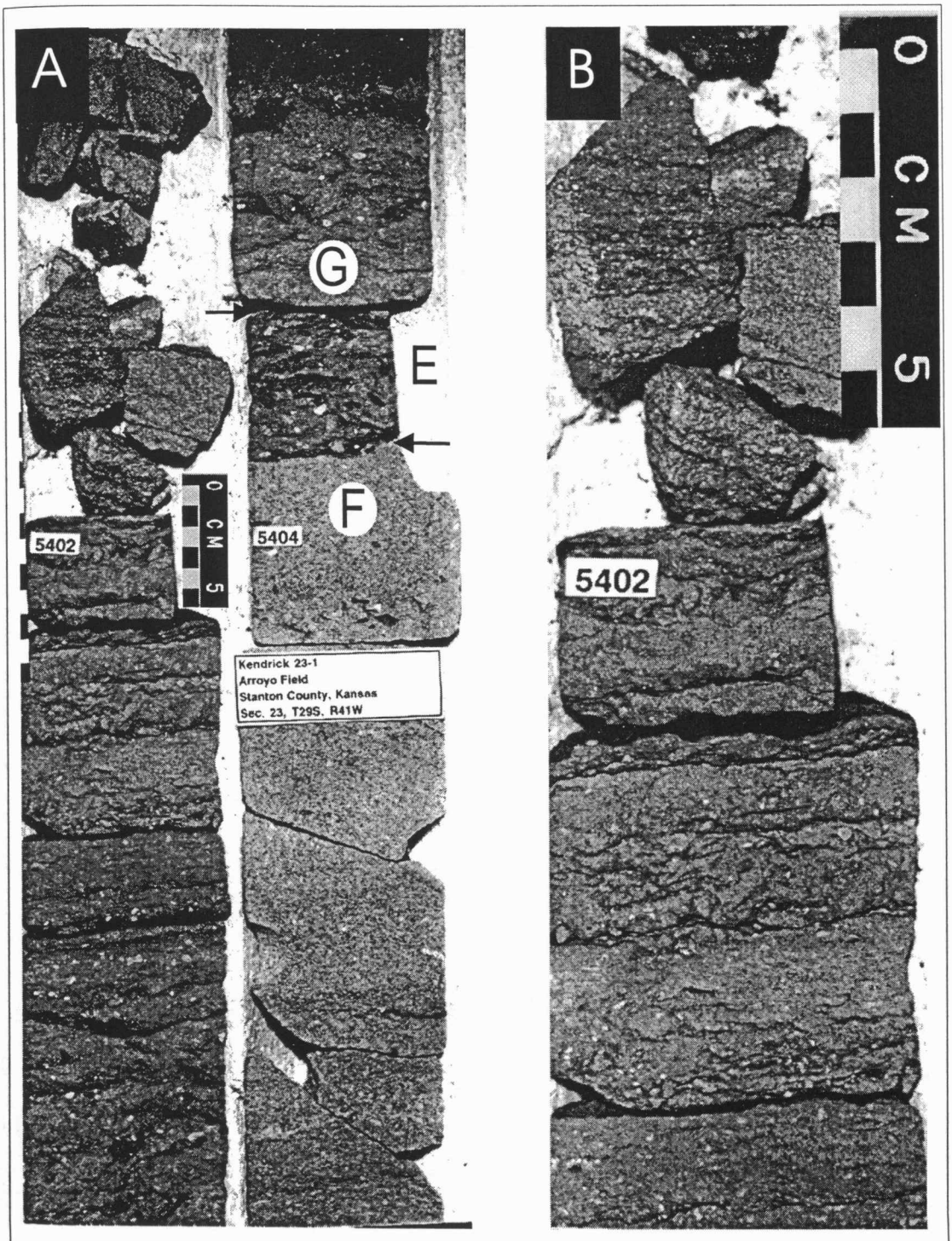

Figure 2.11 a) Photo shows sharp contacts between facies F, E and G (arrows); b) Close-up photo shows low-angle cross bedding (below) and shale laminae (up). Note: the white dots are crinoid and fragments.

Facies H

Facies H (5397.2–5398 ft) consists of a light to dark gray bioclastic, glauconitic, moderately sorted, pebbly, medium-grained sandstone interbedded with pebbly, conglomeratic, medium-grained sandstone. Facies H contains erosive surfaces, a series of normally graded intervals that are locally interbedded with shale laminae and stylolitic structures. Low-angle cross bedding is present (figures 2.12a, b). Lithoclasts increase upward and consist of rounded to subrounded mud and sand clasts 1 to 4 cm in diameter. Bivalves, crinoids, and coral from 1 to 2 cm in diameter are the main bioclastic constituents. Facies H is moderately bioturbated near the top and slightly bioturbated in the middle portion of the unit. Facies H has a sharp contact with the underlying facies E and a gradual contact with the overlying facies D.

Facies H and F are similarly constituted but differ in the following ways. First, compared to facies F, facies H consists of larger lithoclasts and bioclasts. Second, the foreset beds are floored with clasts larger than those in facies F. Finally, the erosive surfaces of facies H are better defined than those in facies F.

An abundance of marine bioclasts, along with a few lithoclasts, suggests a proximal marine setting. Low-angle cross-bedded sandstone without signs of bioturbation or mud drapes indicates rapid sedimentation and high-energy traction deposition in a wave-dominated environment. The presence of a series of fining-upward beds and shale laminae suggests periods of traction deposition followed by suspension deposition. Well-defined erosive surfaces indicate short periods of high-

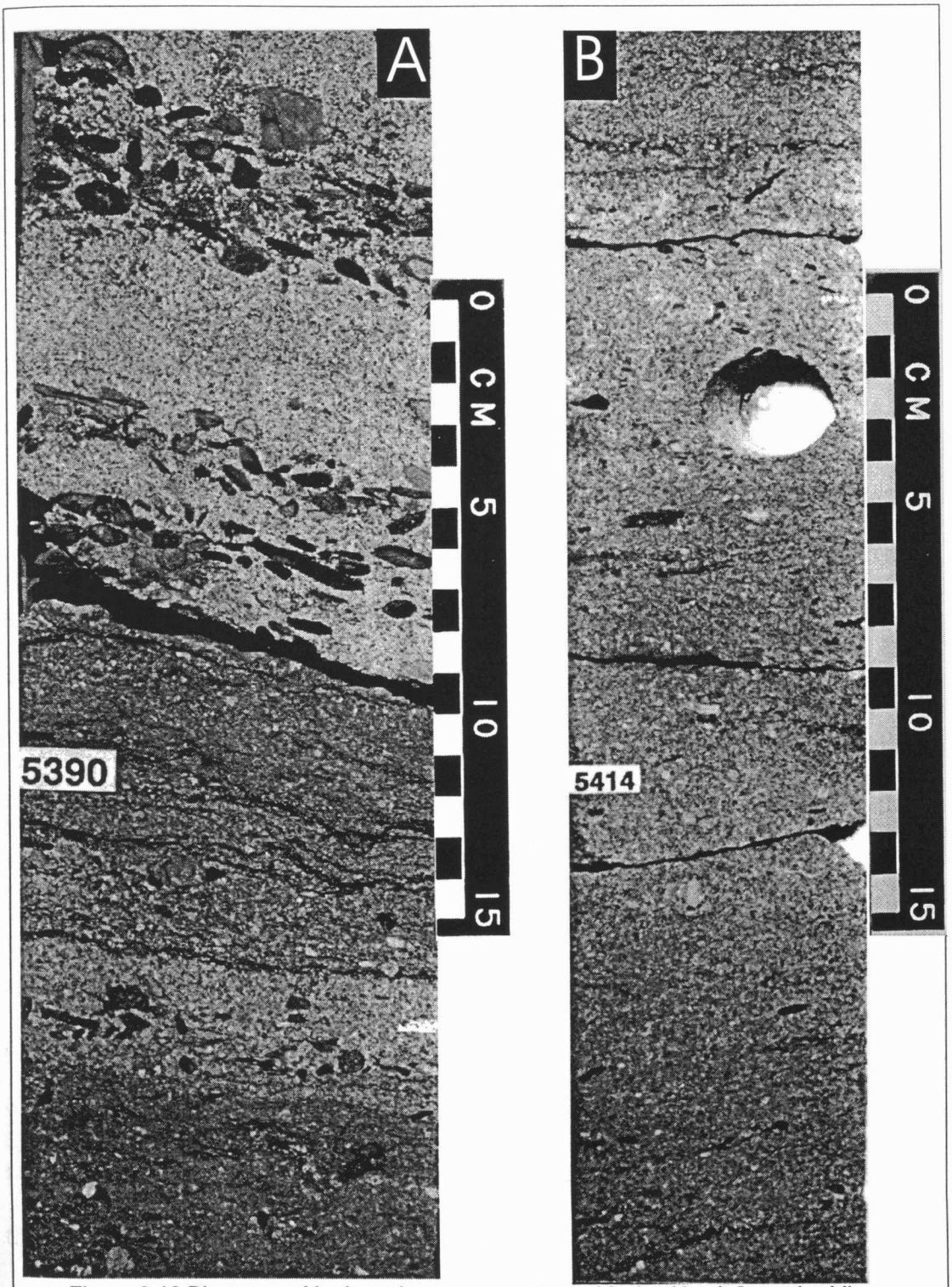

Figure 2.12 Photo a and b show the coarser nature of facies H. a) Cross bedding foresets are floored with pebbles.

energy currents. On the basis of the stratigraphic position and sedimentary structures of facies H, I conclude it was deposited in a wave-dominated environment such as a upper shoreface or proximal tidal channel complex.

Facies I

Facies I (5388–5386.8 ft) is a light-gray, bioclastic, glauconitic, massive, moderately to well-sorted, calcite-cemented, medium-grained quartz sandstone. The base of facies I shows an erosive surface floored with elongated lithoclast pebbles (Figure 2.13a). Facies I consists of locally present scattered bioclasts and lithoclasts (<1 to 1 cm in length). A series of normal graded intervals and stylolitic structures are also present. Bivalves, corals, and echinoderms fragments are the main bioclastic constituents of facies I. Bioclasts and lithoclasts decrease in abundance upward, with a concomitant increase in silt and shale matrix. The upper portion of facies I consists of discontinuous mud laminae and poorly developed ripple marks associated with stylolitic structures (Figure 2.13b). Facies I has an erosional contact with the underlying facies E and the overlying facies J (figures 2.13a, b).

The presence of bivalves, corals, and echinoderm fragments suggests a marine setting. The lower part of facies I suggests erosive events. The well-sorted nature of the sandstone, the clast sizes, the low mud content, the mud drapes and bioturbation indicate a high-energy, wave-dominated condition, resulting from continuous reworking. Gradual upward increases of mud content and shale laminae suggest that the depositional rate and current energy decreased upward. I interpret facies I as

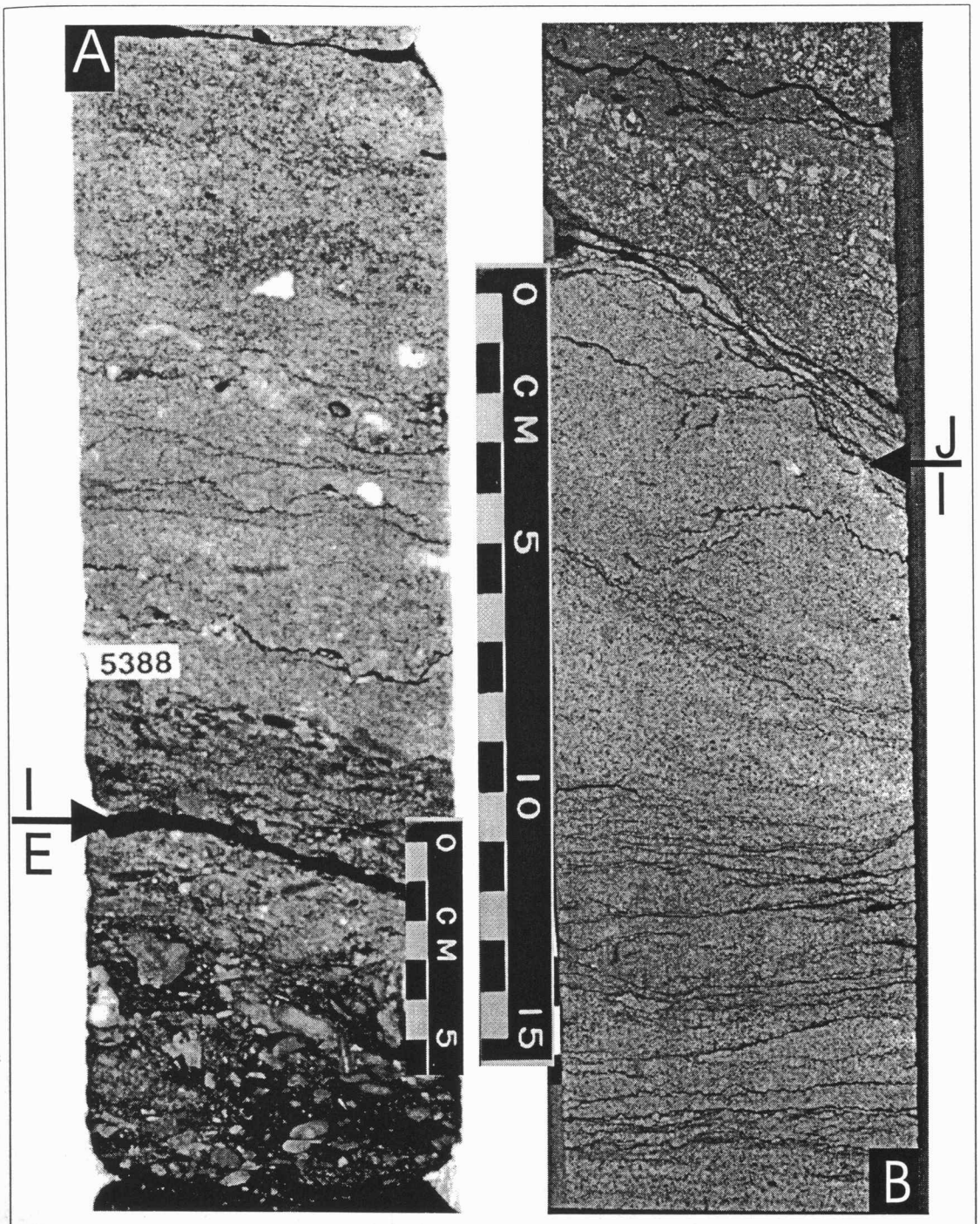

Figure 2.13 a) photo shows the pebbly erosive surface that marks the contact between facies I and E (arrow). Note: the massive nature of the lower part of facies I and the abundance of coral fragments. (white dots); b) Ripple marks, and laminae associated with stylolitic structures. Note: the erosional contact separating facies I from J and the inclined geometry of the beds (arrow).

having been deposited in a proximal high-energy, wave-dominated marine setting, such as an upper shoreface environment.

Facies J

Facies J (5486.8–5475 ft) is a very dark gray, bioclastic, glauconitic, locally pyritic, heavily calcite-cemented, well-sorted, low-angle cross-bedded, very coarse-grained quartz sandstone (Figure 2.14a). The base of facies J consists of a 3-cm lag deposit composed of echinoderm fragments and other undifferentiated bioclasts. This lag deposit grades normally into a well-sorted, coarse-grained sandstone. Low-angle planar cross-bedding, subhorizontal bedding and heavily calcite-cemented intervals are present throughout the facies. Locally present are shale laminae associated with stylolitic structures that are more abundant upward in the facies (figures 2.14a, c). A few scattered mud clasts and bioclasts are also present. Evidence of sparse bioturbation is present in the finer intervals and near the top of facies J. Bivalves and echinoderms, in association with *Planolites* and *Ophiomorpha irregulaire*, are the main biotic components (Figure 2.14b). Facies J has an erosional contact with the underlying facies I (Figure 2.13b).

The base of facies J indicates the presence of a scour-and-fill process. Extensive calcite cement and marine bioclasts indicate a marine setting. The well-sorted nature of the facies, as well as the low-angle cross bedding and subhorizontal bedding, taken together with the low mud content and the absence of mud drapes, indicate a high-energy, wave-dominated environment. Large-scale cross-bedding suggests the migration of underwater dunes. A gradational transition upward into

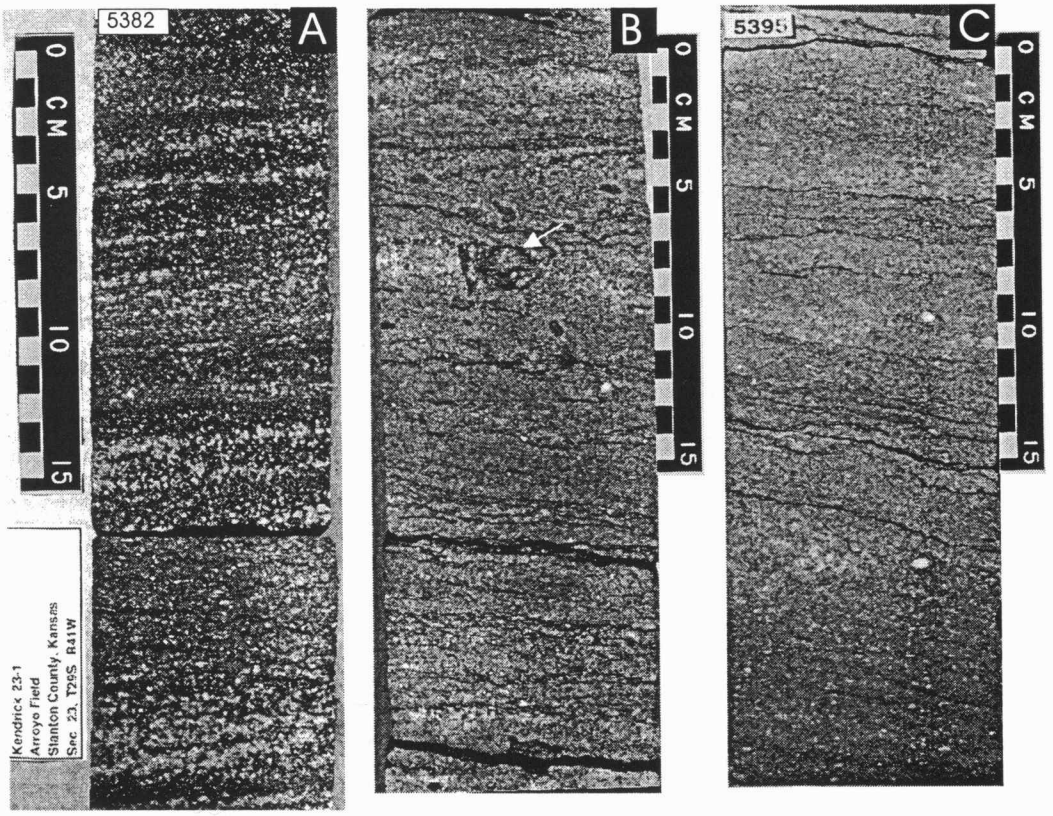

Figure 2.14 A) Low angle cross bedding and heavily cemented intervals (facies J), B) Slightly bioturbated fine-grained sandstone with *Ophiomorpha irregulaire* (arrow) (facies J), C) Shale lamina associated with stylolitic structures (facies J) and low angle cros bedding. Note white dotes are coral fragments.

shale laminae and an increase in mud content indicate shoaling and decrease of deposition rate and current energy. The general fining-upward trend from medium-grained sandstone (facies I) to very coarse-grained, cross-bedded sandstone (facies J) suggests a shoreface. I interpret facies J to have been deposited in a high-energy, wave-dominated, marine setting, such as an upper shoreface.

Fritz 16-1 core

The J. M. Huber Fritz 16-1 core, from Stanton County, Kansas, is composed of 50 ft (5449 ft–5399 ft) of fine-grained siliciclastic lower Morrowan successions (Table 2.3).

Core No.	Top (ft)	Bottom (ft)	Recovered (ft)	Sandstone	Shale
1	5399	5431	32	mixed	mixed
2	5431	5452	11	0	mixed

Table 2.3—Cored intervals from J. M. Huber Fritz 16-1, section 23, T29S, R41W, Stanton County, Kansas.

The cored interval was subdivided based on grain size, and sedimentary and biological structures into three lithofacies, facies K, L and M (Table 2.4 and Figure 2.15). The lowermost part (5449–5430 ft) consists of reddish siltstone with textures and structures that indicate a pedogenic process (facies K). The middle part (5429–5425 ft) is composed of parallel-laminated, calcareous mudstone (facies L). The upper part (5425–5399 ft) consists of interbedded greenish, very fine-grained sandstone and of siltstone showing soft-sediment deformation (facies M).

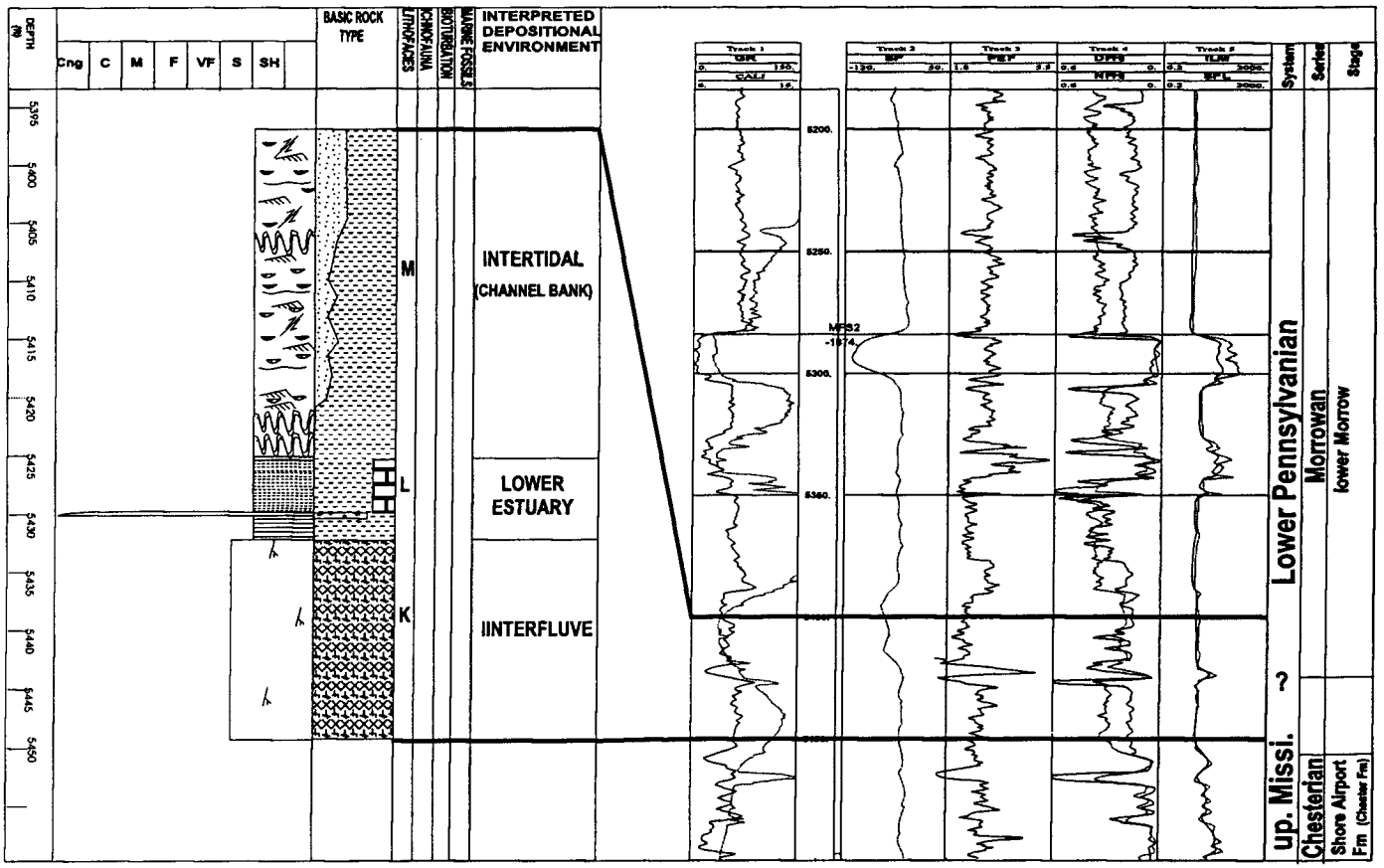

Figure 2.15 Core description and wireline log of the J. M. Huber Fritz 16-1(sec. 23, T 29s, R41 W, Stanton County, Kansas)

Facies K

Facies K (5449–5430 ft) is red-brown to pale green-gray siltstone. Coarse- to fine-grained prismatic peds, slickensides and cutans are the main features of facies K (figures 2.16a, b). Facies K shows a gradual transition from a fragile, blocky siltstone to a green-gray, laminated, fissile mudstone (5431–5429 ft). Facies K has sharp erosional contact with facies L (Figure 2.17a).

Prismatic peds, slickensides and cutans are common features of paleosol. Slickensides and stress cutans are indicative of the periodic shrinking and swelling of clays during cyclic wet–dry periods. I interpret facies K as a paleosol formed in the interfluvial area along the margin of the incised valley during the late Mississippian.

Facies L

Facies L (5429–5425 ft) is a green-gray, very hard, argillaceous, silty mudstone. The base of facies L consists of lag deposits 9 cm thick that are composed of shell fragments (Figure 2.17a). Parallel lamination, discontinuous faint shale laminae, ripple marks, and shale stringers are present. Locally, thin laminae of very fine-grained siltstone are interbedded within facies L. The upper part of facies L shows a gradual transition from a very fine-grained siltstone to a medium- to coarse-grained siltstone. Facies L has an erosional contact with underlying facies K and a gradual contact with overlying facies M (Figure 2.17b).

The absence of bioturbation and soft-sediment deformation suggests a stressful marine to brackish-water condition. The lag deposit at the base of facies L

Figure 2.16 Facies K a) photo shows the paleosol interval; b) Close-up photo shows the paleosol interval .

suggests a scour-and-fill process. I interpret this lag deposit as representing a marine transgressive surface. The presence of shale laminations, shale stringers, and ripple marks suggest a relatively quiet water depositional condition. I interpret facies L to have been deposited in a low-energy setting, such as a lower estuary.

Facies M

Facies M is represented by mudstone and by a light-gray to black, deformed, interbedded siltstone. Interbedded silt and mud laminae; ripple cross laminations; and wavy, lenticular, and flaser bedding are present. Soft-sediment deformation structures, such as load-bedding, convolute lamination, ball and pillow, load casts and slumping features are observed throughout the facies. Facies M has gradual contact with the underlying facies L (Figure 2.17b).

The interbedded mudstone and siltstone suggest periodic fluctuations in sediment supply and current energy. The heterolithic nature of facies M, with its wavy, lenticular and flaser bedding is typical of a tide-influenced setting. Soft-sediment deformation suggests that the sediment was deposited rapidly on an inclined surface. I interpret facies M as having accumulated on a tida- channel bank.

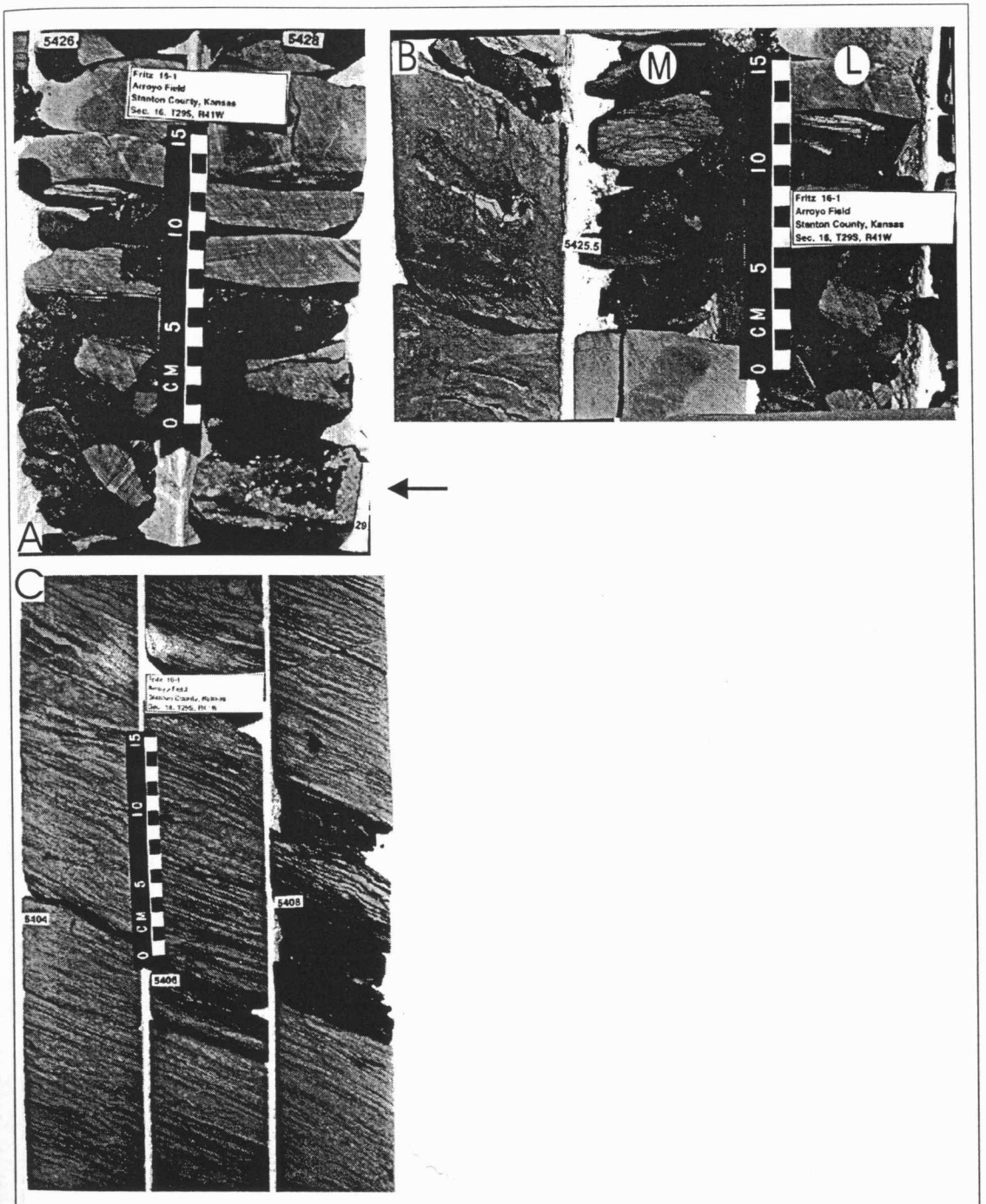

Figure 2.17 Facies L. a) transgressive surface (arrow); b) transition from facies L to M. Note: the soft-sediment deformation within facies M; c) heterolithic nature of facies M. Note: the soft-sediment deformation features.

3.0 THE ELECTROFACIES MODEL

The lithological data and wireline-log responses were integrated to construct an electrofacies model. This model was built by utilizing wells that had cores and lithological descriptions found in their geological reports. Five electrofacies were established in the lower Morrow successions at Arroyo field (Table 3.1). Electrofacies Ae and Be were observed in Kendrick 23-1 core, whereas electrofacies Ee, the paleosol, was observed in the Fritz 16-1 core. Electrofacies Ce and De are inferred based on geological reports from Spikes 1-29, Cockerham 1-33 and Grellner 1-18 wells.

Lithofacies	GR (API)	SP (mV)	PEF (E/B)	Nphi and Dphi (%)	Rhob (g/cc)	Lithology
Ae	Clean	Negative cylindrical shape	Low (~1.8)	D> N	2.8	Clean, quartz arenite sandstone with low mud content
Be	Clean but segmented	Negative fluctuation	High, increasing - upward	D ~ N	2.28-2.55	bioclast–rich sandstone, mud, and conglomerate
Ce	High	Non permeable	High, increasing-upward	N > D	2.49-2.57	Argillaceous mudstone
De	Clean	Negative fluctuation	High, fluctuating	D ~ N	2.47-2.65	Tight, bioclast- rich sandstone
Ee	Mod. high	Non-permeable	High fluctuating	N>D		Paleosol

Table 3.1 Summary of characteristics of electrofacies

Reference	Wireline-log type
Hassan et al., (1976)	Spectral gamma ray log (NSGN) and photoelectric index (PEF)
Serra et al., (1980) and (1985)	Spectral gamma ray(SGN) log and high resolution dipmeter tools (HDT and SHDT)
Doveton (1994) and Watney et al., (1990)	Composite neutron and density, photoelectric index (PEF) and Spectral gamma ray log (SGN)
Carr and Lundgren (1994)	Spectral gamma ray log (NSGN)
Geoffrey et al., (1996)	Composite neutron and density, and Spectral gamma ray log (NSGN)

Table 3.2 Summary of the relevant works concerning the interpretation of depositional environments from wireline-logs.

Well logging and wireline-logs

Well logging is the in situ measurement of the petrophysical properties of subsurface lithological units (Schlumberger, 1989). In this study, several kinds of wireline-logs were available to construct an electrofacies model. These wireline-logs include the gamma ray, spontaneous potential, sonic, photoelectric index, density, and neutron logs. Each wireline-log is described in more detail below.

Gamma ray log

The gamma ray curve records the natural radioactivity of the formation. The amount of radioactivity depends on the concentration of potassium, thorium, and uranium in the sample. Two kinds of gamma ray logs exist: the Standard gamma ray log (SGR) and the natural gamma ray spectrometry (NGRS). SGR measures total radioactivity and is commonly used to differentiate between shaley and nonshaley beds. NGRS measures total radioactivity as well as the concentrations of potassium, thorium, and uranium producing the radioactivity (Schlumberger, 1989). NGRS logs have been used to differentiate between different types of clay minerals, to detect

exposure surfaces, and to determine various depositional environments. For example, the amount of potassium concentration in an arid region is higher than in a humid one (Serra et. al., 1980). Hassan et al., (1976) stated that uranium demonstrates a strong correlation with organic carbon only, and the three radioactive elements show negative associations with calcium carbonate. Carr and Lundgren (1994), pointed out that subaerial exposure commonly includes high uranium but low potassium concentrations, whereas flooding surfaces show high concentrations of both uranium and potassium.

Spontaneous potential curve log

The spontaneous potential curve (SP) log records the electrical potential produced by the interaction of formation water, conductive drilling fluid, and certain ion-selective rocks (Schlumberger, 1989). The magnitude of curve deflection is controlled by the difference in salinity between the formation water and the mud filtrate. If the formation salinity is greater than the mud filtrate, the SP is expected to deflect to the left, called negative potential. When the salinity of the formation water is lower than that of the mud filtrate, the SP will deflect to the right, called positive potential (Schlumberger, 1989). This implies that the SP response to the permeability of ion flow will normally correlate with hydraulic permeability. Generally, the SP log is used to distinguish between permeable and non-permeable units.

Sonic log

Sonic logs record the length of the time that is required for a sound wave to travel a given distance in a formation (Schlumberger, 1989). This measured time is

called interval transit time ($\Delta\tau$). The rock matrix and the porosity control the sonic log reading (Schlumberger, 1989). Therefore, sonic logs are commonly used as porosity logs.

Density log

A density log records the number of Compton-scattering collisions made by gamma rays emitted from a radioactive source (Schlumberger, 1989). The numbers of these Compton-scattering collisions are directly related to the number of electrons in the rock. The electron density of a given formation depends on the density of the rock matrix, its porosity, and the density of the pore fluids. Density logs are primarily used as porosity logs and can be used to evaluate complex lithologies when corrected for specific lithology matrix (Doveton, 1994).

Neutron log

The neutron log reflects the abundance of hydrogen nuclei in the formation. The neutron reading is lower with a higher content of hydrogen. This log is primarily used to evaluate the porosity of sandstone and limestone units and to detect gas zones when combined with other logs, such as density and resistivity.

Photoelectric log

The Photoelectric index (PEF) measures the absorption of low-energy gamma rays by a formation. The reported log responses ranges from 0 to 10 barns per electron. The recorded PEF value is a direct function of the formation element atomic numbers. Pore fluids only slightly affect the photoelectric index, which makes it a great discriminator primarily between calcite (limestone) and non-calcareous

(shale and sand) mineralogies. The PEF log combined with the neutron and density logs is commonly used to differentiate lithologies (Doveton, 1994).

Techniques

Selected lower Morrow wells with cored intervals and geologist reports were first subdivided into distinct intervals based on their wireline signatures as determined from available wireline-logs. The composite neutron-density, photoelectric index, and spontaneous potential logs were emphasized. Next, the entire lower Morrow interval was plotted using the RHOmaa and Umaa crossplot technique and Nphi-Dphi vs. photoelectric index crossplots (Schlumberger, 1989; Doveton, 1994).

RHOmaa-Umaa crossplot

The RHOmaa-Umaa crossplot technique was developed by Schlumberger Company as a formation mineral evaluation tool. The RHOma-Umaa crossplot uses a combination of the PEF, neutron porosity (Nphi), density porosity (Dphi), or bulk density (Rhob) curves. This study adapted the calcite-quartz-dolomite triangle to include shale instead of dolomite as an endpoint. With this shale modification, the gas effect is easily observed in sedimentary successions. By plotting points on this diagram, in conjunction with other data, lithologies can be inferred including type of clay (kaolinite, illite, and chlorite) (figures 3.1, 3.2).

Neutron-density porosity (Nphi-Dphi) vs. photoelectric index (PEF) crossplot

Doveton, (1994) stated that patterns of the density and neutron curves, when used together and calibrated to the appropriate lithological index, can differentiate

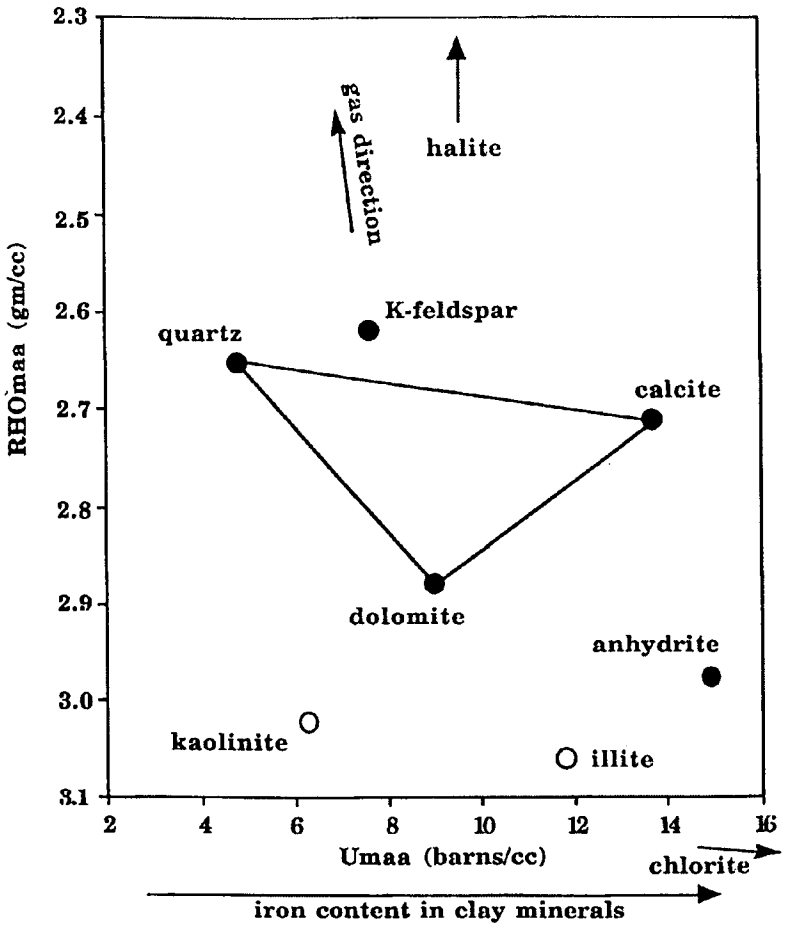

Figure 3.1 RHOmaa-Umaa Crossplot (modified from Schlumberger, 1989).

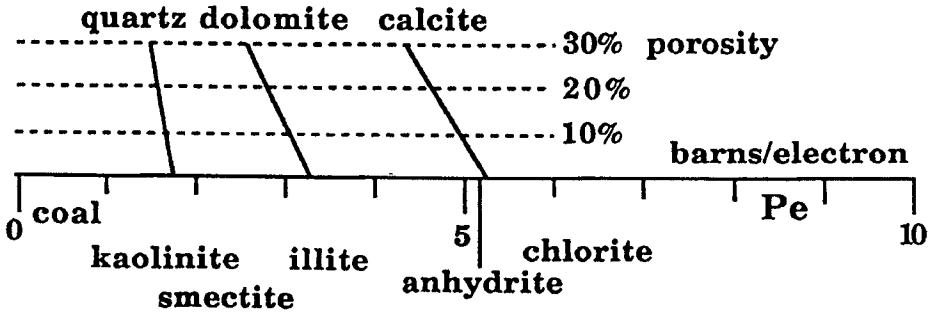

Figure 3.2 PEF lithology scale (modified from Doveton, 1994).

lithologies such as sandstone and limestone (Figure 3.3). The ideas of Doveton were modified by constructing a crossplot of the difference of Nphi and Dphi versus PEF. The crossplot is composed of two axes: The y-axis is represented by the PEF values (0-5) which cover the quartz, dolomite, calcite, and clay mineral spectrum (kaolinite, smectite, illite; Figure 3.2). The x-axis is the difference in values between the neutron and the density porosity curves scaled to limestone porosity. The x-axis has both a positive and negative side with a y-axis intercept of zero (Figure 3.4).

The x-axis scale shows variations in lithologies. A negative sum is obtained when the density porosity is greater than the neutron porosity. Negative values fall to the left side of the PEF curve and are indicative of quartz-rich sandstones and kaolinite or smectite shales or clay. Bioclast-rich and carbonate strata generally produce overlapping neutron and density curves that cancel out and produce a sum near zero. These values will fall near zero on the x-axis and between the values of 2.5-3.5 on the y-axis. When the neutron porosity is greater than the density porosity, a positive sum is obtained, which may be indicative of marine shales (illite and chlorite). These values fall on the right side of the x-axis and between the values of 3 to 5 on the y-axis.

The cluster geometries of shales and clean sand units are controlled by the gas effect (negative side of the x-axis) and the amount of hydrogen (organic content on the positive side of the y-axis). The mineralogy variations will produce cluster plots that may have point clouds surrounding them or produce a tail of points that trend off of the main cluster. When this technique is applied to an entire sequence,

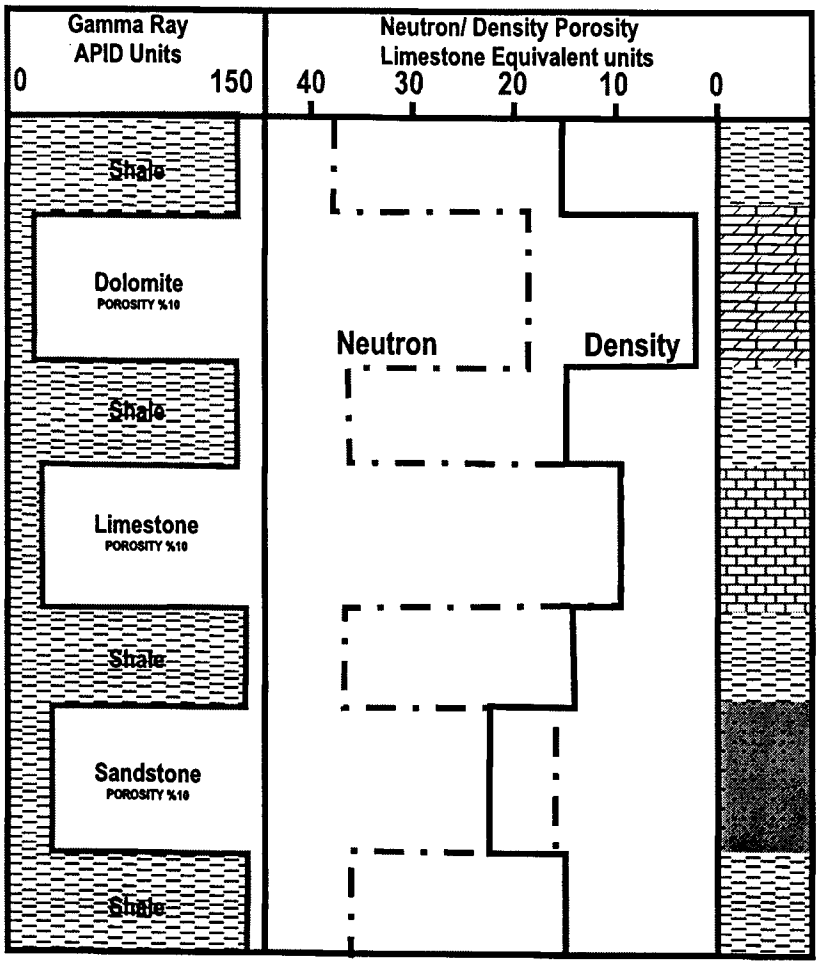

Figure 3.3 Hypothetical neutron-density overlay pattern for simple lithologies (modified from Doveton 1986).

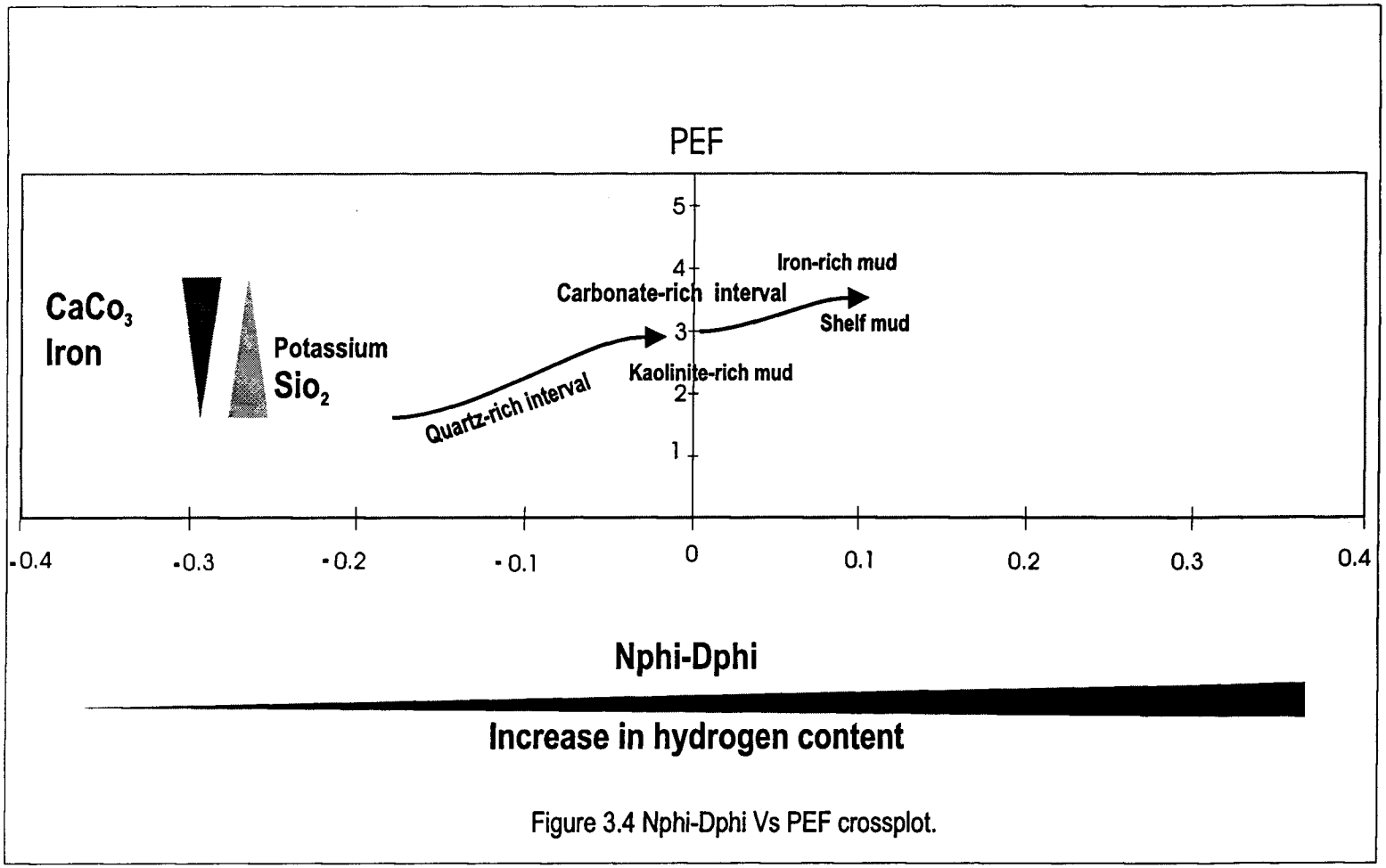

Figure 3.4 Nphi-Dphi Vs PEF crossplot.

depositional environments and lithologies can be distinguished. This crossplot technique has not been utilized in any published papers prior to this case study.

Applications of crossplots

The crossplots primarily served to detect similar clusters that could be correlated between the wells. Similar cluster plots are interpreted to represent similar lithologies that reflect, at least in part, related depositional settings. By correlating crossplot clusters with wireline signatures, core, and geologist reports, an electrofacies model was constructed for the lower Morrow.

Wireline-logs can be used to subdivide facies in the study area in which other lithological data were absent. Each electrofacies has distinct curve signatures and specific lithological successions. The resulting electrofacies model was calibrated with core data to construct lithostratigraphic cross-sections.

Limitations to logging data must always be considered in their application. The vertical resolution of conventional logging tools is of the order of two feet, so thinner beds will not be discerned unless they have radical properties that are not entirely masked by the averaging process. Also, some units that can be discriminated visually in core will be indistinguishable on logs if they have the similar wireline-logging properties.

Due to variations in mineralogy, lateral shifts in depositional environments, wireline tool calibrations and borehole conditions, mineral cross-plots may show variation in data point cluster locations.

Electrofacies

In the cored intervals of the Kendrick 23-1 and Fritz 16-1, the lower Morrow interval was subdivided into four zones based on log signatures, with each zone representing a distinct electrofacies (figures 3.5, 3.11). Electrofacies Ae corresponds to core lithofacies A and B; electrofacies Be corresponds to core lithofacies C, D, E, F, G, I and J, and electrofacies Ee represents lithofacies K, observed in the Fritz 16-1 core (figures 2.2, 2.15). From Spikes 1-29, electrofacies Ce correlates to the shale interval (5312 ft-5410 ft), and electrofacies De represents the glauconitic, calcite-cemented sandstone of the informally called middle Morrow limestone (figures 3.5,3.8, 3.9, 3.10, 3.11).

These different electrofacies were plotted using the RHOmaa (apparent matrix grain density (g/cc)) and Umaa (apparent matrix volumetric cross section (Barns/cc) and density–neuron porosity (Nphi-Dphi) vs. photoelectric index crossplots, as previously described. Each electrofacies shows a distinctive cluster of points.

Electrofacies Ae

Electrofacies Ae as defined in the Kendrick 23-1 (5431-5465 feet) is characterized by relatively cylindrical trends, low gamma ray levels (~20 API), low photoelectric indexes (1.8 barns/electron), high permeability as indicated by a continuous negative cylindrical SP trends (~-80 mV), constant Rhob (2.48) and a relatively high porosity (Dphi~19% and Nphi~9%). The box-like shape of the gamma ray has been described as cylindrical (Emery and Myers, 1996). The upper limit of electrofacies Ae is at 5430 feet, marked by a gradual change in all log curve

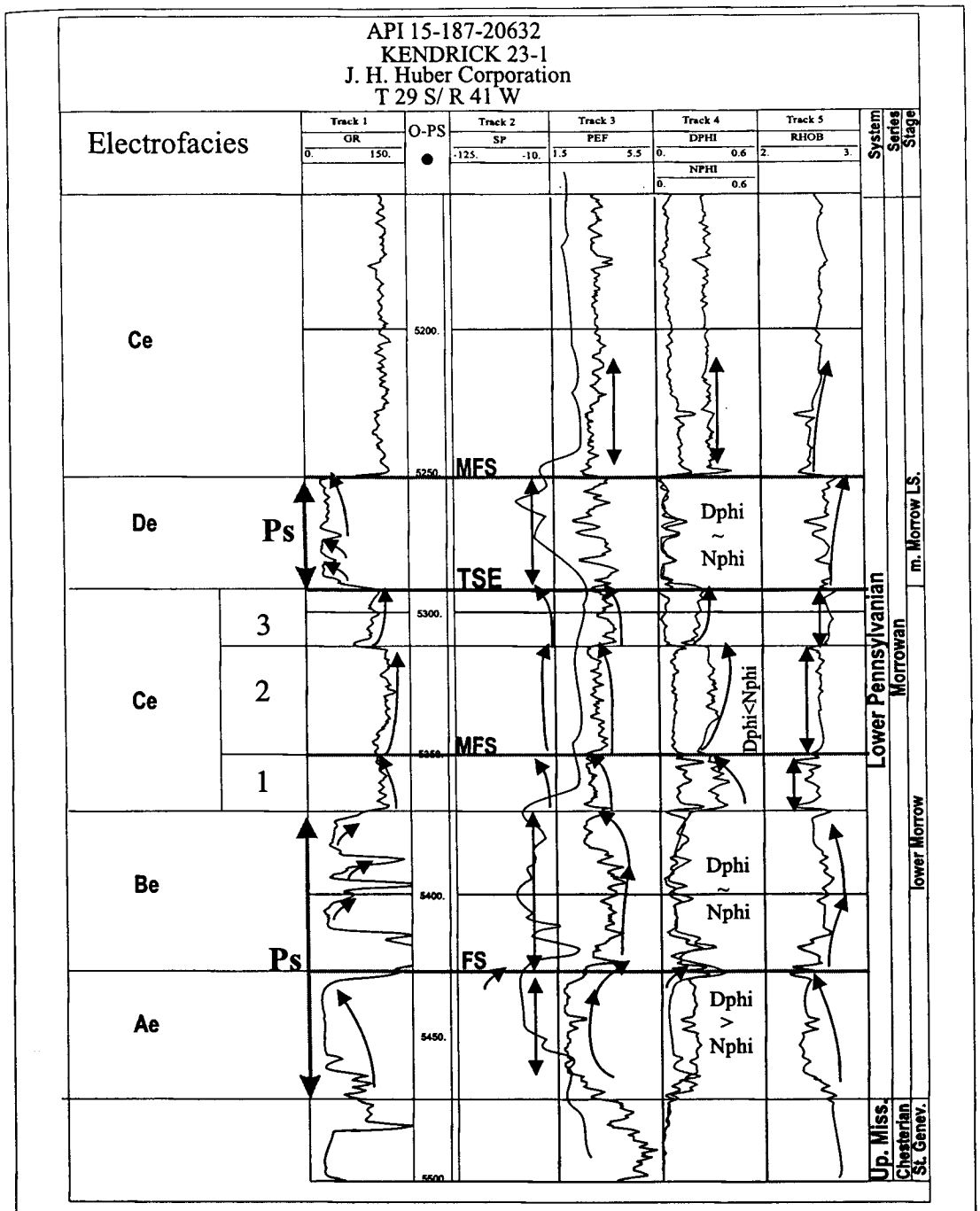

Figure 3.5 Kendrick 23-1 wireline log suite and stratigraphic interprtation. Black arrows show wireline log trends. Note: the stacked parasequence. Ps, parasequence set; MFS, maximum flooding surface; TSE, transgressive surface of erosion; FS, flooding surface.

characters (figures 2.2, 3.5).

The RHOmaa and Umaa crossplot shows that electrofacies Ae has a cluster that is located up and away from the quartz region and has a tail that is parallel to the quartz-shale axis (Figure 3.6). On the Nphi and Dphi vs. photoelectric index crossplot, Electrofacies Ae has a distinct elongated cluster that lies between the values of –0.2 and zero on the Nphi-Dphi axis and trends towards the PEF axis value of 2 (Figure 3.7). Both clusters and their tails indicate a quartz-rich lithology that contains a relatively low mud content (a mixture of kaolinite and smectite). The shifting in the RHOmaa-Umaa cluster above the quartz region may be the result of a gas effect.

Electrofacies Ae reflects the lithological and physical properties that correspond to Lithofacies A and B as defined in the Kendrick 23-1(Figure 2.2, Table 3.3). The low gamma ray level indicates relatively clean sandstones (low clay content). The low photoelectric index reflects the quartz-rich sandstone facies (quartz arenite) with little to no calcium carbonate content (e.g. cement or bioclasts). Based on the depositional environment as defined in core and on observed stratigraphic geometry, I would interpret Electrofacies Ae as quartz-rich brackish-water sandstone that was largely restricted within the valley.

The wireline signatures will differ slightly from well to well because of lateral variations and the shifting of lithologies and mineral compositions. Variations in glauconite and pyrite concentrations, for example, could have a significant effect on log signatures (Table 3.4).

ELECTROFACIES	LITHOFACIES ASSEMBLEGES		GR (API)	SP (mN)	PEF (E/B)	Dphi (%)	Nphi (%)	Rhob (g/C3)	Drho (g/C3)
Ae	A and B		20	-80	1.8	19	9	2.48	0.015
Be	C		145	0	2.6-3.2	28	39	2.25	-0.09
	D and E		125	-48	4.0-3.5	11	8	2.54	0.02
	F, G, H, I and K		75	-68	~3.02	~8	10	2.45	0.03
Ce	Black and gray shale (Kendrick 1-23)	upper	9	0	3.7	24	24	2.65	-0.09
		Middle	118	0	3.3	9	32	2.55	-0.08
		Lower	108	0	3.14	12	36	2.48	-0.09
De	Middle Morrow Sandstone		28	-50	2.9	4	3	2.6	-0.028
Ee	L		85	0	3.7	18	30	2.42	.08

3.3 Summary of petrophysical responses of the key surfaces observed in the Arnold 1-1 wireline logs.

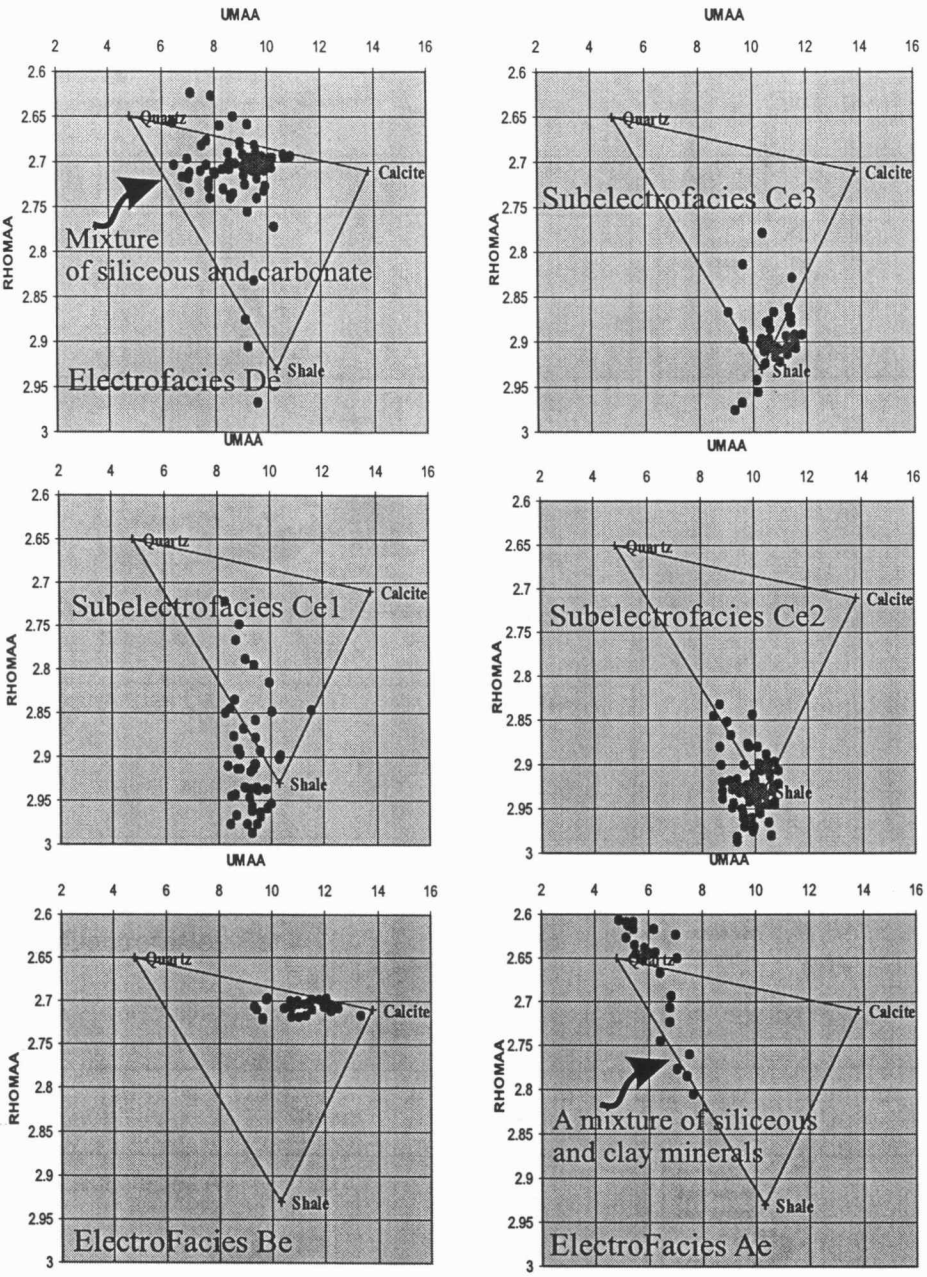

Figure 3.6 RHOmaa and Umaa cross plots show the electrofacies found within the Kendrick 23-1: Note: the variation in carbonate and siliceous content between electrofacies Ae, Be and De, and the clay minerals between subelectrofaciesCe2, Ce2 and Ce3.

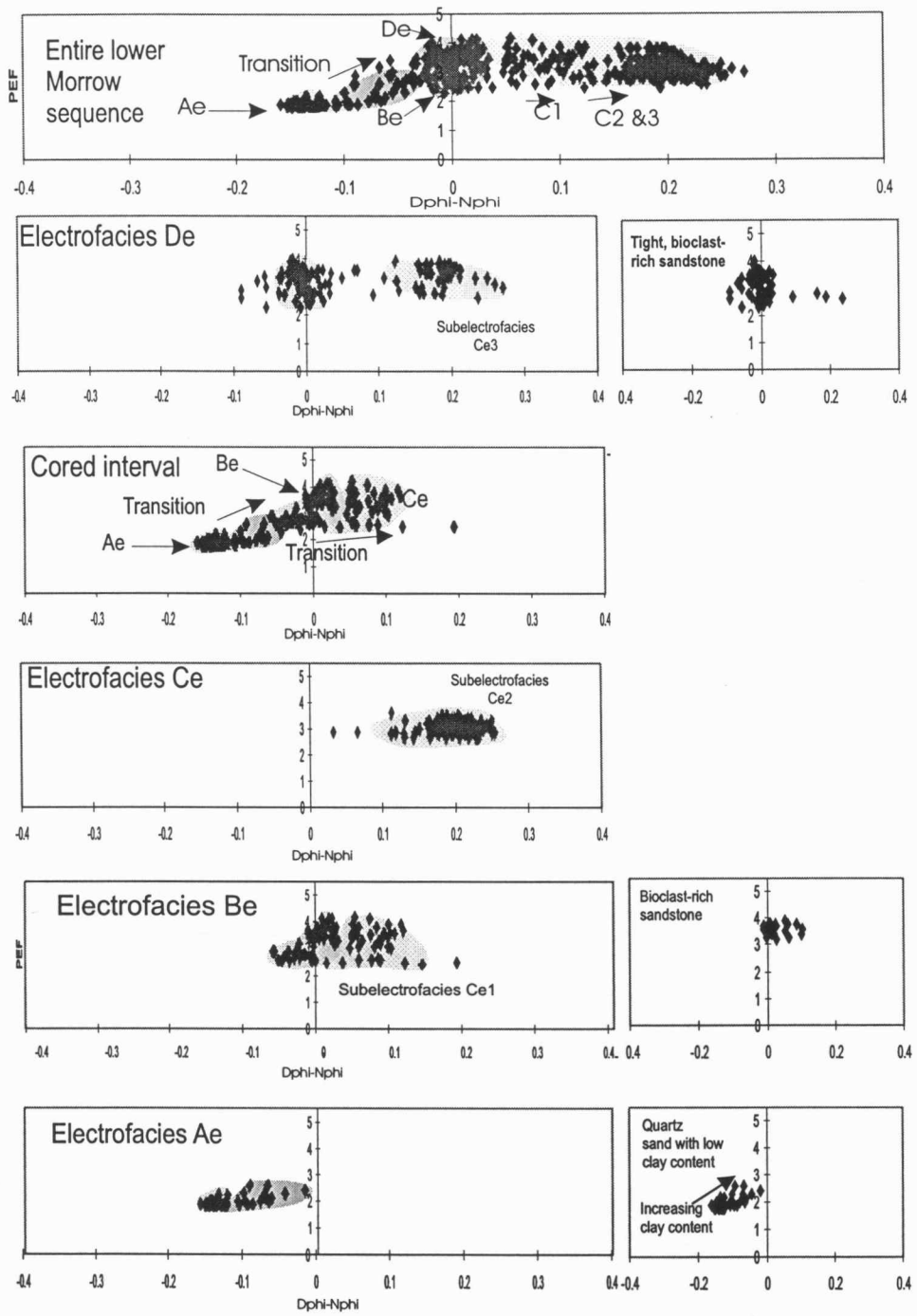

Figure 3.7 Nphi-Dphi vs PEF cross-plots of the electrofacies Ae, Be, Ce, and De, that are found within Kendrick 23-1. Black arrows show the transition trends between the electrofacies as a result of variations in mineral content.

Mineral	ρ log g/cc	ΦSNP P.U.	ΦCNL P.U.	τc μS/ft	PEF B/E
Glauconite	~5.54	~23	~38	-	6.3
Pyrite	4.99	-2	-3	62.1	16.94

Table 3.4 Different logging tool responses to glauconite and pyrite (modified from Schlumberger, 1989). ρ log is the Density Log, ΦSNP is the Sidewall Neutron Porosity, ΦCNL is the Compensated Neutron Log, τc is interval transit time.

Electrofacies Be

Electrofacies Be represents the interval of 5370-5430 feet within the Kendrick 23-1 core (Figure 2.2). The PEF, Rhob and SP values, along with the small magnitude of separation between the Nphi and Dphi values, distinguished electrofacies Be from electrofacies Ae. The wireline-log signatures of electrofacies Be show cylindrical and bell GR trends (45-145 API), high PEF (2.6-4 barns/electron), fluctuating SP (0-68 mV), high Rhob (2.5-2.54), and moderately high porosity (Dphi 8-28% and Nphi 10-35%; Figure 3.5; Table3.3).

The RHOmaa and Umaa crossplot shows a recognizable cluster, near calcite on the quartz-calcite axis, surrounded by a scattered cloud of points (Figure 3.6). The Nphi and Dphi vs. photoelectric index crossplot also produced two elongated clusters that have two different PEF value (2.5 and 3.5 B/E) across the PEF axis. The lower cluster has negative Nphi and Dphi values whereas the upper cluster has positive Nphi and Dphi values (Figure 3.7). Both cluster locations and observed trends indicate that Electrofacies Be is primarily composed of carbonate minerals with

appreciable amounts of quartz and contains a relatively high mud content (smectite to illite).

Electrofacies Be reflects the lithological and physical properties that correspond to fine- and coarse-grained, marine-influenced facies that was defined in the Kendrick 23-1 (Table 3.3). The high photoelectric index, overlapping Nphi and Dphi curves, and moderately high Rhob reflects carbonate rich-sandstone. Fluctuating gamma ray (45-145API), SP (0-68 mV), and PEF (2.6-3.5 B/E) values indicate periodic high mud content (smectite–illite) within electrofacies Be.

Electrofacies Be wireline-log profiles of Nphi and Dphi do not contradict Doveton's hypothetical neutron-density overlay patterns (Doveton, 1986). Doveton argues that when properly calibrated on a limestone porosity scale (10%), the neutron and density curves will coincide. However, siliciclastic intervals that are calcite cemented or contain appreciable amounts of carbonate material such as bioclasts will show the same limestone Nphi-Dphi character (Figure 3.3).

Electrofacies Ce

Electrofacies Ce is the interval of 5370 ft–5290 feet that was not covered by the Kendrick 23-1 core (figures 2.3, 3.5). High gamma ray (99-108 API), PEF (3.13-3.7 B/E), Nphi (24-36 %), moderately high Rhob (2.48-2.65 g/cc) and low permeability (SP~ 0 mV.) are the main wireline signatures that characterize the argillaceous black fissile shale inferred from cutting descriptions in the geologist reports of Spikes 1-29, Cockerham 1-33 and Grellner 1-18 wells (figures 3.5, 3.8, 3.9, 3.10).

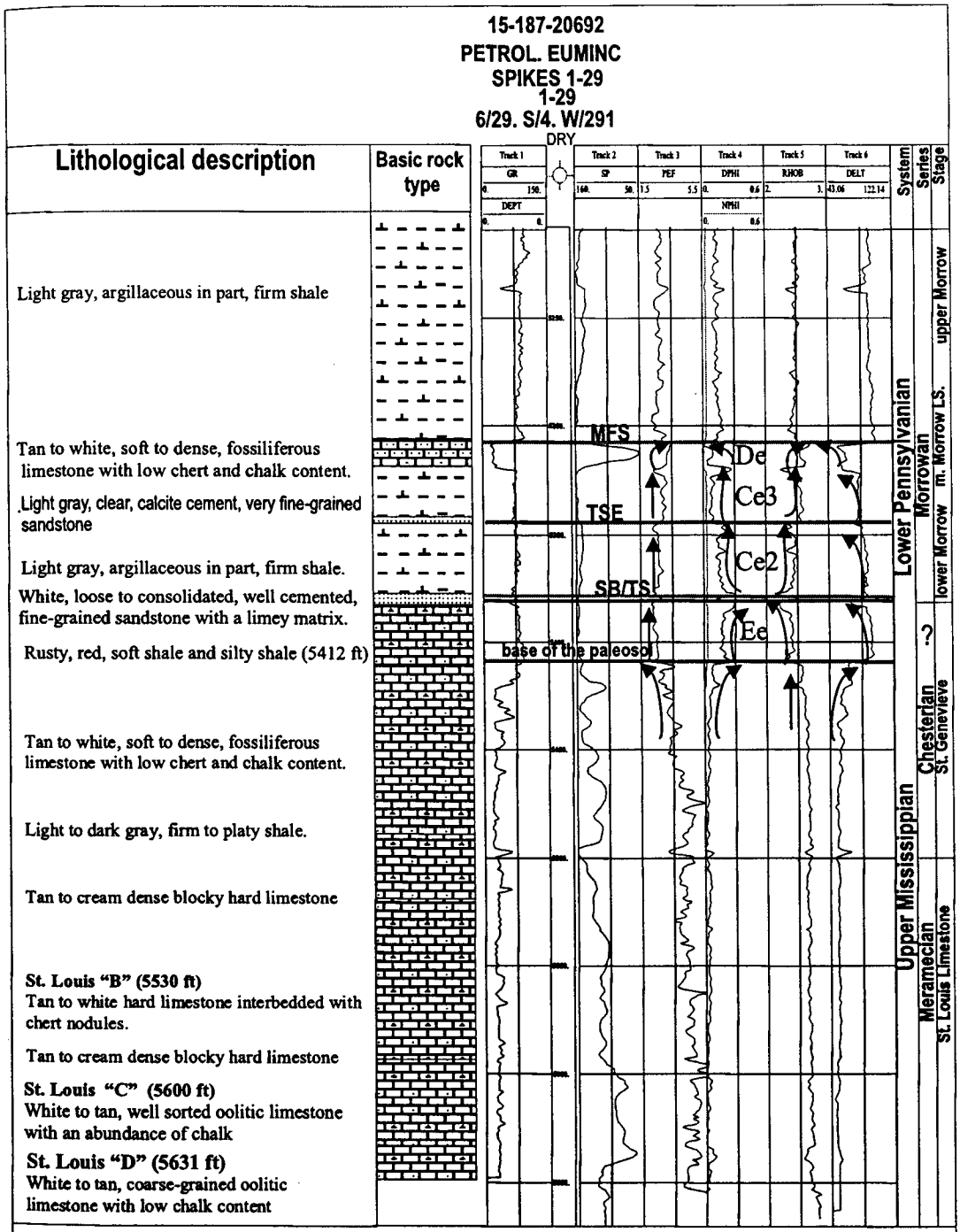

Figure 3.8 Stratigraphic interpretation for the Spike wireline log suite and geologist report from the Spike 1-29 well. Black arrows show wireline log trends. MFS, maximum flooding surface; TSE, transgressive surface of erosion; TS, transgressive surface; m.ML, middle Morrow limestone.

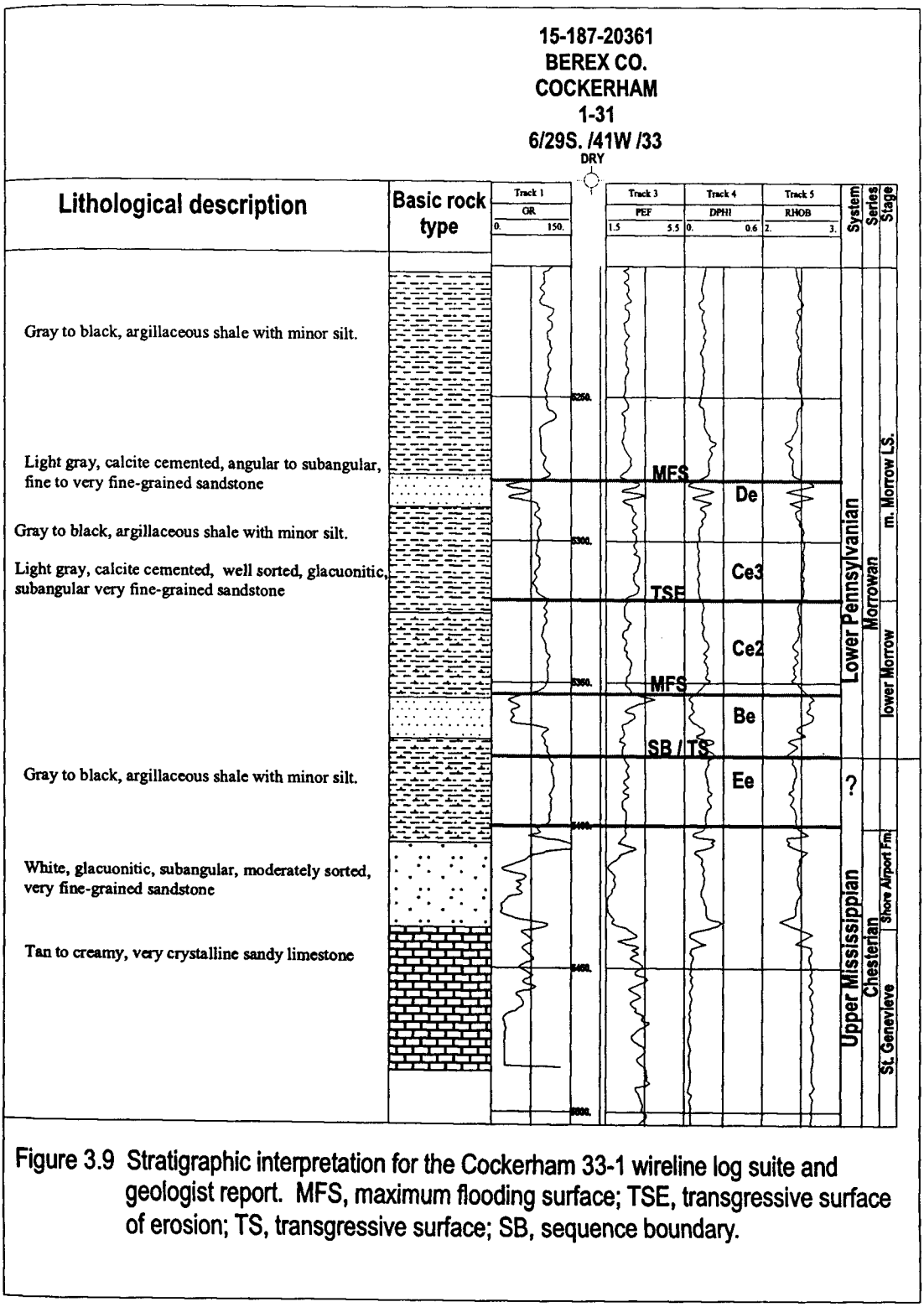

Figure 3.9 Stratigraphic interpretation for the Cockerham 33-1 wireline log suite and geologist report. MFS, maximum flooding surface; TSE, transgressive surface of erosion; TS, transgressive surface; SB, sequence boundary.

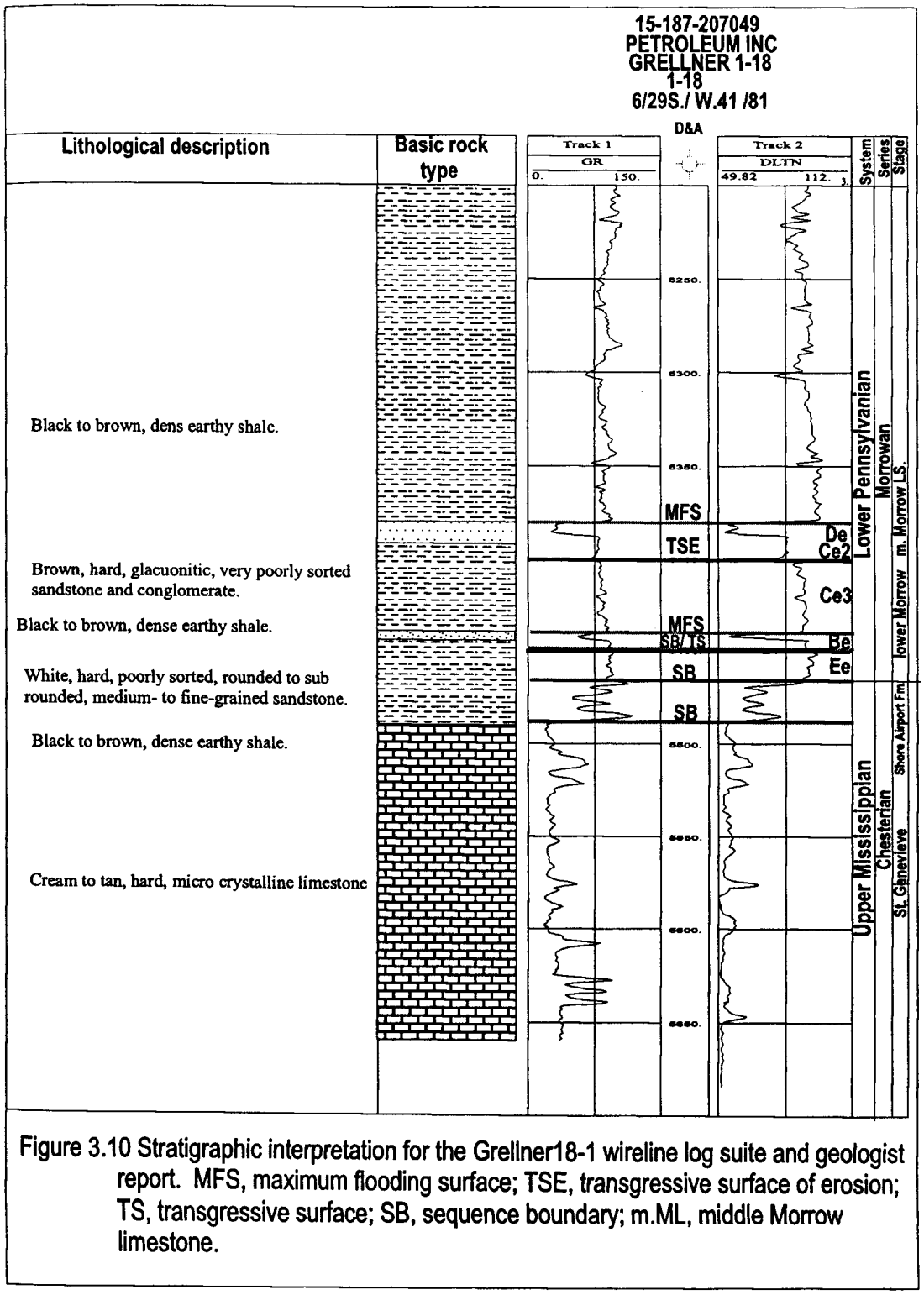

Figure 3.10 Stratigraphic interpretation for the Grellner18-1 wireline log suite and geologist report. MFS, maximum flooding surface; TSE, transgressive surface of erosion; TS, transgressive surface; SB, sequence boundary; m.ML, middle Morrow limestone.

Ideas for distinguishing among different types of shale using neutron–density curves (Doveton, 1994) were used to subdivide the shale intervals within the lower Morrow. Based on gamma ray, photoelectric index, density, neutron porosity, and bulk density curves, the lower Morrow in the Kendrick 23-1 was classified into three subelectrofacies, Ce1, Ce2 and Ce3. The subelectrofacies show cycles reflecting three distinct averages of wireline-log values (Figure 3.5 and Table 3.3).

The RHOmaa and Umaa crossplots combined with Schlumberger (1989) published charts and Doveton (1994) photoelectric factor scale indexes, portrays three different, recognizable clusters corresponding to these three shale intervals (Figure 3.6). On the RHOmaa-Umaa crossplot, subelectrofacies Ce1 is an elongated cluster deflected away to the left from the shale area towards the kaolinite region and has a tail along the bisection of the quartz-calcite axis. The cluster deflection suggests that subelectrofacies Ce1 is composed of mixed kaolinite and smectite minerals whereas the trend of the tail indicates a mixture of fine-grained silt and sand siliceous grains. The RHOmaa-Umaa plot of subelectrofacies Ce2 is located in the shale area with a slight deflection towards the kaolinite region while the subelectrofacies Ce3 cluster deviates toward the illite region. The scattered cloud associated with these clusters is interpreted as fine-grained siliceous and argillaceous material deposited within these shale intervals, as observed in the Spikes 1-29, Cockerham 1-33, and Grellner 1-18 geologist reports (figures 3.8, 3.9, 3.10).

The Nphi and Dphi vs. photoelectric index crossplot displays two distinct elongated clusters parallel to the positive axis of Nphi and Dphi. Subelectrofacies

Ce1 shows an elongated cluster cloud near the PEF axis. Subelectrofacies Ce2 and Ce3 have two, narrow, overlapping, dense, elongated clusters located to the right of the PEF curve on the positive side of the Nphi and Dphi axis (Figure 3.7). These shape and trend differences can be attributed to variations in fine-grained siliceous content that have been observed in RHOmaa-Umaa crossplots and the different amounts of hydrogen content (organic matter) that was inferred from the high Nphi-Dphi values.

Lithostratigraphic correlations (Appendix A; Figure A.1) show that subelectrofacies Ce have downlap relationships with the lower and the middle Morrow units (Figure 3.5 and Appendix A; Figure A.1). Proceeding upward, subelectrofacies Ce1 generally overlies electrofacies Be in the deeper part of the valley. Subelectrofacies Ce2 overlies a thin unit of fine-grained sandstone (Kearny sandstone C). In Appendix A; Figure A.1, electrofacies De is underlined by subelectrofacies Ce3 and overlain by subelectrofacies Ce1. In Fritz 16-1, only subelectrofacies Ce2 and Ce3 are found. The lithostratigraphic correlation (Appendix A; Figure A.1) shows that subelectrofacies Ce1 is commonly encountered within the deeper part of lower Morrow strata.

Electrofacies Ce may imply several stages of sea-level rise. The mineral compositions of subelectrofacies Ce2 and Ce3 suggest flooding events during relatively starved periods of the shelf (e.g. low siliceous material), whereas subelectrofacies Ce1 may indicate a major flooding event and a shutting down of the sediment sources.

Not all of these subelectrofacies are found in every well. When tracing these subelectrofacies, lateral shifting of the depositional environments and changes in paleogeographic highs were taken into account.

Electrofacies De

Electrofacies De represents the interval of 5262-5270 feet that was not part of the cored interval of the Kendrick 23-1 and Fritz 1-16 core. This electrofacies has a serrated, cylindrical GR trend (28 API), fluctuating SP (-50 mV), high PEF (2.9 barns/electron), high Rhob (2.6) and low porosity (Dphi~4 % and Nphi~3 %) 9 (figures 3.5, 3.11). The wireline-logs are responding to the bioclastic, calcite-cemented, glauconitic, pyritic, coarse- to medium-grained sandstone (informally called middle Morrow limestone) that was inferred from the geologist reports of the Spikes 1-29, Cockerham 1-33, and Grellner 1-18 wells (Table 3.3 and figures 3.8, 3.9, 3.10).

The RHOmaa and Umaa crossplots show a cluster of points located approximately at the middle of the quartz-calcite axis with a scattered cloud pointed towards the quartz-rich area (Figure 3.6). Cross-plots of Nphi-Dphi vs. photoelectric index show a recognizable cluster near the calcite-rich area that was similar to the electrofacies Be cluster plots (Figure 3.7). This cluster of points along with the scattered cloud suggests that electrofacies De has a lower mud and higher calcium carbonate content than electrofacies Be. The relatively low permeability and porosity of electrofacies De compared to electrofacies Be suggests that electrofacies De may be more heavily calcite-cemented and has secondary porosity such as voids and vugs

that cannot be detected by the sonic log but is shown in the neutron-density porosity logs (figures 3.8 and 3.10). Based on its stratigraphic position with respect to the other electrofacies, electrofacies De is interpreted to represent an open marine environment such as the upper shoreface.

Electrofacies Ee

The lower 12 feet of the Fritz 16-1 core interval represents electrofacies Ee that corresponds to the paleosol interval (facies L). A serrated, cylindrical moderately high gamma ray trend (~70 API), high photoelectric index (~3.4 B/E), high porosity (Dphi~15 % and Nphi~30%) and low permeability (0 mV) are the wireline-log responses that characterize electrofacies Ee (5427-5460ft) (Table 3.3 and figures 2.16, 3.11).

The RHOmaa and Umaa crossplot shows that electrofacies Ee displays an elongated cluster of points located in the shale region and parallel to the quartz–shale axis (Figure 3.12). The Nphi-Dphi vs. photoelectric index crossplot reveals that electrofacies Ee delineates a distinctive cluster trend with a positive slope (Figure 3.13). The electrofacies Ee cluster differs from those of electrofacies Ce in terms of cluster geometry and position with respect to the chart's axis and to photoelectric index values. Such variations in cluster geometry and position are attributed to the existence of iron oxide minerals in lithofacies L.

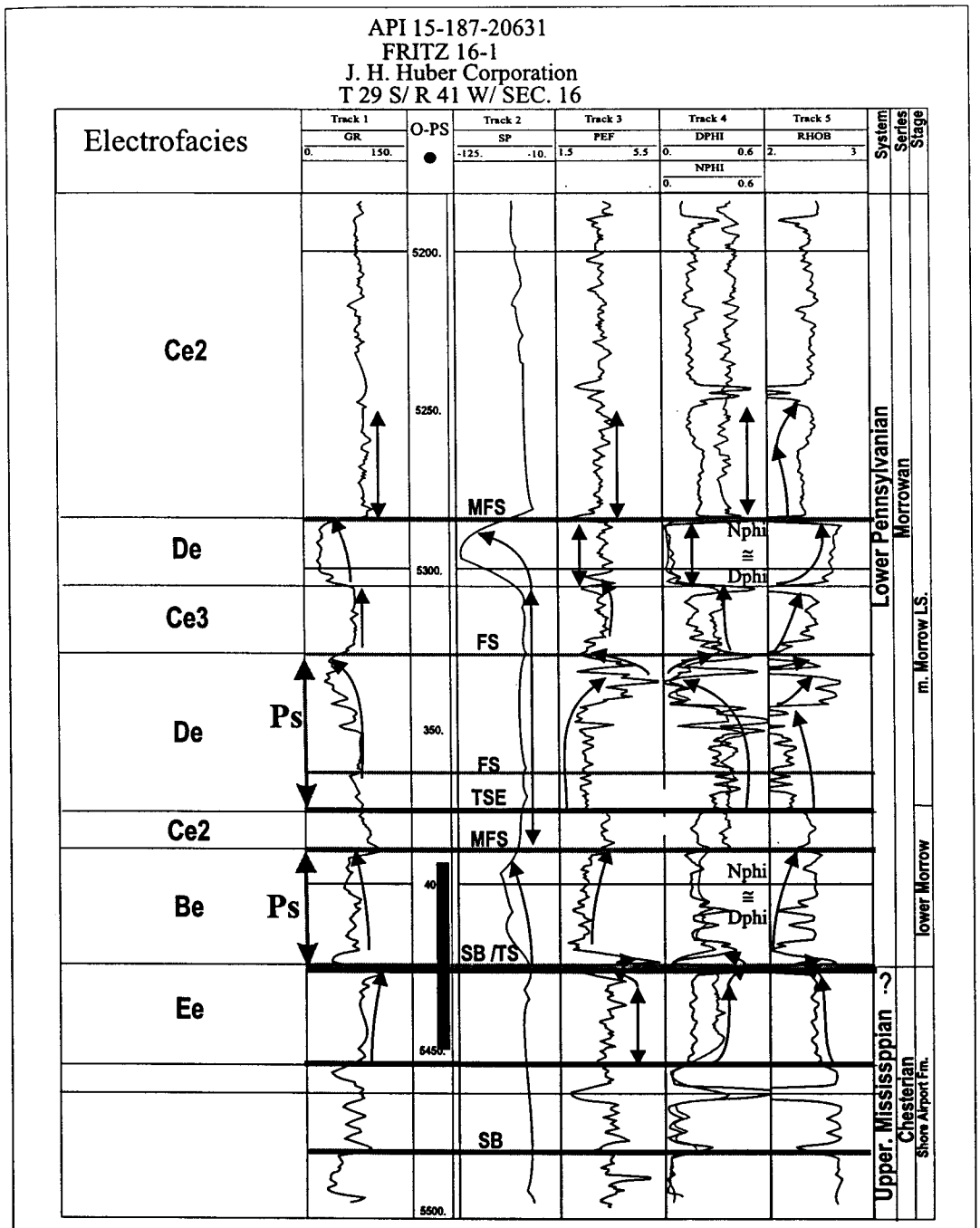

Figure 3.11 Fritz 16-1 wireline log suite and stratigraphic interpretation. Black arrows show wireline log trends. Ps, parasequence set; MFS, maximum flooding surface; TSE, transgressive surface of erosion; FS, flooding surface; m.NL, middle Morrow limestone

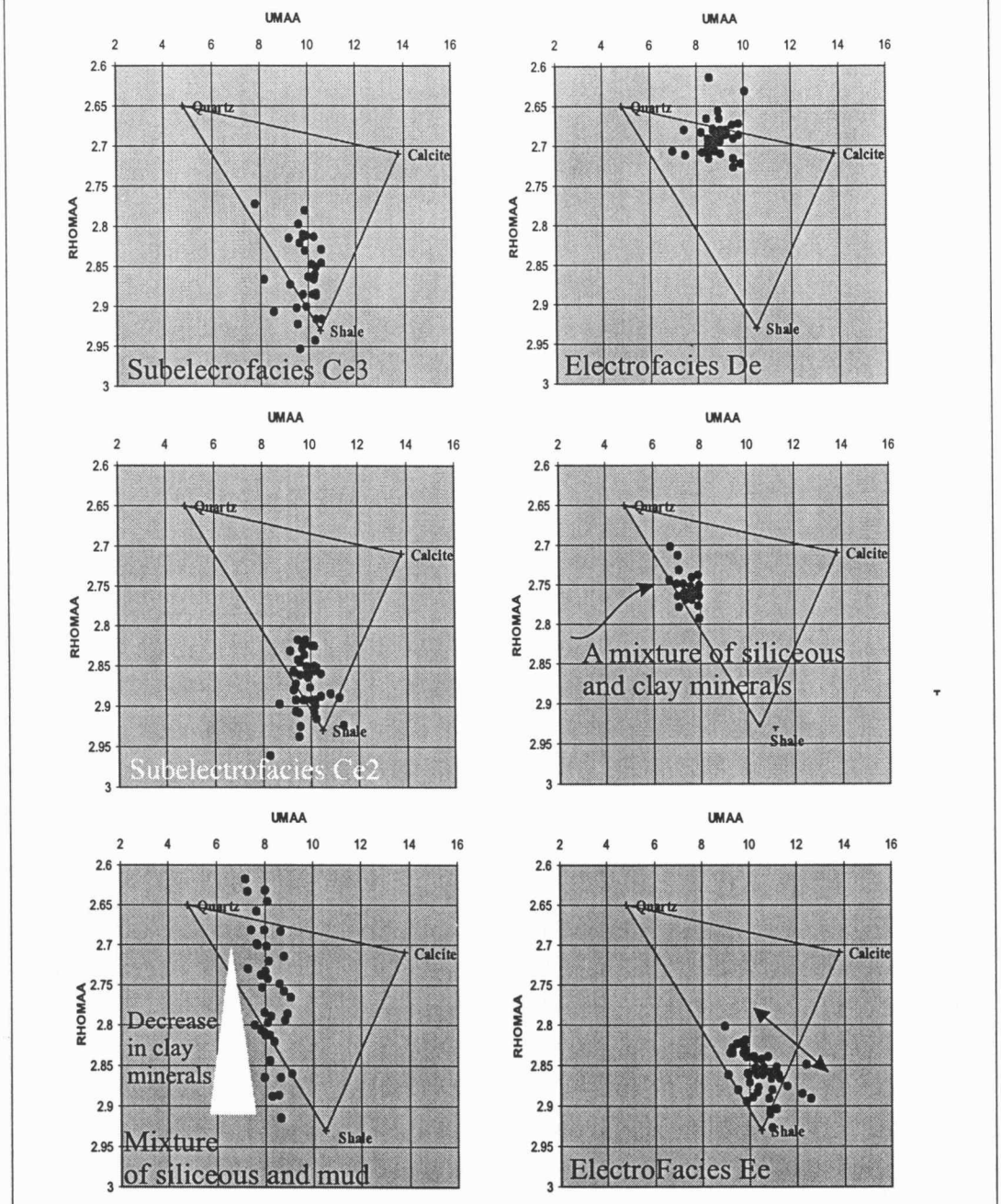

Figure 3.12 RHOmaa and Umaa cross-plots depict the elecrofacies found within Fritz 16-1 Note: The variation in clay mineralogy within subelectrofacies Ce. The paleosol trend is denoted by an arrow parallel to the shale-quartz axis.

4.0 RECOGNITION OF SEQUENCE BOUNDARIES AND MAXIMUM FLOODING SURFACES

A sequence boundary is a allostratigraphic surface that is developed as a result of subaerial erosion or exposure; this boundary separates younger strata from older strata (Mitchum and Vail, 1977; Van Wagoner et al., 1988). Sequence boundaries are laterally continuous and have correlative surfaces basinward (Vail et al. 1977, 1984; Vail and Todd, 1981; Haq et al., 1988). The criteria used to identify a sequence boundary includes subaerial erosional truncation, lateral correlative subaerial exposure, landward shift in facies onlap relationships with the surrounding older strata, and vertical change in parasequence stacking patterns (Van Wagoner et al., 1988).

A maximum marine flooding surface is a surface that indicates an abrupt increase in water depth and separates older, proximal water successions from younger, distal successions. Maximum flooding surfaces are laterally continuous and have correlative surfaces landward. These surfaces commonly overlie parasequence sets (Van Wagoner et al., 1988).

The electrofacies model developed at Arroyo Field, identified five major depositional environments: interfluve (Ee), upper estuarine (Ae), lower estuarine and upper shoreface (Be and De) and lower to offshore shoreface (Ce). The interpreted depositional environments were placed within a sequence-stratigraphic framework using key surfaces identified in core (Fritz 16-1) and spectral gamma-ray logs (Arnold 1-1).

In the Arroyo Field, the subaerial erosional truncation surface (sequence boundary) that indicates the separation of the Morrowan strata from the Mississippian strata was not cored. However, a sequence boundary and a transgressive surface were recognized in the Fritz 16-1 core and two maximum flooding surfaces and sequence boundaries were inferred from natural gamma-ray spectrometry analysis of logs from the Arnold 1-1 (figures 2.15, 3.11, 4.1). Each sequence-stratigraphic bounding surface has petrophysical characteristics that can be used to correlate across the field (Table 4.1).

Application of spectral gamma-ray logs in sequence stratigraphy

Generally, natural gamma-ray spectrometry logs measure the individual concentrations of potassium in percent, thorium in parts per million, and uranium in parts per million in a given formation (Schlumberger, 1989; Doveton, 1994). Accurate interpretation of the natural gamma-ray spectrometry log requires a good understanding of the nature of these ions and their degree of mobility.

The mobility of thorium ions is limited because thorium is easily hydrolyzed. Therefore, thorium is commonly concentrated in residual minerals such as clay minerals and bauxite (Table 4.2). The thorium curve is generally used as a clay mineral indicator (Hassan et al., 1976).

Unlike thorium, uranium is easily mobilized; and migrates during leaching and dissolution. Under high pH conditions, uranium ions (uranyl $(UO_2)^{+2}$) react with carbonate ions to form ionic complexes such as $(UO_2(CO_3)_2)^{-2}$ that increase the

API 15-187-20521
ARNOLD 1-1
J. M. Huber Ccorporation
T 29 S./ R 41 W./ SEC. 1

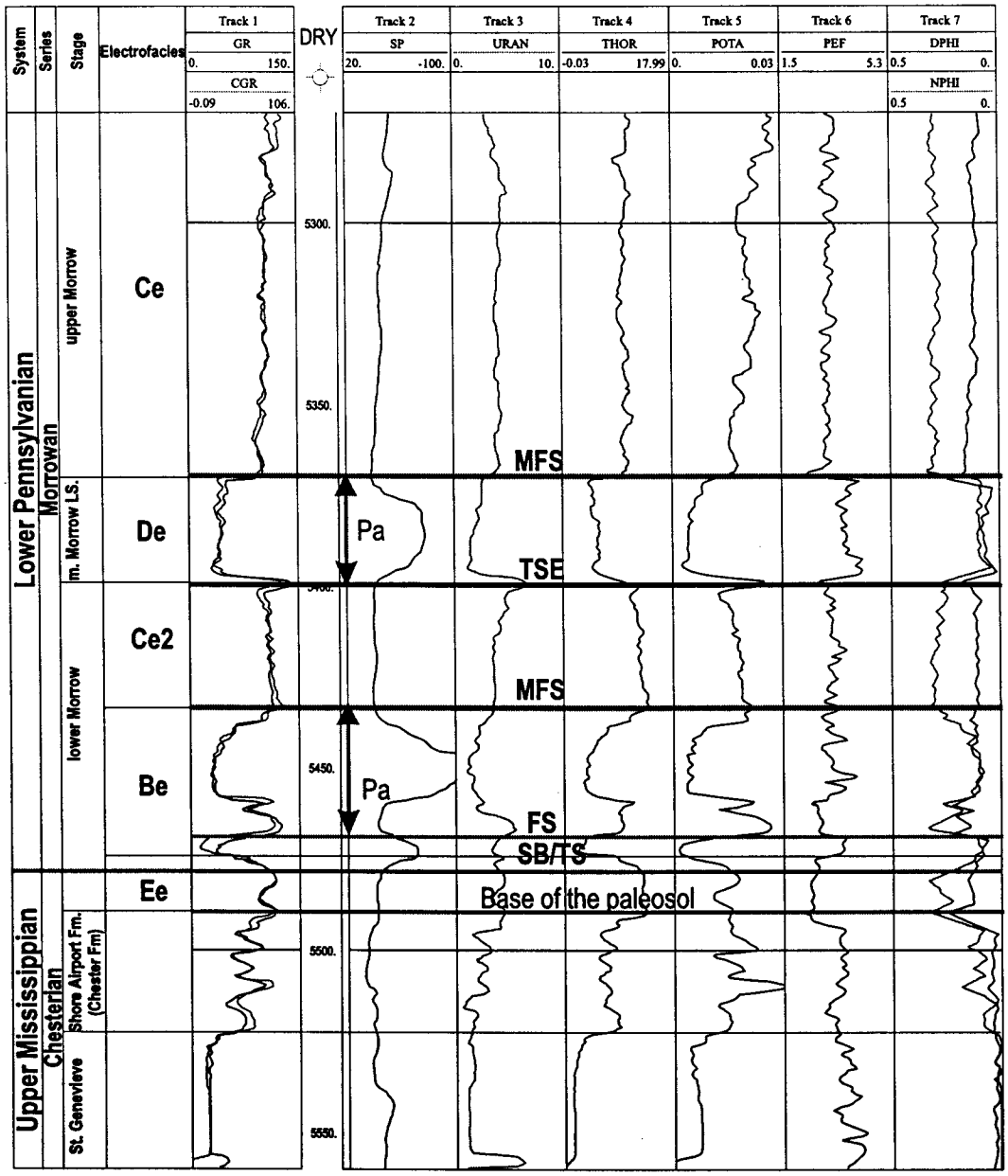

Figure 4.1 Sequence-stratigraphic interpretation of the Arnold 1-1 wireline log suite. Pa, para-sequence; MFS, major flooding surface; FS, flooding surface; TSE, transgressive surface of erosion; SB, sequence boundary; TS, transgressive surface.

Key surfaces	Th (ppm)	U (ppm)	K (%)	Th/U	PEF (B/E)	Dphi (%)	Nphi (%)
Upper sequence boundary	11.5	6.4	2.4	1.8	2.8	18	28
Upper flooding surface	10	4	1.7	2.5	3	18	32
Middle flooding surface	13.5	3.5	1.7	3.9	3.5	10	32
Lower flooding surface	5	3.4	2.2	1.5	2.8	18	34
Paleosol	12.8	3.9	3.3	3.247	2.5	13	28

Table 4.1 Petrophysical characteristics of sequence-stratigraphic bounding surfaces.

Mineral	Bauxite	Kaolinite	Illite	Montmorillite	Glauconite
Thorium (ppm)	40-50	30-20	20-15	15-10	10-1
K (ppm.)	?	0 - 1.94 (av.:0.63)	3.51-8.31 (av.:5.2)	0.60 (av.: 0.22)	3.2-5.8 (av::4.5)

Table 4.2 Thorium and Potassium responses to clay minerals, Glauconite and Bauxite.

mobility of the uranium (Hassan et al., 1976). Under reducing conditions, uranium ions are reduced to tetravalents that can be concentrated in several ways (in organic complexes, for instance) and absorbed by clay (Adams and Weaver, 1958; Hassan et al., 1976). The uranium curve is commonly used to identify hot shale units, to differentiate between potassium feldspar and uranium-rich sandstone, show fracture porosity and identify sequence boundaries (Adams and Weaver, 1958; Hassan et al., 1976; Doveton, 1994; Schlumberger, 1989).

Potassium ions have a weak ionic potential and are commonly absorbed by fine sedimentary particles, generally micaceous clay minerals. The potassium curve is commonly used to discriminate between micaceous clay minerals (Hassan et al., 1976). Generally, illite has a higher potassium level than does smectite or a mixed clay layer, whereas kaolinite has little or no potassium (Doveton, 1994; Table 4.1).

Several researchers have pointed out the importance of using spectral gamma-ray analysis as a tool for identifying subaerial exposures (Adams and Weaver, 1958; Carr and Budd, 1987; Watney and French, 1988). Subaerialy exposed settings commonly show a high uranium concentration (Carlisle, 1983; Chung and Swart, 1990). Uranium is transported to such settings by the lateral movement of the groundwater or by a downward movement through the vadose zone (Carr and Lundgren, 1994). Rainfall, dust, seaspray, and surface runoff are examples of possible uranium sources (Guide and Trucker, 1991). The distribution of uranium concentration along a vertical profile within a subaerially exposed setting is controlled by climate, pedogenic process, degree of vegetation, and rate of erosion

and sedimentation (Adams and Weaver, 1958; Mann and Horowitz, 1979; Ettensohn et al., 1988).

In the Arnold 1-1 well (section 1, R29S, T41W), the lower Morrow successions were subdivided into four intervals based on uranium, thorium, and potassium concentration and the vertical succession of facies as determined by the electrofacies model (figures 4.1, and 4.2).

Correlating Fritz 16-1 (section 16), Spikes 1-29 (section 29), and Grellner 1-18 (section 18) with Arnold 1-1 suggests that the lower interval (5478–5494 ft) of Arnold 1-1 is composed of rusty red shale and siltstone. The wireline-log responses for the lower interval are similar to that of electrofacies Ee (lithofacies L, interfluve) (figures 2.11, 3.9, 3.10, 3.11, 4.1). The spectral gamma-ray response for the lower interval is summarized in Table 4.1. In the Arnold 1-1, the base of the paleosol interval that separates the Chester Formation from the lower Morrowan strata is located at 5492 ft. Beneath the paleosol interval, the uranium curve shows relatively high values while the thorium and potassium curves show relatively low values (figures 4.1, 4.3). Continuing up-section, thorium and potassium concentrations increase and decrease upward, respectively, whereas uranium concentration levels remain fairly constant. The top of the paleosol interval (electrofacies Ee) is located at 5478 ft, where the uranium, potassium, and thorium show decrease (Table 4.2).

The spectral gamma-ray potassium, uranium, and thorium (KUT) ratio, litho-density vs. natural gamma-ray spectra and generalized mineral field charts (figures 4.4, 4.5, 4.6) suggest that a mixture of kaolinite and smectite clay minerals are the

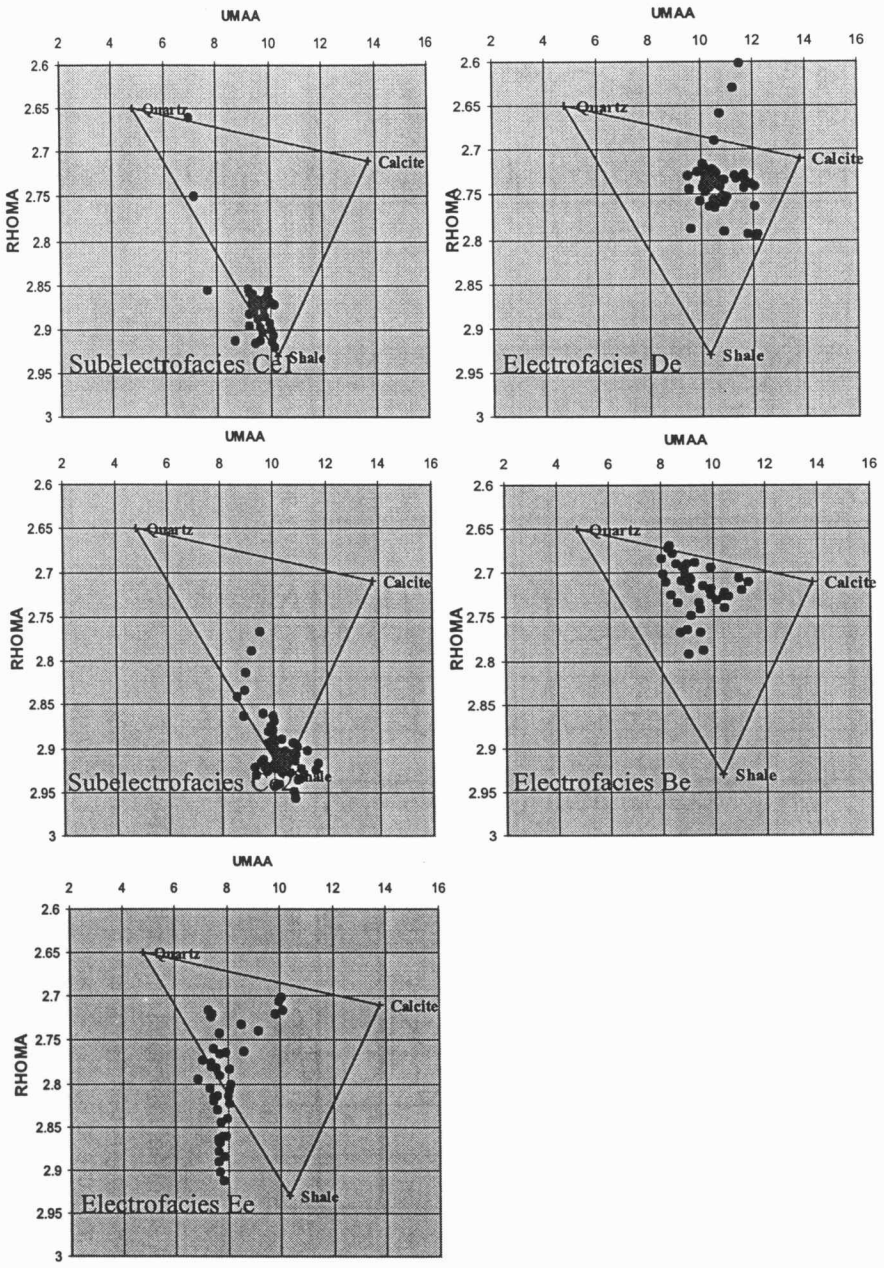

Figure 4.2 RHOmaa and Umaa crossplots show the electrofacies found within Arnold 1-1. Note: Electrofacies De contains more mudcontent, electrofacies Be has more siliceous grains and the interfluve interval (electrofaice Ee) has more kaolinitic and siliceous material.

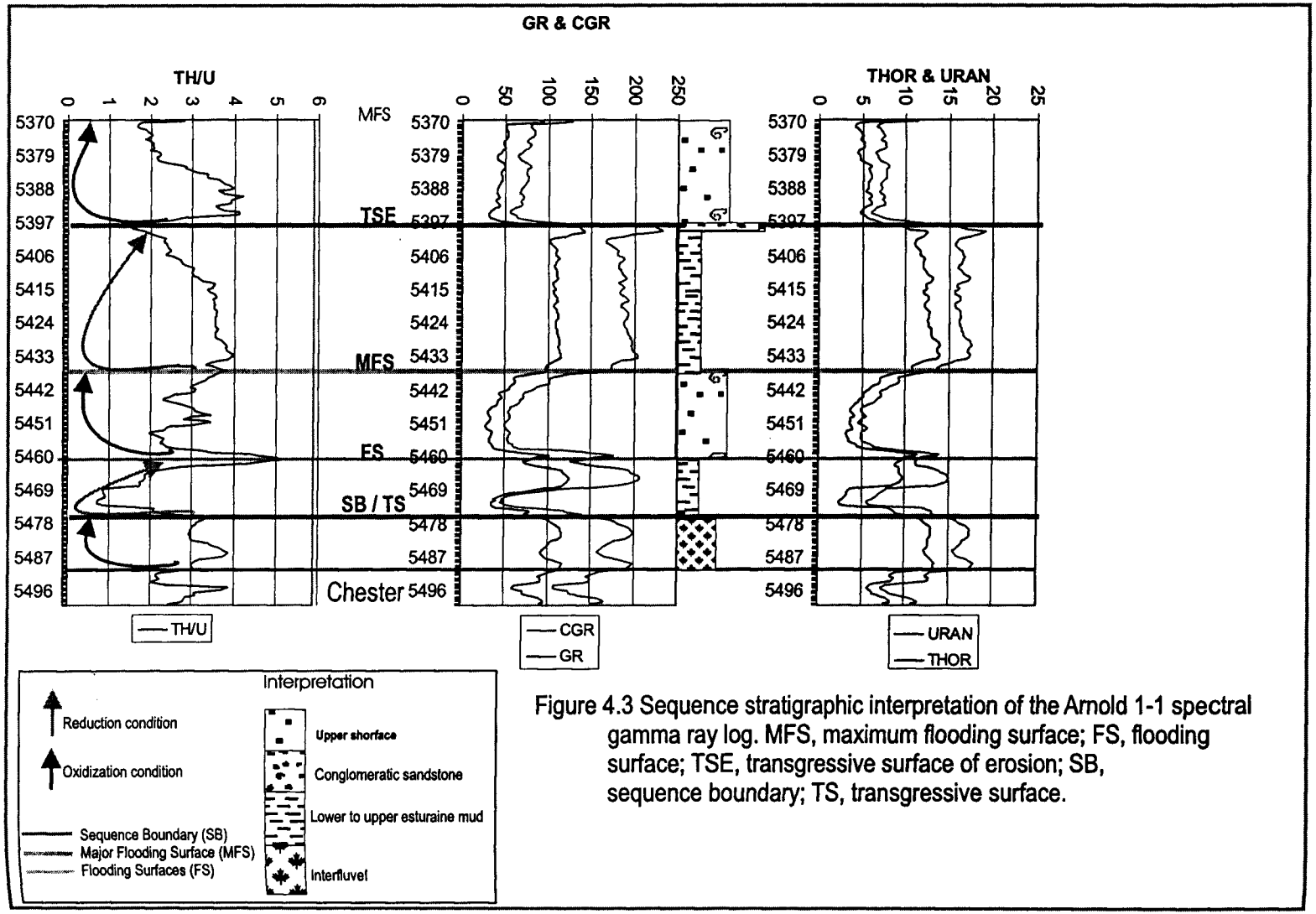

Figure 4.3 Sequence stratigraphic interpretation of the Arnold 1-1 spectral gamma ray log. MFS, maximum flooding surface; FS, flooding surface; TSE, transgressive surface of erosion; SB, sequence boundary; TS, transgressive surface.

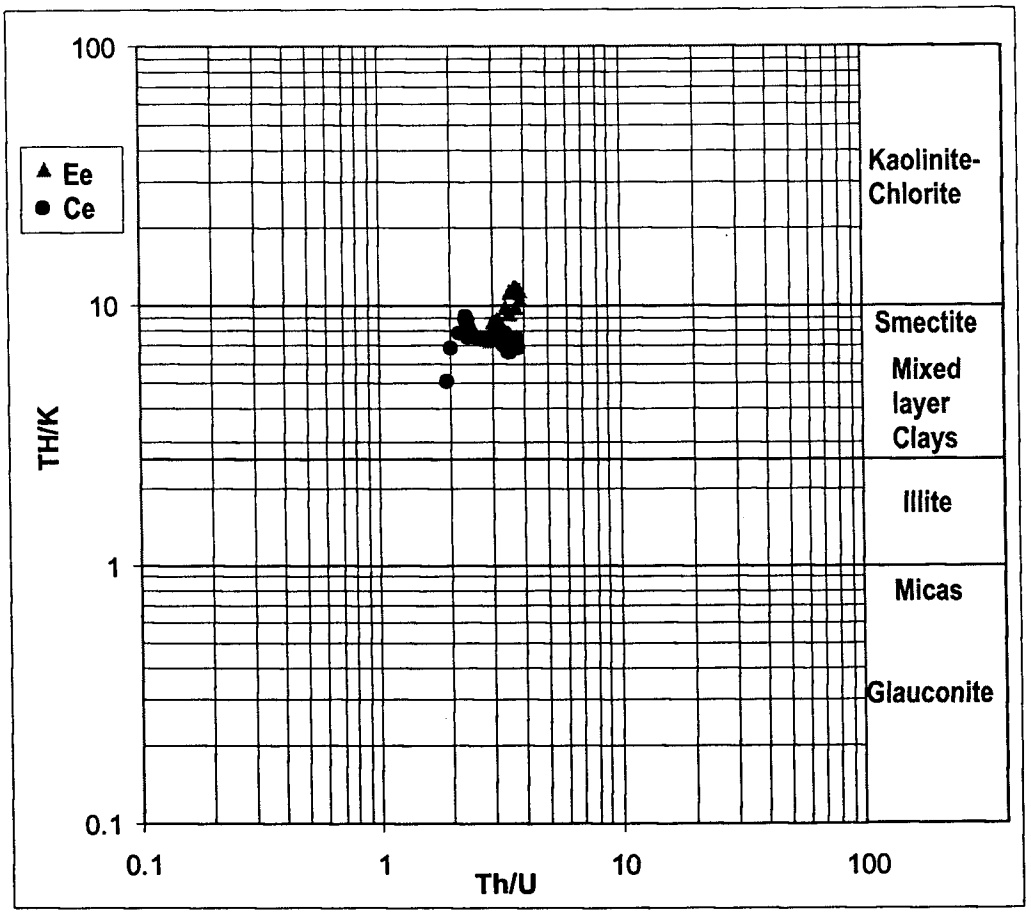

Figure 4.4 Spectral gamma ray KUT ratio chart. Note: black circles represent electrofacies Ce whereas the triangles represent electrofacies Ee.

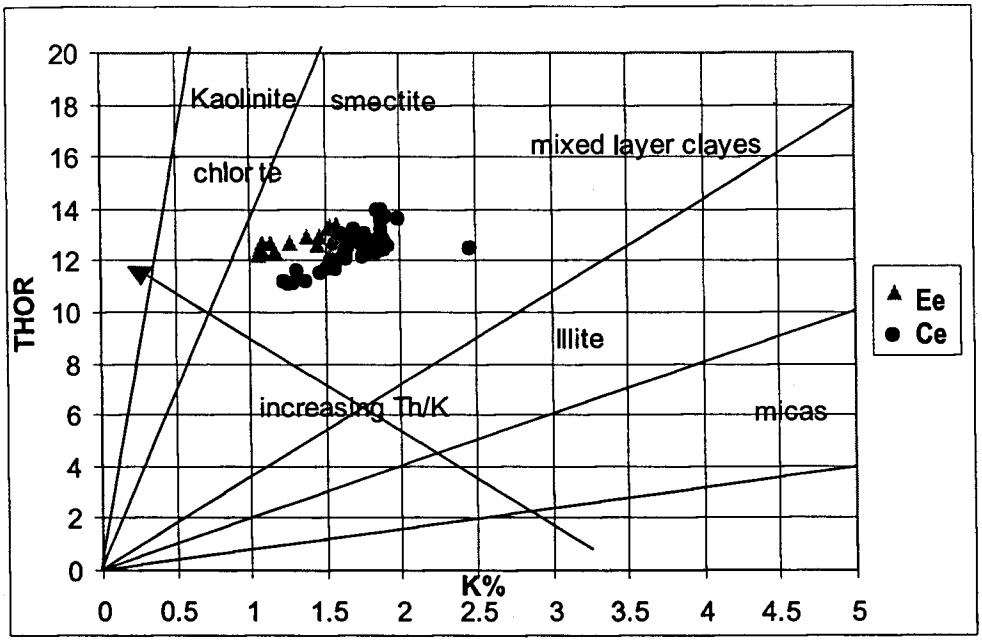

Figure 4.5 Generalized mineral fields on a potassium-thorium crossplot (Modified from Serra et al.,1980). Note: black circles represent electrofacies Ce whereas the triangles represent electrofacies Ee.

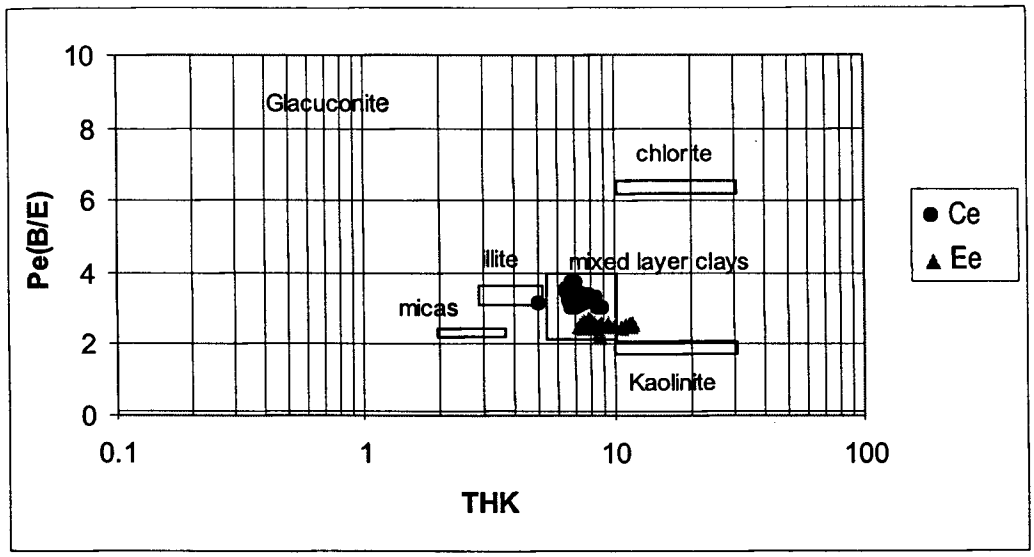

Figure 4.6 Mineral identification from Litho-Density log and natural gamma ray spectrometry (modified from Schlumberger, 1988).Note: black circle dots represent electrofacies Ce whereas the trigonal represents electrofacies Ee.

main components of the lower interval. Kaolinite and smectite suggest alkaline conditions and the weathering of acidic minerals such as feldspar (Deer et al., 1985). The presence of ferrous mudstone and moderate concentrations of uranium suggest that leaching occurred during exposure to atmospheric oxygen. Moderate thorium/uranium ratios suggest less weathering or reworking of old paleosol. Electrofacies Ee cluster plots (paleosol) as observed on the mineral crossplots, have an overlapping relationship with the shelf mud of electrofacies Ce (figures 4.3, 4.4, 4.5). The overlapping between electrofacies Ee and Ce were also supported by the similar separations in their Nphi and Dphi curves. These correlations suggest that electrofacies Ee (paleosol) may have formed as the product of the subaerial weathering of electrofacies Ce that was originally deposited in the previous highstand systems tract (HST).

A highly radioactive horizon (6.4 API) was identified above subelectrofacies Ce2 and below electrofacies De (5400 ft; figures 4.1, 4.3). Lithological correlation across the study area shows that the radioactive-rich horizon is irregular and has a scouring geometry with underlying shelf mud (subelectrofacies Ce2). A distinct 10 ft of brown, hard, poorly sorted, conglomeratic, coarse-grained sandstone in a silty matrix was reported in the Grellner 1-18 geological report (5380 ft; Figure 3.10). The conglomeratic sand unit overlies a black, hard, fossiliferous, argillaceous shale interval (subelectrofacies Ce2). The position of this conglomeratic sand unit resembles the highly radioactive horizon observed in Arnold 1-1 and is interpreted as a transgressive surface of erosion (TSE) that capped the lower Morrow sequence in

the Arroyo Field area (figures 4.1, 4.3; Weimer et al., 1988). High uranium, thorium, and potassium concentrations and high photoelectric index and porosity spikes were the wireline-log responses for this sequence boundary (Table 4.1).

Three flooding surfaces are inferred from the Arnold 1-1 spectral gamma-ray analysis. The lower (5468 ft) and middle (5434 ft) flooding surfaces are located within electrofacies Be and at the base of subelectrofacies Ce2, respectively, whereas the upper flooding surface was located at the base of electrofacies De (5370 ft; figures 4.1, 4.3). Both the middle and upper flooding surfaces cap parasequence sets that are considered to be maximum flooding surfaces (figures 4.1, 4.3; Van Wagoner et al., 1988). High uranium, thorium, and potassium concentrations, as well as a high photoelectric index and high porosity, are the wireline-log responses of the flooding surfaces (Table 4.1). The high concentrations of radioactivity coincide with low thorium/uranium ratios, which suggests that the fine-grained facies composing these surfaces were deposited slowly under low Eh conditions (Adams and Weaver, 1958).

Correlation of sequence-stratigraphic boundaries

Eight lithostratigraphic cross sections were constructed across the Arroyo Field (Figure 4.7). Cross sections A-A' to E-E' are east–west and are relatively perpendicular to the depositional strike, whereas cross sections F-F' to H-H' run north–south and are relatively parallel to the depositional dip (Appendix A; A.1-A.9).

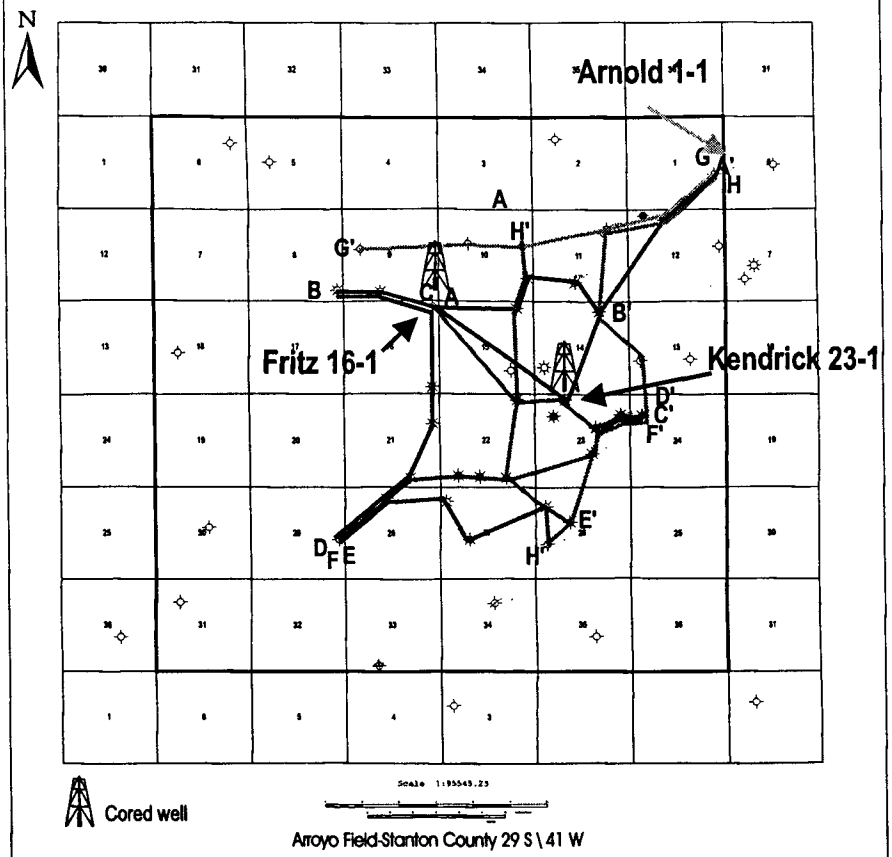

Figure 4.7 Location of the cross section lines used in the Arroyo Field. Light arrow points to well containing spectral gamma ray log.

The east–west cross sections datumed on the middle maximum flooding surface, show that the lower Morrow successions were deposited within a paleovalley that was incised into underlying Mississippian strata (Chester Formation, St. Genevieve Limestone, or St. Louis Limestone).

Cross section A-A' (Appendix A; Figure A.1) demonstrates the components of the electrofacies model and its chronostratigraphic surfaces. The sequence boundary that separates the lower Morrow from the underlying Mississippian strata was identified based on core descriptions (Fritz 16-1; lithofacies M; electrofacies Ee), spectral gamma-ray logs (Arnold 1-1), and variations in the thickness and truncation of the underlying Mississippian strata (Appendix A; figures A.1-A.9).

The maximum flooding surfaces (MFS) were mapped at the top of the parasequence sets of electrofacies Ae, Be and Ce1 within the deeper part of the incised valley; Be, and subelectrofacies Ce2 at within the shallower part and the valley walls, and subelectrofacies Ce and electrofacies De. These surfaces were identified based on the combination of abrupt changes in at least two of the following: an increase in radioactive elements, a decrease in porosity and permeability, an increase in the calcium carbonate content (variation in PEF curve), or a decrease of the bulk density.

A rapid transition from electrofacies Ce (commonly subelectrofacies Ce2) into electrofacies De identifies the transgressive surfaces of erosion (TSE) that separate the lower Morrowan strata from the middle Morrow limestone (electrofacies De). The wireline-log responses are relatively similar to those of the flooding surfaces;

however, the transgressive surface of erosion (TES) showed scouring geometry with underlying electrofacies Ce2 (Appendix A; A.1-A.9).

The upper-estuary facies (electrofacies Ae) was found only in the deepest part of the paleovalley and showed onlap relationships with the pre-Pennsylvanian sequence boundary. North of the study area (line B-B' Appendix A; Figure A.2), the upper-estuary facies was deposited in a relatively deep narrow channel that widened in the middle of the study area (lines C-C' and D-D', Appendix A; figures A.3, A.4) and bifurcated both the southeast (section 26) and southwest (section 28) (line E-E', Appendix A; Figure A.5). The cross sections also revealed that either the interfluve (electrofacies Ee) or the Chester Formation truncated against the upper-estuary facies. A flooding surface separates the upper-estuary facies from the overlying electrofacies Be. The lower-estuary and shoreface successions (electrofacies Be and Ce1) overlay the upper estuarine facies (electrofacies Ae) in the deepest part of the paleovalley, or overlay either the interfluve (electrofacies Ee) or the pre-Pennsylvanian unconformity at the main paleovalley walls (lines A-A' and B-B', Appendix A; figures A.1, A.2). The mud–sand ratio of the marine-influenced sandbodies (electrofacies Be) increased both east and west toward the paleovalley walls (lines B-B', C-C', E-E', Appendix A; figures A.2, A.3, A.5). Variations in thickness of these sand units can be observed across the study area, which suggests that the paleotopographic highs controlled the distributions and the deposition of these sandbodies (lines D-D' and E-E', Appendix A; figures A.4, A.5).

Offshore successions (electrofacies Ce2) are separated from the underlying upper-estuary and shoreface deposits by the middle MFS and from the overlying shoreface (electrofacies De) by a transgressive surface of erosion (TSE). The shelf mud successions overlie either the upper estuarine and shoreface strata in the main paleovalley or the pre-Pennsylvanian unconformity at the paleovalley walls (lines C-C' and E-E', Appendix A; figures A.3, A.5). The thickness of the offshore successions varies across the study area. Such variations in thickness suggest a relative fall of sea-level followed by a shoreface progradation and subsequent erosion of the underlying shelf mud (electrofacies Ce). Shoreface successions (subelectrofacies Ce3 and electrofacies De) are separated from the overlying offshore facies (subelectrofacies Ce1) by the upper flooding surface and from the underlying shelf mud by a TSE.

5.0 DEPOSITIONAL MODEL FOR THE ARROYO FIELD

Introduction

I have interpreted the lower Morrow successions in the Arroyo Field to represent deposits of a wave-dominated estuary in an incised valley. I based this conclusion on the geometry of the sequence boundary, the facies relationship with the sequence boundary and the key surfaces, the diversity and abundance of ichnofauna and marine fossils, and the internal sedimentary structures.

Review

The Incised Valley

An incised valley is a low, elongated, paleotopographic feature that formed as result of a fall in sea-level and the erosion of an exposed shelf by fluvial processes (Van Wagoner et al., 1988; Emery and Myers, 1996; Figure 5.1a). Many valley incisions attributed to a relative sea-level fall have been documented, such as the Pleistocene valley system of the Gulf of Mexico, and in the Pennsylvanian and Cretaceous of the western interior of the United States (Weimer et al., 1988; Anderson et al., 1990).

The length of an incised valley is a function of the coastal zone gradient and the magnitude and duration of the relative sea-level fall. In a broad, gently dipping coastal plain, an incised valley may be longer than the incised valley of a narrow,

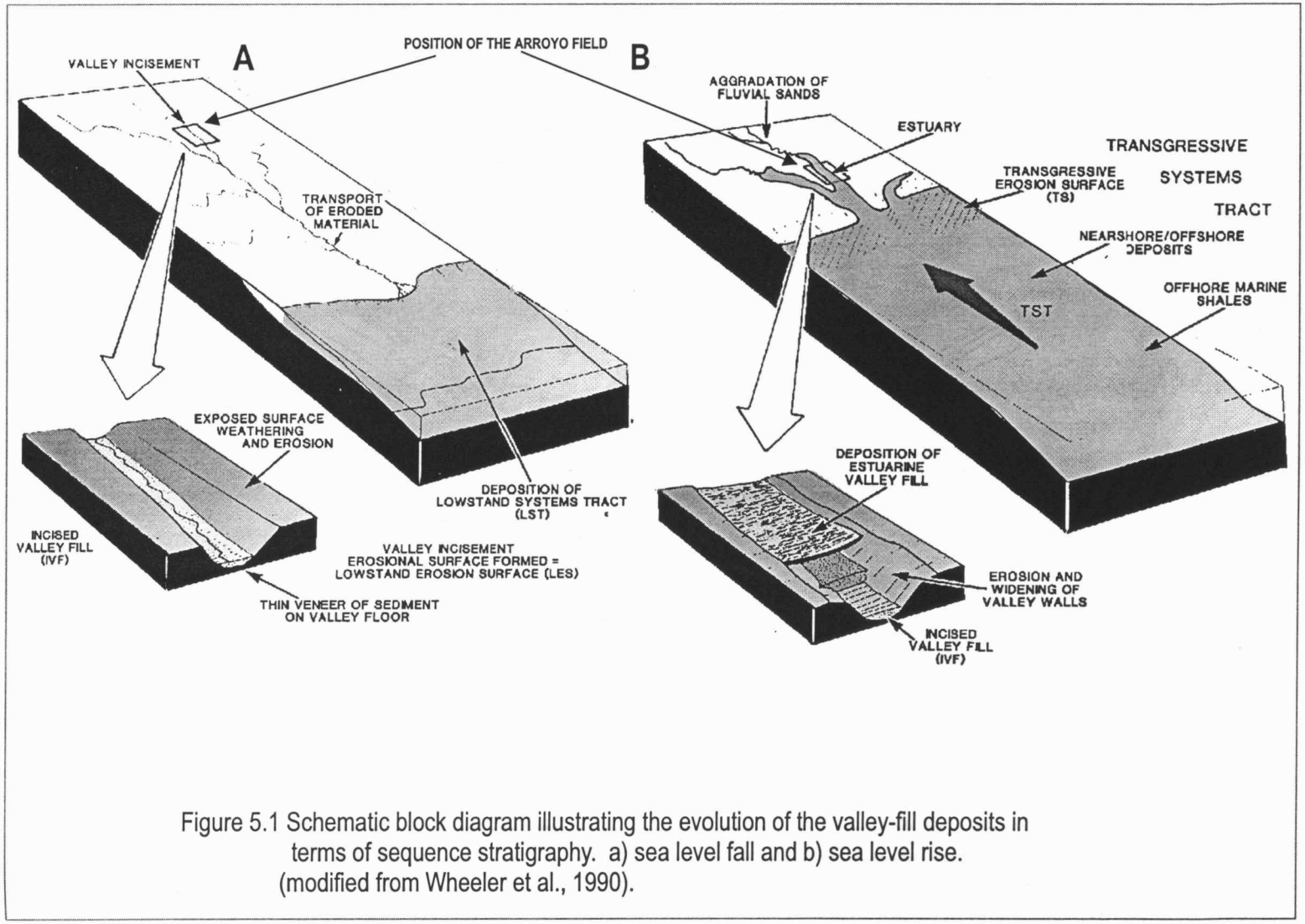

Figure 5.1 Schematic block diagram illustrating the evolution of the valley-fill deposits in terms of sequence stratigraphy. a) sea level fall and b) sea level rise. (modified from Wheeler et al., 1990).

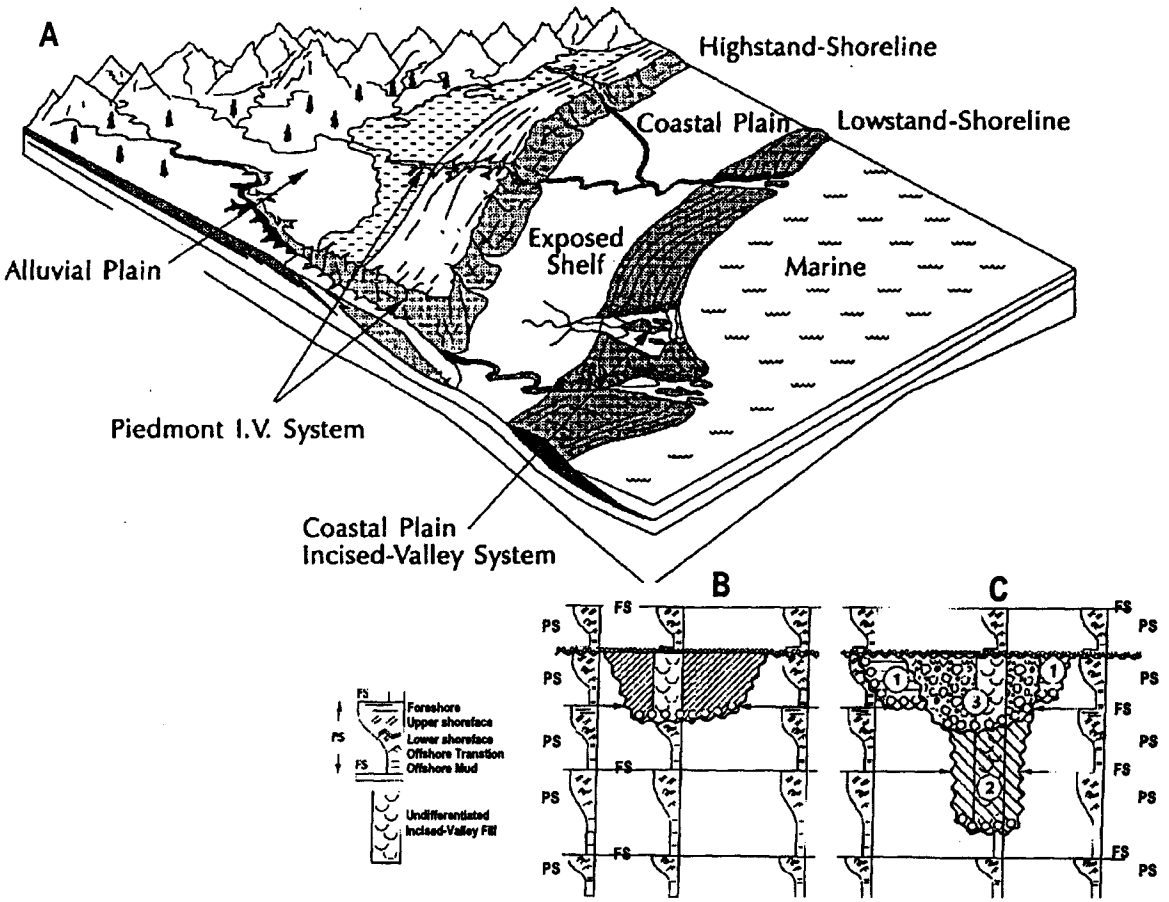

Figure 5.2 Schematic diagrams illustrating a) the distinction between piedmont and coastal-plain incised valley systems b) simple and c) compound incised-valley systems. Numbers 1-3 refer to successive episodes of erosion and deposition within the incised valley. PS = parasequence; FS = flooding surface (modified from Rosenthal, 1988 and Zaitlin et al.,1994)

steep, inclined coast (Wood et al., 1993). If the duration of the sea-level fall is long, the incised valley will extend further landward.

Incised valleys are generally characterized by the following: (1) Incised valleys commonly are aligned and tend to increase in dimension down-valley. (2) The walls and the bases of the incised valleys are bound by sequence boundaries that may be correlated to subaerially erosional surfaces (paleosol, interfluve). (3) Incised valleys are larger and deeper than individual and have valley-like features. (4) Incised valley incisions take the form of terraces. (5) Within an incised valley, basinward shifts in facies are present across a sequence boundary. (6) The fill of an incised valley records a trend of increasing accommodation space (sea-level rise) and an onlap relationship with the valley walls (Van Wagoner et al., 1988; Reynolds, 1994; Zaitlin et al., 1994; Emery and Myers, 1996; Hampson et al., 1997).

As the sea-level rises, an incised valley is converted into a drowned river-mouth estuary and the valley-fill sediment begins to accumulate (Figure 5.1b). The drowned valley receives sediment from two major sources: from the land via a river and from the sea via waves and tides currents, longshore drift, and storms. The balance between the rate of the relative sea-level rise and the volume of sediment input controls the type and the geometry of the valley fill (Nichols and Biggs, 1985). Therefore, an incised valley can be filled completely or partially with fluvial sediments (e.g., Pennsylvanian Morrow, USA) or with open marine sediment (e.g., Viking Formation, Canada; Krystinik and Blackeney-DeJarnett, 1990; Allen and

Posamentier, 1993). However, estuarine deposits are the most common fill of drowned valleys (Allen and Posamentier, 1993).

Incised valley fills have been classified into single valley fills with only one episode of filling, and compound valley fills combining several cycles of erosion and filling (figures 5.2a, b, c; Rahmani, 1988; Wood and Hopkins, 1989). Simple incised valleys are relatively small valleys and are composed of one sequence that filled during a high-frequency sea-level cycle (Figure 5.2b). The sedimentary fill of a simple valley commonly consists of fine-grained and mature deposits recycled from coastal plain sediments (Zaitlin et al., 1994) (Figure 5.2b). The compound valley fill consists of multiple sequences that were deposited during several fluctuations of sea-level. The compound valley fill often contains coarse-grained, immature, fluvial sediments. Simple valley-fill systems commonly characterize low-gradient coastal plain settings, whereas compound valley-fill systems are typical of a steeper gradient piedmont setting (Zaitlin et al., 1994; Figure 5.2.c).

The Estuary

Dalrymple et al. (1992) defines an estuary as:

"The seaward portion of a drowned valley system which received sediments from both fluvial and marine sources and which contain facies influenced by tide, wave, and fluvial processes. The estuary is considered to extend from the landward limit of the tidal facies at its head to the seaward limit of the coastal facies at its mouth." (p. 233)

Modern estuaries developed as a result of the rapid, glacially influenced, Holocene, sea-level rise that flooded river valleys. In a modern setting, well-developed estuaries are found on mid-latitude coastal plains with wide continental shelves that are undergoing marine submergence (Reinson, 1992). The type and distribution of estuary fill is controlled by the rate of sedimentary supply by both fluvial and marine process relative to the rate of transgression (Reinson, 1992). Estuaries have been classified based on the dominance of wave and tidal processes into two end members, wave- and tide-dominated estuaries (Reinson et al., 1988; Nichols et al., 1991; Dalrymple et al., 1992; Allen and Posamentier, 1993; Zaitlin et al., 1994; figures 5.3, 5.4). In a wave-dominated setting (e.g., the James Estuary, Virginia, USA), wave currents and longshore drift dominate the marine process at the estuary's mouth, whereas the fluvial processes dominate the upper part of the estuary. Energy of the current for both processes decreases dramatically in the middle part of the estuary. Therefore, wave-dominated estuaries show tripartite zonation of sand–mud–sand, with minimal tidally influenced structures (Figure 5.3). In tide-dominated estuaries (e.g., the Cobequid Bay–Salmon River in the Bay of Fundy, Canada), onshore and shoreface sands are transported further landward into the estuary, mainly by tidal currents. Therefore, a tidal-dominated estuary shows a gradual transition from coarse-grained tidal bars seaward to intertidal fluvial mud flats landward, with an abundance of tidally influenced structures (Figure 5.4; Dalrymple et al., 1992; Nichols et al., 1991). The presence of estuarine successions is not necessarily an indicator of an incised valley-fill system. A modern example shows that the Schelde

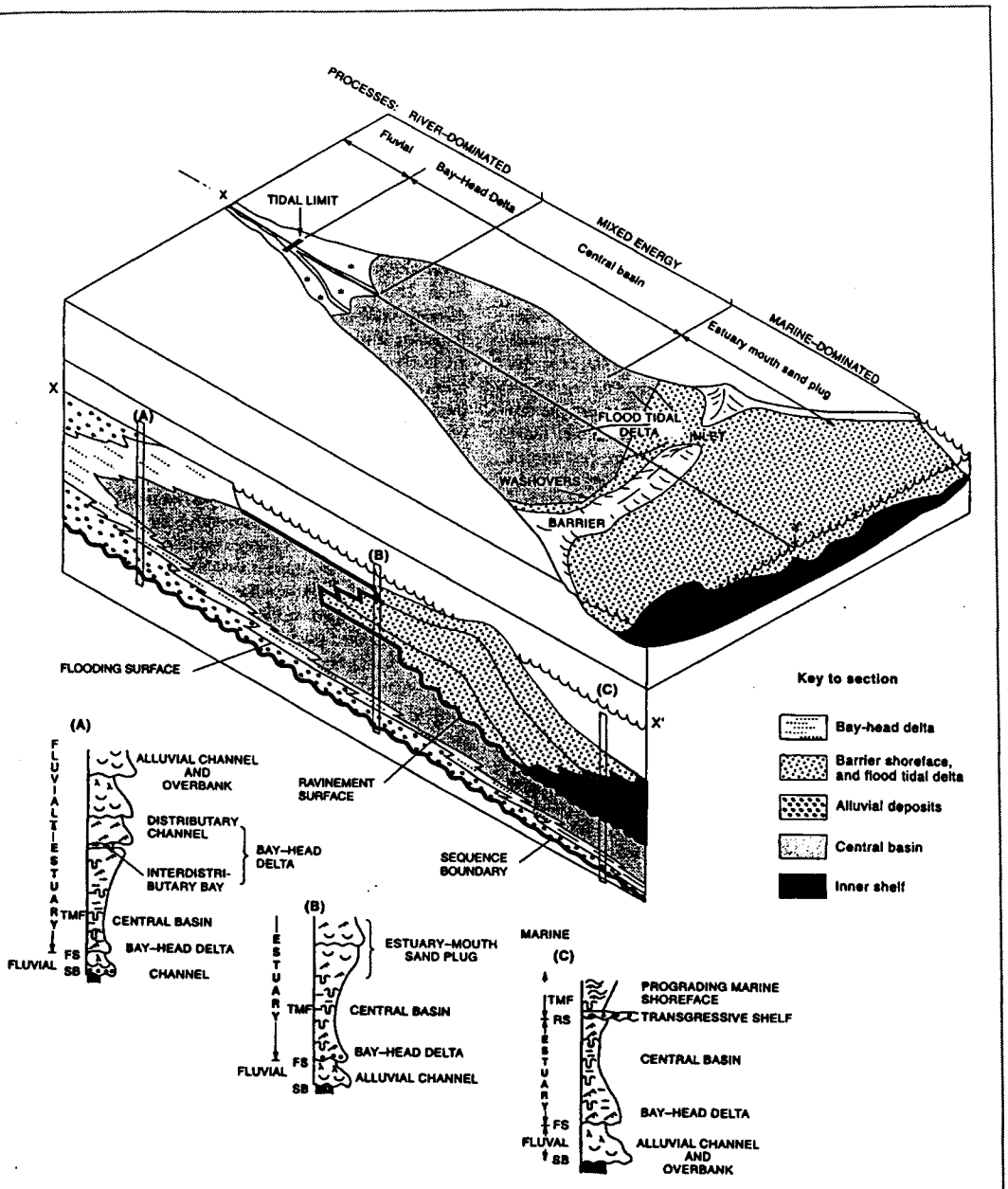

Figure 5.3 Schematic block diagram illustrating wave-dominated estuary (modified from Zaitlin et al., 1994)

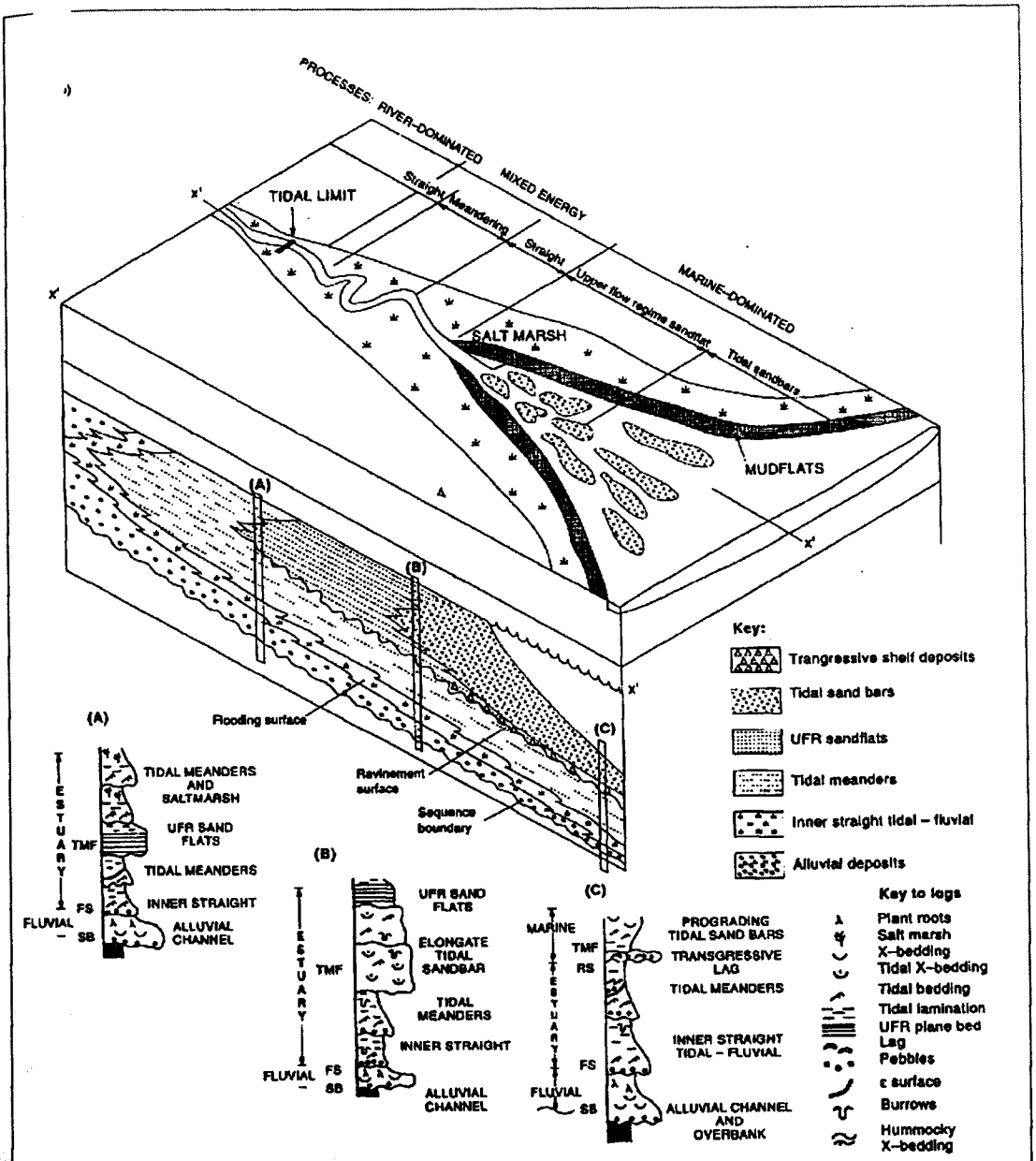

Figure 5.4 Schematic block diagram illustrating tide-dominated estuary (modified from Zaitlin et al., 1994)

Estuary in the Netherlands was formed by tidal scouring during Holocene transgression, not as the result of a drowned valley (Ebbing and Laban, 1986).

An estuarine complex can be composed of any number of the following environments: braided or meandering river, tidal flat, lagoon, back barrier island, tidal channel complex, and shoreface environments. The degree of preservation and the dominance of both marine and fluvial facies within an estuary environment are mainly controlled by the rate of the rise in sea-level, the intensity of wave and tidal currents, and fluvial discharge of sediment.

Ancient estuarine deposits are difficult to compare with the facies distribution in the modern estuary (Reinson, 1992). Few geological models for estuarine environments have been proposed that can be applied to the stratigraphic record. The widely accepted models are those proposed by Zaitlin et al. (1994) and Nichols et al. (1991). Both models are built on the assumption of steady, continuous transgression and sediment supply. These models also are based on key surfaces that can be recognized only in the outcrop and, to a degree, in cores. Both models were used as a general guide in this study.

Estuarine environments are characterized by fluctuations in salinity, fluctuations in current energy, particular sedimentary structures and constituents, and during periods of transgression increased accommodation space and landward progression of marine facies. Increases in salinity (fresh -brackish-marine) can be inferred from the following: (1) an increase of ichnofauna size, abundance and diversity seaward; (2) a seaward increase in bioturbation; (3) the presence of coal and

carbonaceous material overlying marine sediments; and (5) a seaward increase in bioclastic diversity and size. Fluctuation in salinity can be inferred from alternation of pyrite, sidrite and glauconite dominated intervals. Fluctuations in current energy can be inferred from the following: (1) an alternation between high-energy (unidirectional or bi-directional cross-bedding) and low-energy sedimentary structures (characterized by ripple marks and mud drapes); (2) the presence of high-energy ichnofauna such as *Skolithos* alternating with low energy ichnofauna such as *Cruziana*; (3) interbedding of highly bioturbated and unbioturbated intervals; and (4) the presence of fining-upward intervals. The existence of two sources of sediments can be inferred from the presence of at least two sandbodies of the same age that: differ in their biological (diversity and abundance), physical sedimentary structures (unidirectional, bi-directional, asymmetrical and symmetrical), constituents (in situ marine fauna), and show a gradual transition in their constituent and sedimentary structures in both landward and seaward directions.

Sequence-stratigraphic interpretation

Cross sections and detailed mapping reveal that the lower Morrowan siliciclastic successions deposited directly on the Mississippian carbonates represent a basinward shift in environments and, along with the truncation, define the sequence boundary. The pre-Pennsylvanian unconformity can be tied laterally to an interfluve. The pre-Pennsylvanian unconformity takes the form of terraced valley (Emery and Myers, 1996; Appendix A; Figure A.1). The paleovalley interpretation is supported by the distribution of electrofacies Ae of the lower Morrow, which is confined to the

valley wall and lies on the pre-Pennsylvanian sequence boundary. Figure 5.5 shows that electrofacies Ae has an axial geometry that follows the paleoslope trend. Lower Morrow deposits also illustrates an onlap relationship with the pre-Pennsylvanian sequence boundary (Appendix A; Figure A.1). The depth of the paleovalley was larger than that of an individual channel; however, the paleovalley was less than 300 ft in magnitude, which suggests that the paleovalley resulted from a glacially induced eustatic sea-level fall (Reynolds, 1994; Haq et al., 1988; Appendix A; Figure A.5).

The sandstone deposits at the base of the valley fill (lithofacies A and B of electrofacies Ae) are much different from those at the top of the valley fill (lithofacies F, H, I and J of electrofacies Be) in regard to the grain size, the sedimentary structures and the abundance and diversity of marine fossils and ichnofauna. In Kendrick 23-1, the overall lithofacies trend is an upward increase in grain size, degree of bioturbation, abundance of marine bioclasts, and diversity of ichnofauna (Figure 2.1a). The upward increase in ichnofauna diversity and the abundance of marine fauna indicate a transition from stressful brackish-water to open marine conditions. The association of the facies within the paleovalley records a trend of increasing accommodation space (rise of relative sea-level; Dalrymple et al., 1992).

Lithofacies A and B show brackish- and tidal-influenced features, such as very low diversity of ichnofauna and marine fossils and the presence of mud drapes. The low diversity of ichnofauna and marine fossils suggests stressful brackish-water conditions during deposition. This interpretation is consistent with the variation in pyrite concentrations observed within lithofacies A (Stumm and Morgan, 1970;

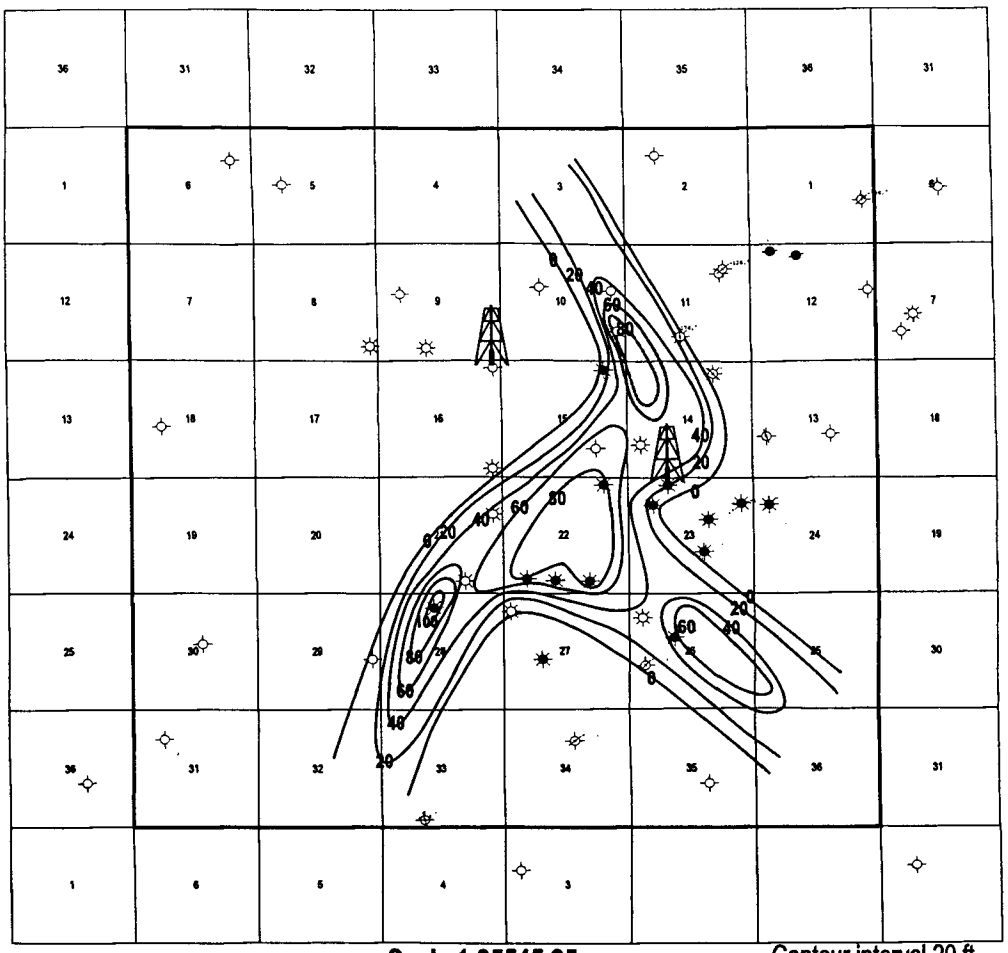

Arroyo Field-Stanton county 29S \ 41W

Figure 5.5 Isopach map showing the axial geometry of electrofacies Ae.

Cassgrande et al., 1977; Berner et al., 1979; Martens and Goldhaber, 1978; Postma, 1982; Berner and Raiswell, 1984). The tidally influenced structures observed within lithofacies B might result from the amplification of wave–tide currents caused by the irregularity of the paleovalley surface area. Lithofacies B shows a gradual upward transition into bioturbated and interbedded mudstone and sandstone (Lithofacies C). This transition indicates a dramatic change in current energy (from high to low energy). Dalrymple et al. (1992), distinguish bay-head delta from fluvial sediments by the presence of brackish-water fauna and tidally influenced structures. They also state that at the base of transgressive successions, bay-head delta sediments are more common. Therefore, lithofacies A and B could represent a bay-head delta, whereas lithofacies C might indicate a central basin facies.

Marine fauna and planar cross-bedding, along with the absence of any tidally influenced structures, dominate the rest of the valley fill succession (lithofacies D–J), which suggests a high-energy, wave-dominated marine setting. The lower and middle parts of the marine succession (lithofacies D–H) show a general fining-upward trend, which suggests a tidal inlet complex developed during transgression periods (Herbert, 1979; Heron et al., 1984; Molsow and Tye, 1985; Dalrymple et al., 1992). The thick inlet floor (lithofacies D) suggests a rapid lateral migration of a tidal inlet complex in a wave-dominated setting (Kumar and Sanders, 1974; Moslow and Tye, 1985; Reinson et al., 1988). This interpretation is supported by the presence of channel geometry and the absence of spit platforms, washover and ebb delta facies (Cheel and Leckie, 1990; Appendix, A, figures A.1, A.3). Lithofacies I and J show a

general coarsening-upward trend. With respect to these lithofacies' positions within the marine succession, this interval is interpreted to represent shoreface deposits (Moslow and Tye, 1985).

Depositional model

The sequence stratigraphy framework, as proposed by Vail et al., (1977, 1984) and Wagoner et al., (1987), is composed of three systems tracts: lowstand systems tract, transgressive systems tract, and highstand systems tract. The lowstand systems tract is separated from the underlying successions by a sequence boundary (subaerial exposure) and from the overlying transgressive systems tract by a transgressive surface. The highstand systems tract is separated from the underlying transgressive systems tract by a maximum flooding surface and from the overlying strata by a sequence boundary.

Incised-valley fills are placed within the lowstand systems tract by Van Wagoner et al., (1987). Reinson et al., (1992), suggest that an incised-valley fill as an accumulation within the valley during the early stages of a rise in sea-level; therefore, these deposits are placed in the transgressive systems tract rather than the lowstand systems tract. The Reinson et al., (1992) modification is being accepted in the geologic community, and applied in Hugoton Embayment, Morrowan incised-valley fills (Sonnenberg et al., 1990; Walker, 1992; Dalrymple, 1992).

In the Arroyo Field area, during Late Mississippian time, a relative drop in sea-level resulted in the exposure of the Hugoton Shelf and the development of the Pre-Pennsylvanian sequence boundary (top of electrofacies Ee of lithofacies K;

figures 5.1a, 5.6a, b). The Hugoton Embayment became a bypass margin that was dominated by southeast-flowing fluvial systems that were eroding the shelf. During the early Morrowan, the incised valley became a sediment trap as a result of a rise in sea-level (transgression). The incised valley-fill was deposited during the transgression period with two different sandbodies (figures 5.1a, 5.4, 5.6a, b, c). These sandbodies are different in their biological and physical sedimentary structures and constituents, which suggests two different sources and depositional environments. The sediments of lithofacies A and B (electrofacies Ae) appear to be derived from the land by fluvial processes. The sediments of lithofacies D–J (electrofacies Be) indicate marine sources and processes; longshore drift, wave currents, and storms. Core descriptions and lithological correlations suggested that the lower Morrow siliciclastic successions at the Arroyo Field were deposited in a wave-dominated estuary during transgression within an incised valley and represent a transgressive system tract (Reinson et al., 1988; Nichols et al., 1991; Van Wagoner et al., 1988; Dalrymple et al., 1992; Allen and Posamentier, 1993; Reynolds, 1994; Zaitlin et al., 1994; Emery and Myers, 1996; Hampson et al., 1997).

In overlying siliciclastic successions at the Arroyo Field, subelectrofacies Ce2 represents a time where the sea-level rose dramatically, inundating the incised valley and creating a maximum flooding surface at the top of the estuarine succession. During this period, both terrestrial and marine siliciclastic sediment sources were shut down. The shelf became a starved setting and deep-water black shale was deposited (Figure 5.6d). Subelectrofacies Ce2 is interpreted as the highstand systems tract (Van

Wagoner et al., 1988; Emery and Myers, 1996). The highstand systems tract was terminated by the fall of the sea-level, which developed the upper sequence boundary (Appendix A; A.1–A.9).

Within the context of the incised valley classifications of Zaitlin et al., (1994), the lower Morrow incised valley at Arroyo Field represents a simple valley fill. This interpretation is consistent with the low gradient of the Hugoton Embayment shelf and with the degree of maturity of the valley fill (Krystinik and Blackeney-DeJarnett, 1990; Allen and Stephen, 1995).

6.0 APPLICATION OF THE ELECTROFACIES MODEL IN GENTZLER FIELD

The lithofacies interpretations and electrofacies model developed for the lower Morrow at Arroyo Field were applied to the equivalent stratigraphic interval at the Gentzler Field in Stevens County, Kansas (Figure 6.1). Lithofacies were described for cored intervals of the Morrow and Chester in Gaskill "2A" and Nell "A" in Gentzler Field (figures 6.2, 6.3). Wireline-log responses were used to construct and evaluate a sequence-stratigraphic framework using the criteria developed at the Arroyo Field. The cored intervals at the Gentzler Field were previously described by Wheeler et al., (1990), Radar (1987) and Franz (1985). I first applied the electrofacies model directly to the field by constructing a cross section connecting the cored wells (Appendix B, Figure B.1). Second, I applied the interpretation, which I inferred from the electrofacies model previously described in chapter III, to the cored intervals in Gaskill "2A" and Nell "A" (figures 6.2, 6.3).

Lithostratigraphic correlation

It is difficult to determine the exact location of the pre-Pennsylvanian sequence boundary across the field. As noted by other workers in the area, the log signatures of the sandstone units in the lower Morrow and the Shore Airport Formation (Chester Formation) s are similar (Abels, 1962, Radar, 1987). Sequence boundaries and other key surfaces, such as flooding surfaces, were identified based on

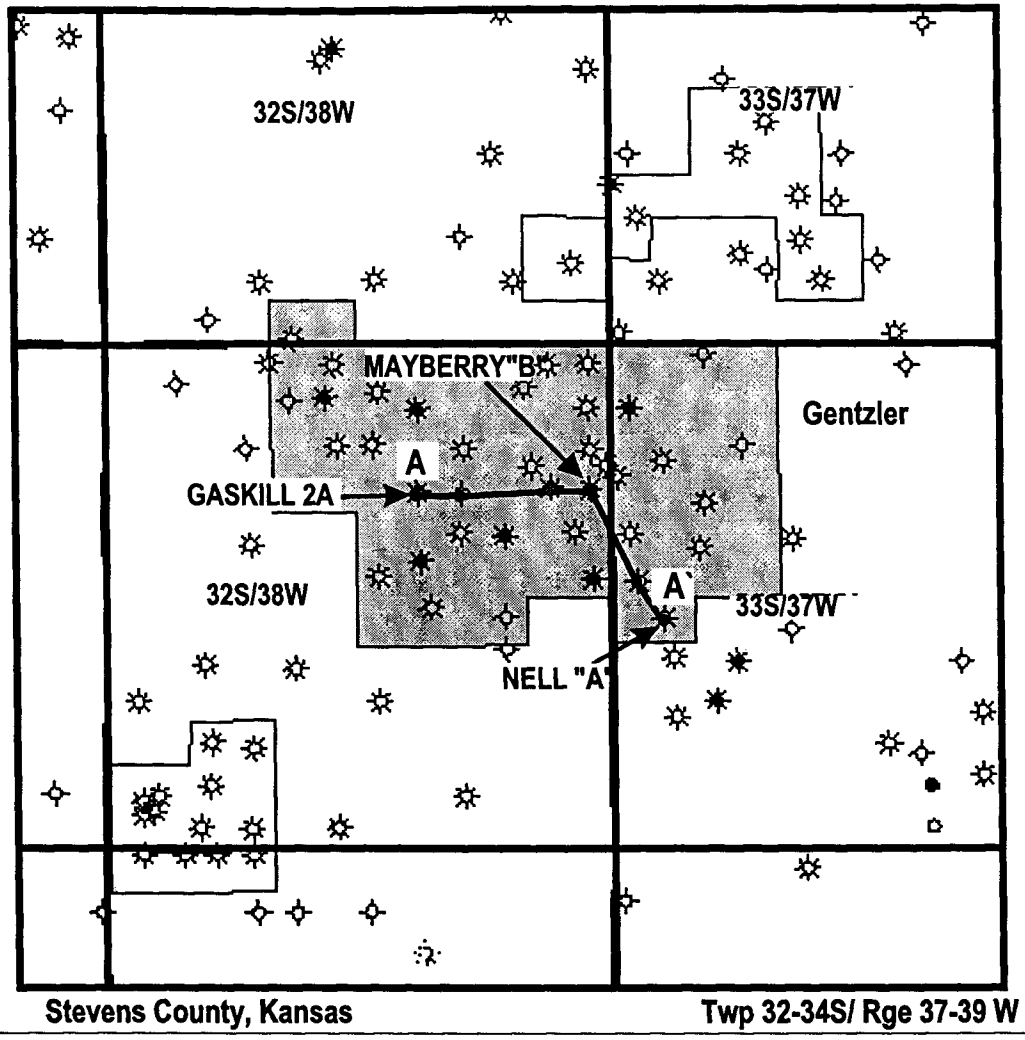

Figure 6.1 Gentzler Field base map showing location of cross section A-A`. Black arrows and light arrow indicate wells with cores and the type log respectively (Modified from Digital Petroleum Altas, http://www.kgs.ukans.edu/PRS/petroIndex.html).

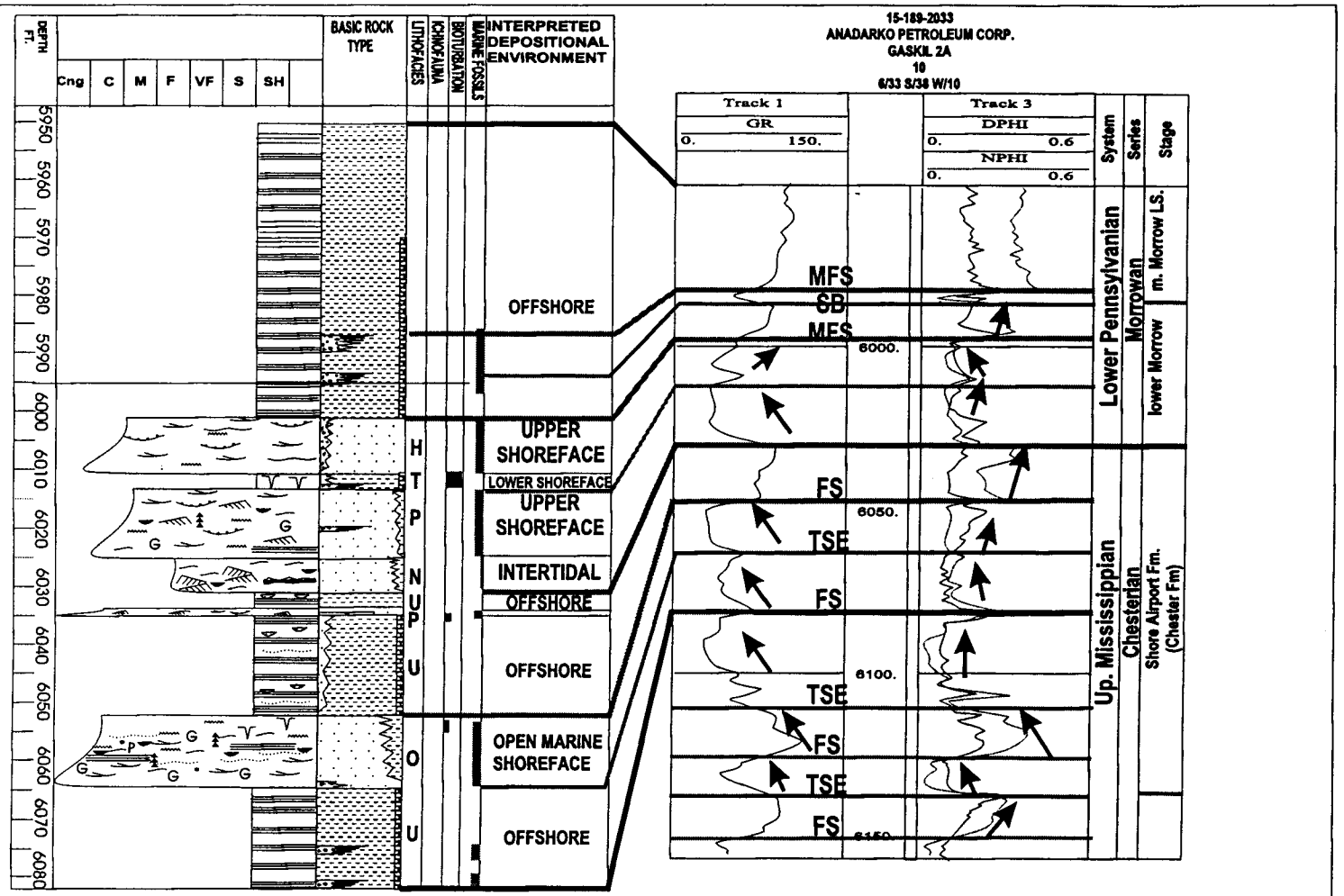

Figure 6.2 Core description and wireline log suite for the Gaskill "2A". Black arrows show wireline log trends of gamma ray, neutron porosity and bulk density. Note: the stacked parasequences; MFS, major flooding surfaces; TSE, transgressive surfaces of erosion; FS, flooding surfaces. See figure 2.1a for explanation of symbols used on core description.

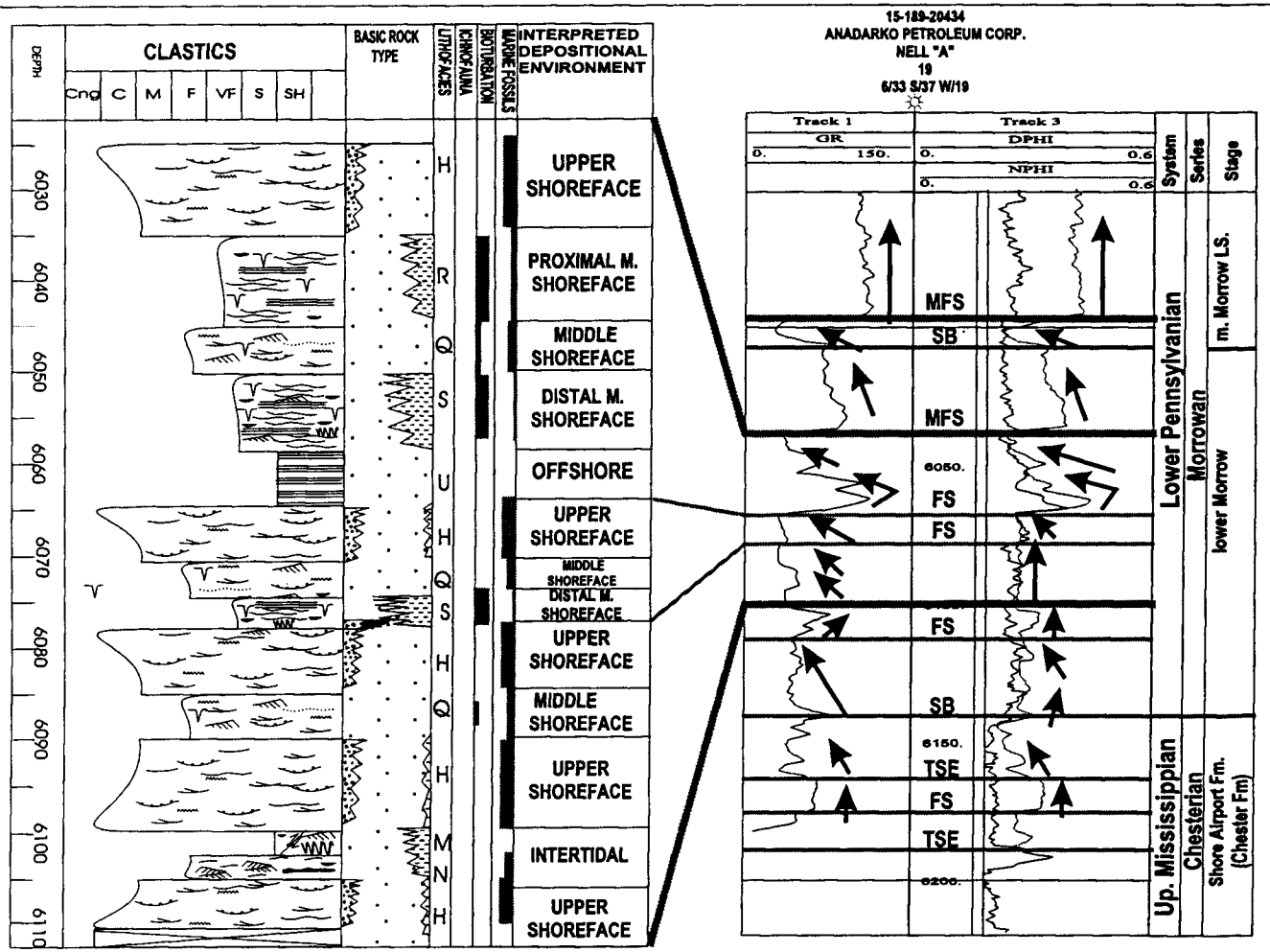

Figure 6.3 Core description and wireline log suite for the Nell "A". Black arrows show wireline log trends of gamma ray, neutron porosity and bulk density. Note: the stacked parasequences; MFS, major flooding surfaces; TSE, transgressive surfaces of erosion; FS, flooding surfaces. See figure 2.1a for explanation of symbols used on core description.

stratigraphic, published unit tops (Radar, 1987), combined with sequence-stratigraphic concepts.

A northwest–southeast cross-section was constructed between the cored wells (figures 6.2, 6.3). The middle Morrow flooding surface as determined by the wire-line logs served as datum for the cross-section (Appendix B, Figure B.1).

Core description

In Gentzler Field, two cores representing 206 feet of the lower Morrow and Mississippian rocks, were recovered from Gaskill "2A" (section 10, township 33S, range 38W) and Nell "A" (section 10, township 33S, range 37W) (figures 6.2, 6.3). The rock succession in Gentzler Field was subdivided into 10 facies based on grain size, sedimentary structures, biogenic structures, and constituents (Table 6.1). In general, the rock successions in both cores display shoaling-upward successions from a deep-water environment (Facies U) to a tidal channel and intertidal sand flat (Facies M and N). Two facies (Facies M and H) were encountered previously in the lower Morrow succession at Arroyo Field. Based on the lithostratigraphic correlation and the electrofacies model, the entire cored interval of the Nell "A" and the upper Gaskill "2A" (6035–5952 ft) represents lower Morrow strata (figures 6.2, 6.3).

Facies N

Facies N is a yellowish, herringbone cross-laminated, well-sorted, very fine-grained silty sandstone. Facies N is present in both the Gaskill "2A" (Figure 6.2) and

Facies	Lithofacies Description	Sedimentary Structures	Depositional Environments
M	light gray to black, deformed, interbedded siltstone and mudstone	Soft-sediment deformation structures (e.g. load bedding, convolute lamination, ball and pillow, load casts, and slumping features), mud laminae, ripple cross-laminations, wavy, lenticular and flaser bedding)	Tidal channel bank.
N	Yellowish, herringbone cross-laminated, well-sorted, very fine-grained silty sandstone	herringbone cross-lamination, ripple cross-lamination, climbing ripples, mud drapes, flaser bedding, bifurcated laminae, planar lamination and low and high angle cross lamination	Intertidal sand flat
H	Bioclastic, slightly bioturbated, moderately-sorted, pebbly medium-grained sandstone; Interbedded with pebbly conglomeratic medium-grained sandstone	Low angle cross-bedding and graded bedding	Upper shoreface
O	Greenish gray, very glacuonitic, moderately to very well-sorted, coarse to medium-grained sandstone	Low angle and planner cross- bedding, mud drapes, horizontal mud laminae, flattened mud lenses, discontinuous mud laminae, fining upward beds, and stylolitic structures	Upper shoreface
P	Light to dark gray fossiliferous, glacuonitic, low angle cross-bedded, medium to coarse-grained sandstone	Low angle cross bedding, ripple cross lamination, mud drapes, flaser bedding, shale laminae and ripple cross lamination	Upper shoreface
Q	Gray to brownish, well-sorted, calcite cemented, low angle cross-bedded, fine-grained sandstone	Low angle cross-bedding and discontinuous lamina associated with stylolitic structures	Middle shoreface
R	Bioturbated, yellowish, fine to medium-grained sandstone; interbedded with thin mud laminae and beds	Parallel lamination, wavy bedding, non-bioturbated sand and discontinuous shale laminae	Middle shoreface
S	Highly bioturbated interbedded gray to greenish fine-grained silty sandstone and black mudstone	Cross and parallel laminations, lenticular and wavy bedding, and soft-sediment deformation features (e.g. pillow and contorted bedding).	Middle shoreface
T	Black intensely bioturbated, fine to very fine-grained sandstone and siltstone	Intense bioturbation	Lower shoreface
U	Dark greenish-gray, parallel laminated, argillaceous mudstone	Parallel lamination and locally present erosive surfaces floored with bioclastic fragments.	Offshore

Table 6.1 Summary of lithofacies and interpreted depositional environments observed in Gentzler Field.

Nell "A" (Figure 6.3). Ripple cross-lamination, reactivation surfaces, climbing ripples, mud drapes, flaser bedding, bifurcated laminae, planar lamination, low- and high-angle cross lamination, and herringbone cross lamination are the dominant sedimentary structures observed within Facies N (figures 6.4a, b). Abundant carbonized wood fragments and rare marine bioclasts were observed. Facies N has a sharp contact with Facies M, H, P, and U (figures 6.2, 6.3). The wireline-log responses of Facies N were a relatively low gamma-ray, a high PEF, and a relatively low porosity that were similar to electrofacies Be (figures 6.2, 6.3).

The presence of well-developed herringbone cross-laminations, along with mud drapes, flaser bedding, bifurcated laminae and reactivation surfaces, indicate a strong bi-directional current. The high degree of sorting and grain size suggests high-energy conditions. From the presence of carbonized wood fragments, I inferred a nearshore setting. Facies N was previously assigned to Facies 9 and Facies D, which were described by Wheeler et al., (1990) and Franz (1985), respectively. Wheeler et al., (1990), interprets this facies to be a fluvial or marine shoreface deposit, whereas Franz (1985) argues that it represents a relatively low energy, shallow nearshore deposit. On the basis of its stratigraphic position in relationship to facies M, H, and P and its internal sedimentary structures, I interpret Facies N to have been deposited in a high-energy intertidal environment, such as a tidal flat.

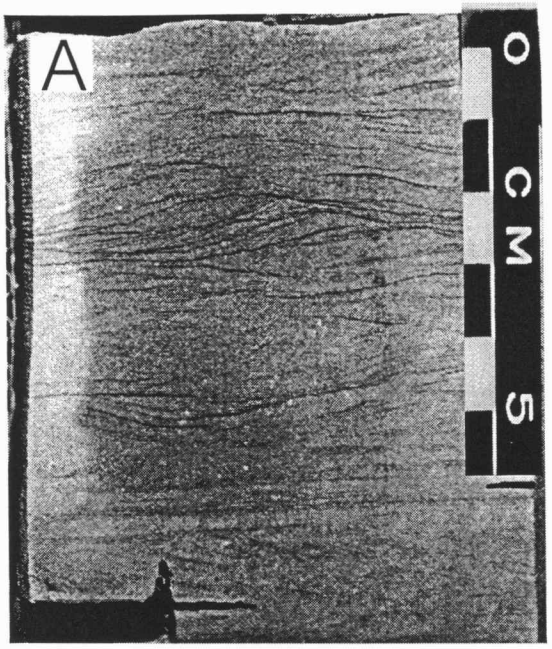

Figure 6.4 Facies N. a) Climbing ripple marks and mud drapes (Gaskill "2A" 10-1); b) Herringbone structures, ripple cross lamination marks and mud drapes (Nell "A"19-1) .

Facies O

Facies O is a greenish-gray, very glauconitic, moderately- to very well-sorted, coarse- to medium-grained sandstone. Facies O is present only in Gaskill "2A" (Figure 6.2). High concentrations of glauconite, relatively high mud content, and low degree of bioturbation and fossil content characterize Facies O (Figure 6.5a). The base of Facies O shows a few mud clasts and abundant fossil fragments. The primary sedimentary structures in Facies O are low-angle and planar cross-bedding, mud drapes, horizontal mud laminae, flattened mud lenses, discontinuous mud laminae, fining-upward beds and stylolites. Scattered pyrite nodules were also observed. *Palaeophycous* and *robust Arenicolites* are the ichnofauna observed in Facies O (figures 6.5b, c). Facies O shows a general fining-upward trend that coincides with improved sorting and with the absence of cross stratification. Facies O has sharp contact with Facies C and an erosional contact with Facies U (figures 6.3, 6.5a). The wireline-log responses of Facies O were a relatively low gamma-ray, high PEF, and relatively low porosity (Figure 6.2). The wireline-log responses were similar to electrofacies Be. The lithostratigraphic correlation suggests that Facies O should be interpreted as Chesterian (Radar, 1987).

The high concentrations of glauconite indicate an open marine condition. The lag deposits at the base of Facies O suggest a scouring and filling process that may be related to a relative fall of sea-level and the end of a flooding event. This interpretation is consistent with the presence of shelf mud (Facies U) both above and below Facies O (Figure 6.13). Weimer et al., (1988), and Sonnenberg et al., (1990),

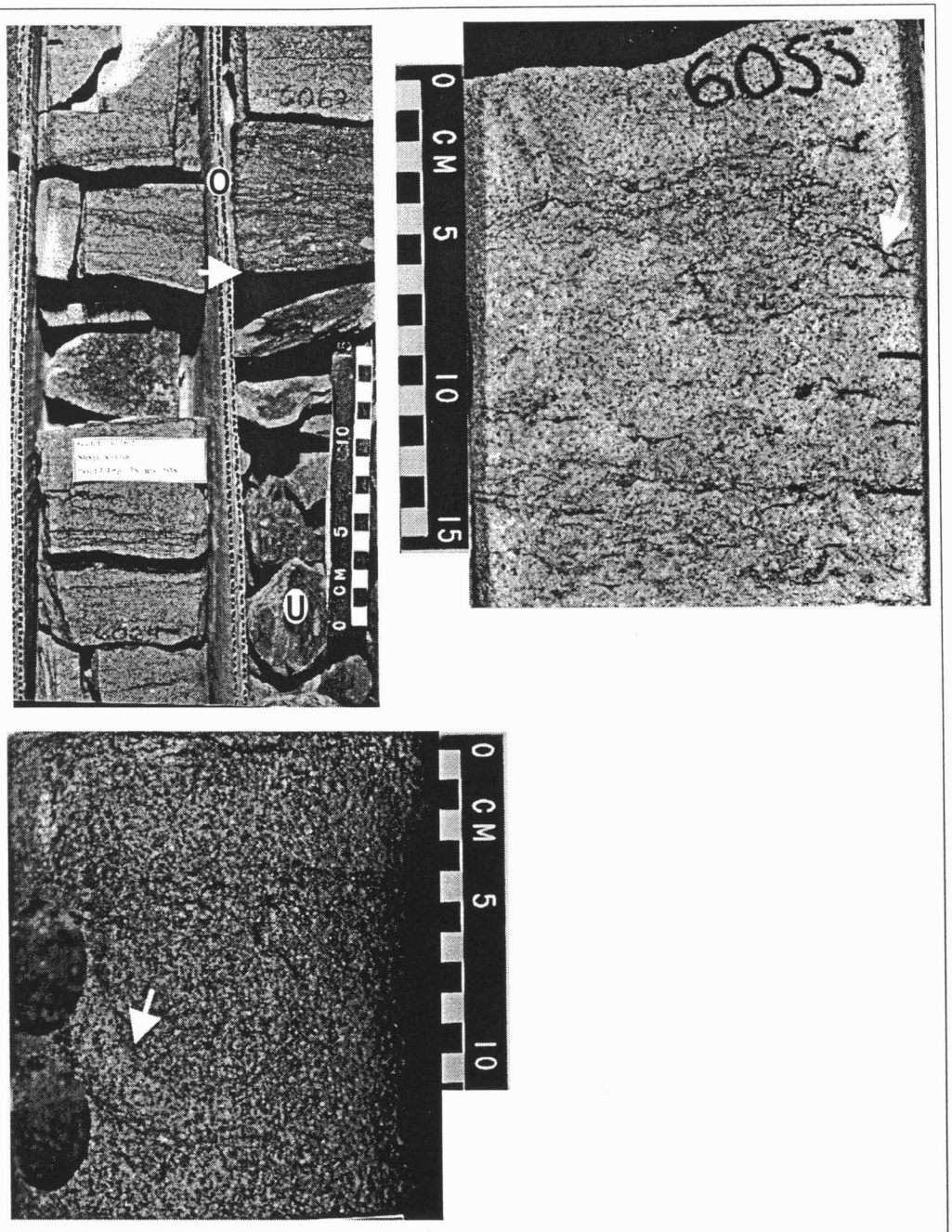

Figure 6.5 Facies O. a) The erosional contact (arrow) between facies U and O. Note: the abundance of shale laminae. White dots are fossils fragment;
b) slight bioturbation and possible *Palaeophycous* (arrow);
c) robust A*renicolites* (arrow) (Gaskill "2A" 10-1).

interpreted the erosive surface as transgressive surface of erosion (TSE). *Palaeophycous* and *robust Arenicolites* provide examples of the *Skolithos* ichnofacies (Pemberton and MacEachern, 1992). Low-angle cross bedding, the *Skolithos* assemblage, and the absence of hummocky cross-stratification indicate a shallow, high-energy environment. Fining-upward beds and the low degree of bioturbation suggest periodic fluctuations in the current energy. This interpretation is consistent with the presence of mud drapes and laminae, which indicate a slight tidal influence. The fining-upward sequence and the improved sorting that can be seen in the upper part of Facies O suggest periods of high-energy events and a reworking of sediments. This interpretation is supported by the absence of trace fossils and by the facies' high-energy sedimentary structures.

Facies O was previously assigned to Facies 6 and Facies C, which were described by Wheeler et al. (1990) and Franz (1985), respectively. Wheeler et al. (1990) interpret this facies to be a fluvial or estuarine deposit, whereas Franz (1985) argues that it represents an offshore sandbar deposit. On the basis of its erosional contact with the underlying facies U and its internal sedimentary structures, I interpret Facies O to have been deposited in a shallow, open marine shoreface environment.

Facies P

Facies P is light- to dark-gray, fossiliferous, glauconitic, low-angle cross-bedded, medium- to coarse-grained sandstone. Facies P is only present in Gaskill "2A" (Figure 6.2). Abundant marine fossil fragments, sparse mud drapes and shale

laminae characterize Facies P. Low-angle cross bedding and ripple cross lamination are present (Figure 6.6). Erosive surfaces floored with scattered mud clasts and quartz-pebbles are locally present. Mud drapes, flaser bedding, shale laminae and ripple cross lamination are common within the finer-grained intervals. Articulate brachiopods and echinoderm fragments are the main bioclastic constituents. Facies P has erosional contact with Facies U and sharp contact with Facies N (Figure 6.2). The wireline-log responses of Facies P were a relatively low gamma-ray and high porosity that were similar to electrofacies Be (Figure 6.2).

The presence of articulate brachiopods, echinoderm fragments, and glauconite suggest an open marine condition. The absence of bioturbation and hummocky cross stratification, along with the presence of low-angle cross-bedding, indicate a shallow, high-energy depositional environment. Large-scale foresets beds suggest migration of subaqueous megaripples. The presence of mud drapes, cross-lamination, and flaser bedding, as well as the presence of erosive surfaces, suggest a tidal influence and periodic fluctuations in current energy. The erosive surface at the base of Facies P was interpreted as transgressive erosional surface (TSE; Weimer et al., 1988; Sonnenberg et al., 1990). Facies P corresponds to Facies 6 and A (Wheeler et al., 1990; Franz, 1985). Wheeler et al., (1990) interpret Facies 6 to have been deposited in an upper shoreface or a tidal channel environment, whereas Franz (1985) interprets Facies A to have been deposited in a shallow marine environment under moderately fluctuating conditions.

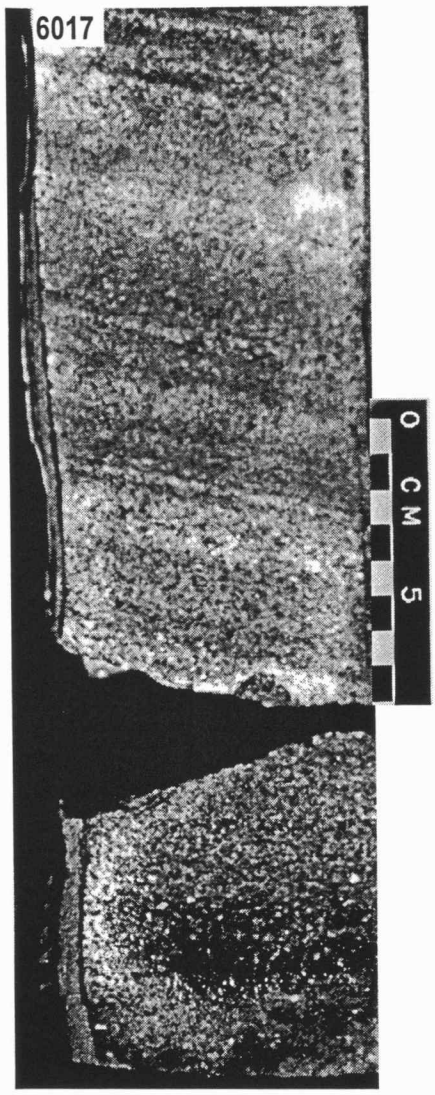

Figure 6.6 Facies P from the Gaskill "2A" 10-1. Low-angle cross-bedded coarse to medium-grained sandstone.

On the basis of its stratigraphic position between facies U and the overlying facies N, and its sedimentary structures, I believe Facies P was deposited in a high-energy upper shoreface environment, such as a barrier island.

Facies Q

Facies Q is gray to brown, well-sorted, calcite-cemented, low-angle cross-bedded, fine-grained sandstone. Facies Q is only present in Nell "A" (Figure 6.3). Low-angle cross bedding, ripple cross-lamination and a high degree of sorting characterizes Facies Q. Facies Q differs from Facies N by the absence of herringbone cross-stratification. Thin, coarse-grained sandstone beds with erosional bases are occasionally interbedded in Facies Q. Discontinuous laminae that are associated with stylolitic structures are locally present. Bioclasts are rare except for a few echinoderm fragments. *Skolithos, Ophiomorpha, Rosselia, Asterosoma* and *Conichnus* are the trace fossils observed in Facies Q (Figure 6.7a). Facies Q has a sharp contact with Facies R, S and H (Figure 6.7b). The wireline-log responses of Facies Q were a relatively low gamma-ray and a high porosity that were similar to electrofacies Be.

The presence of echinoderm fragments and well-developed and diverse trace fossils, along with the absence of carboniferous fragments, suggest an open marine environment. The trace fossils found within Facies Q represents suspension feeding species and suggest a *Skolithos* assemblage (Pemberton and MacEachern, 1992).

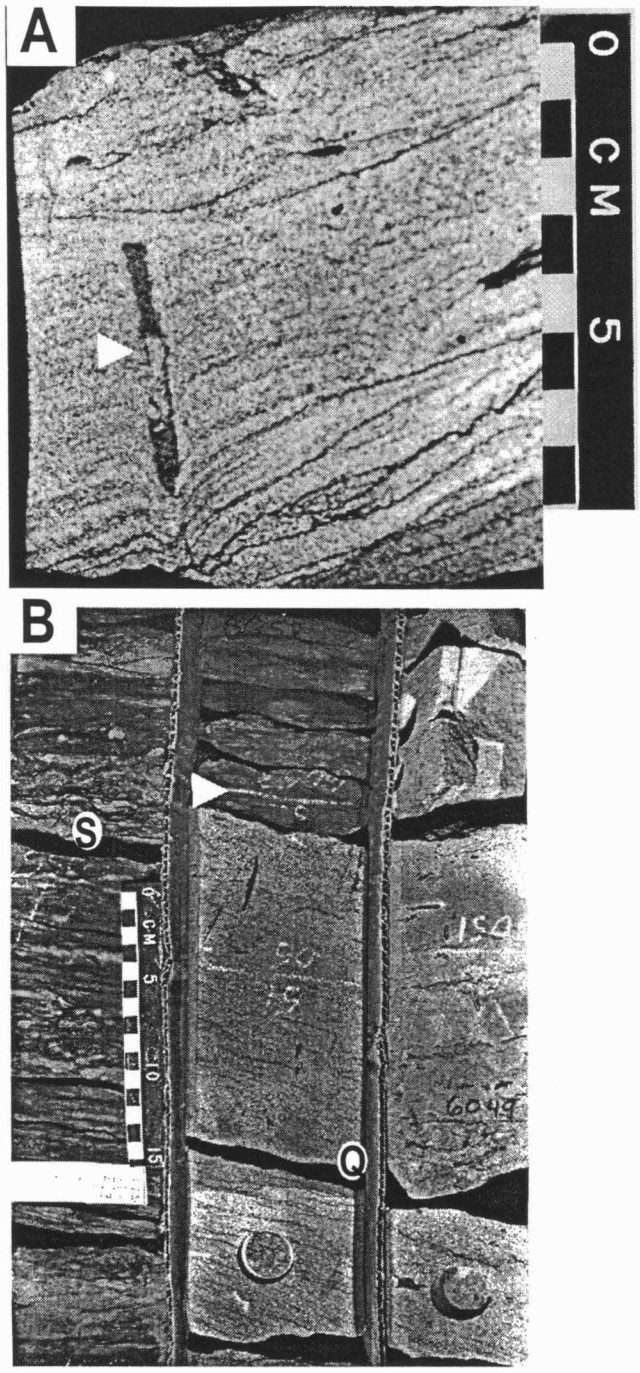

Figure 6.7 Facies Q from the Nell "A"19-1. a) Low-angle cross-bedding and shale laminae within well sorted fine- to medium-grained-sandstone. Note: The *Skolithos* burrow (arrow); b) a sharp contact between facies Q and S (arrow).

From the presence of low-angle cross bedding and ripple cross-lamination, along with the well-sorted nature of Facies Q, I infer a high-energy depositional setting. This interpretation is supported by the dominance of the *Skolithos* assemblage, which requires high-energy conditions in order to keep organic particles suspended (Pemberton and MacEachern, 1992). Periodic appearance of thin beds of coarse-grained sandstone with erosive bases (interbedded occasionally with *Skolithos* burrows), the well-sorted, fine-grained sandstone, and the absence of herringbone cross stratification, mud drapes, reactivation surfaces suggest periodic fluctuations in the current energy and in sediment supply. The variation in sediment supply may have been the result of storm events.

Facies Q resembles Facies 9 of Wheeler et al. (1990) and Facies G of Franz (1985). Wheeler et al., (1990) interpreted Facies 9 as fluvial or middle shoreface deposits, whereas, Franz (1985) interpreted Facies G as back barrier deposits. On the basis of its stratigraphic position and internal structures, Facies Q is interpreted to have been deposited in middle shoreface environments.

Facies R

Facies R is a yellow, bioturbated, fine- to medium-grained sandstone interbedded with thin mud laminae and beds. Facies R is only present in Nell "A"(Figure 6.3). A higher sand content distinguishes Facies R from other bioturbated facies. Parallel lamination, flaser and wavy bedding are observed within the

Figure 6.8 Facies R from the Nell"A" 19-1. *Palaeophycous* (arrows). Note: the high-sand content, flaser and shale laminae, low angle cross-bedding and shale laminae.

unbioturbated sand. *Teichichnus, Palaeophycous, Planolites, Chondrites* and *Rhizocorallium* are the main trace fossils (Figure 6.8). The burrows found within Facies R are filled with a fine- to medium-grained sandstone. Facies R has sharp contact with Facies H and Q (Figure 6.3). The wireline-log responses of Facies R were a relatively high gamma-ray, and a high porosity. Based on the wireline-log responses Facies R is assigned to electrofacies Ce.

In Facies R the trace fossils are dominated by the vertical and horizontal feeding structures of deposit feeders and represent the *Cruziana* ichnofacies (Pemberton and MacEachern, 1992). The diversity and abundance of the ichnofauna suggest an open marine condition. The dominance of *Planolites* and *Chondrites* indicates low oxygen bottom-water conditions (Pemberton and MacEachern, 1992). A high degree of bioturbation and the presence of shale laminae suggest a low-energy condition and a relatively slow sedimentation rate.

Facies R is similar to Facies 9 of Wheeler et al. (1990) and Facies G of Franz (1985). Wheeler et al., (1990) interpreted Facies 9 as fluvial or middle shoreface deposits whereas Franz (1985) interpreted Facies G as back barrier deposits. On the basis of its stratigraphic position and sedimentary structures, I believe that Facies R was deposited in a proximal middle shoreface environment.

Facies S

Facies S comprises highly bioturbated, interbedded, gray to green-gray, fine-grained, silty sandstone and black mudstone. Facies S is only present in Nell "A" (Figure 6.3). Facies S can be distinguished from facies T by the degree of bioturbation and the presence of the primary sedimentary structures. It can be distinguished from Facies R by the abundant mud content. Cross and parallel-laminations and lenticular and wavy bedding are observed within the sand intervals (figures 6.9a, b). Soft-sediment deformation features, such as pillow and contoured bedding, can be seen. Facies S shows an up-section increase in mud content. *Teichichnus*, *Palaeophycous*, *Planolites*, and *Chondrites* are forms that dominate the ichnofauna found within Facies S (Figure 6.9c). Facies S has sharp a contact with Facies R and U (Figure 6.3). The wireline-log responses of Facies S were a relatively high gamma-ray, and a high porosity. Based on the wireline-log responses Facies S is assigned to electrofacies Ce.

The diversity and abundance of the ichnofauna suggest an open marine environment. The trace fossils are dominated by the vertical and horizontal feeding structures of deposit feeders and represent the *Cruziana* ichnofacies (Pemberton and MacEachern, 1992). An abundance of *Chondrites* and *Planolites* suggests low oxygen bottom-water conditions (Pemberton and MacEachern, 1992). The interbedded silty sandstone and black mudstone suggest alternations between high-.

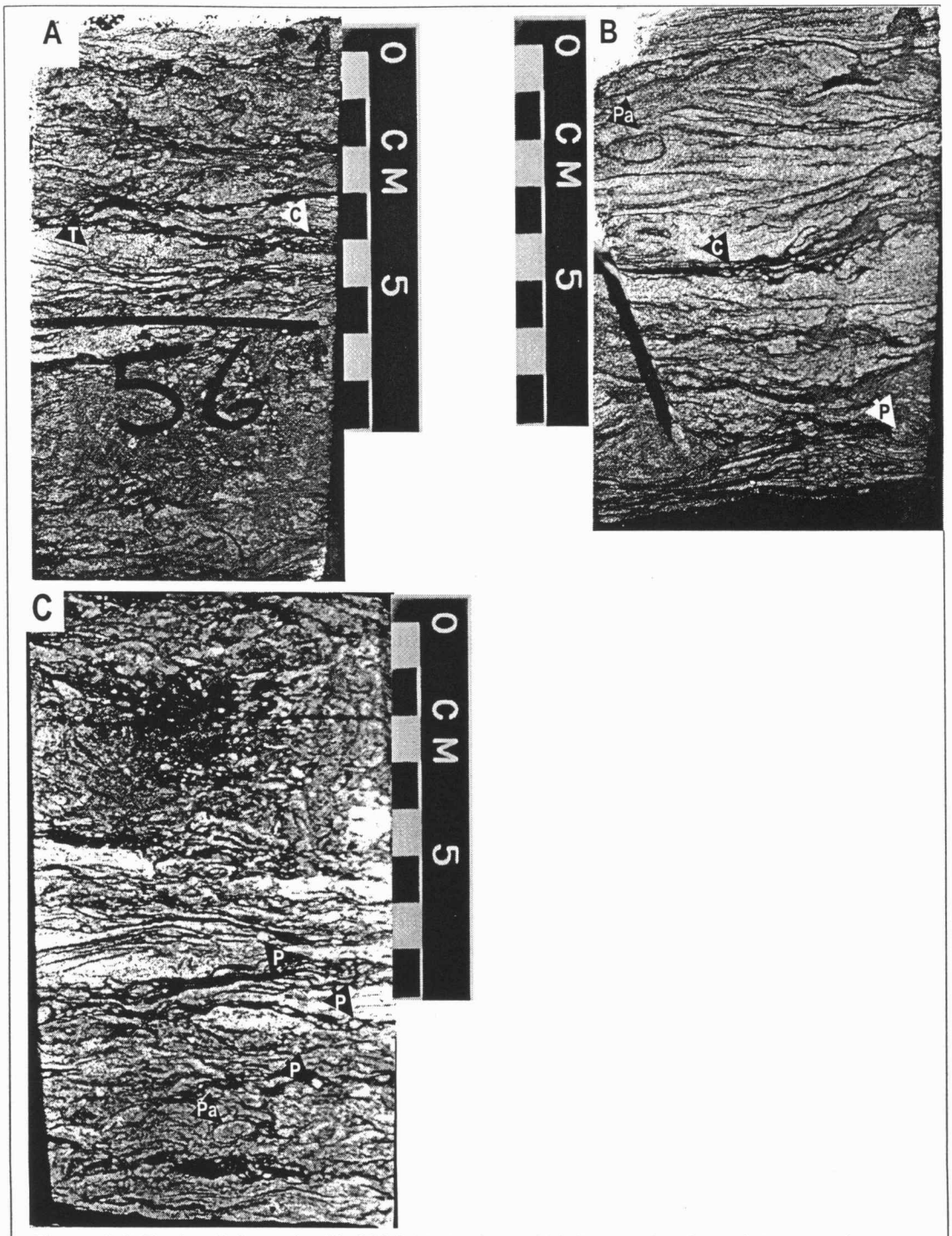

Figure 6.9 Facies S from the Nell "A" 19-1. a), and b) fine-grained sandstone and mudstone with ripple and mud laminae; c) Cruziana ichnofauna assemblage. P, *Planolites*; Pa, *Palaeophycous*; T, *Teichichnus*; C, *Chondrites*.

and low-energy conditions. The high degree of bioturbation indicates a relatively slow sedimentation rate (Pemberton and MacEachern, 1992).

Facies S is similar to Facies 9 of Wheeler et al. (1990) and Facies G, of Franz (1985). On the basis of its stratigraphic position and sedimentary structures, I interpret Facies S to have been deposited in a distal to middle shoreface environment

Facies T

Facies T is a black, intensely bioturbated, fine to very fine-grained sandstone and siltstone. Facies T is only present in Gaskill "2A" (Figure 6.2). Intense bioturbation and a lack of preservation of any primary sedimentary structures distinguish Facies T from other bioturbated facies (Figure 6.10a). The base of Facies T consists of lag deposit (3 cm) that is composed of round mud and sand clasts (Figure 6.10b). The primary ichnofauna observed in Facies T are *Planolites, Chondrites, Rhizocorallium, Diplocraterion, Teichichnus, Zoophycos, Cylindrichnus, Palaeophycous, Ophiomorpha,* and *Skolithos.* Facies T has a sharp contact with Facies U and an erosional contact with Facies O (figures 6.2, 6.10b). The wireline-log responses of Facies T were a relatively high gamma-ray and a high porosity that were similar to electrofacies Ce.

The trace fossils are dominated by the vertical and horizontal feeding structures of deposit feeders, representing the *Cruziana* ichnofacies (Pemberton and MacEachern, 1992). The diversity and abundance of the ichnofauna suggests open

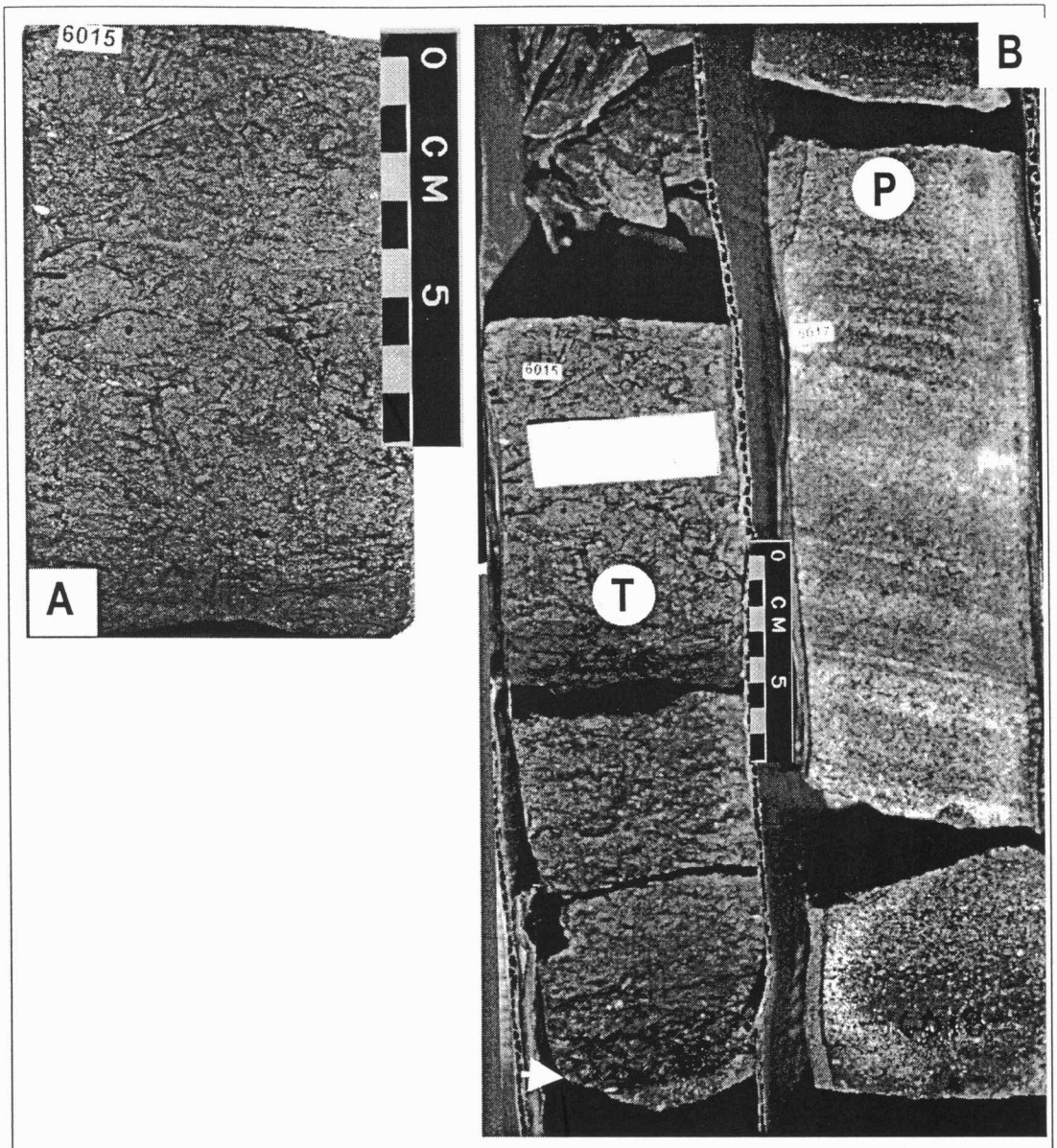

Figure 6.10 Facies T from the Gaskill "2A" 10-1. a) Intensely bioturbated fine-grained sandstone; b) Erosional contact between facies P and T. Note: the lag deposits at the base of facies T (arrow).

marine conditions. The high degree of bioturbation indicates a low-energy condition and a slow sedimentation rate (Pemberton and MacEachern, 1992). The lag deposits at the base of Facies T are interpreted to represent a period of sea-level fall and erosion followed by a rapid rise of sea-level. Facies T is similar to Facies 9 and Facies G, which were described by Wheeler et al. (1990) and Franz (1985), respectively. On the basis of its stratigraphic position and sedimentary structures, Facies T is interpreted to have been deposited in a lower shoreface environment.

Facies U

Facies U is a dark greenish gray, parallel-laminated, argillaceous mudstone. Facies U was observed in both Gaskill "2A" and Nell "A" (figures 6.2, 6.3). Parallel laminations and occasional erosive surfaces floored with bioclastic fragments are present in Facies U (Figure 6.11a). Brachiopods and echinoderm fragments are the primary bioclastic constituents. Facies U has erosional contacts with Facies O, H, and D (figures 6.2, 6.3, 6.11b). The wireline-log responses of Facies U, a high gamma-ray, and low porosity, were similar to electrofacies Ce.

The absence of siltstone and sandstone suggest a starved depositional setting. The preservation of thin mud laminae and the absence of trace fossils and bioturbation indicate a low-energy and a slow sedimentation rate under anoxic bottom-water conditions of a deep-water environment. The local presence of erosive surfaces, overlain by bioclast-rich intervals, suggests short periods of high-energy

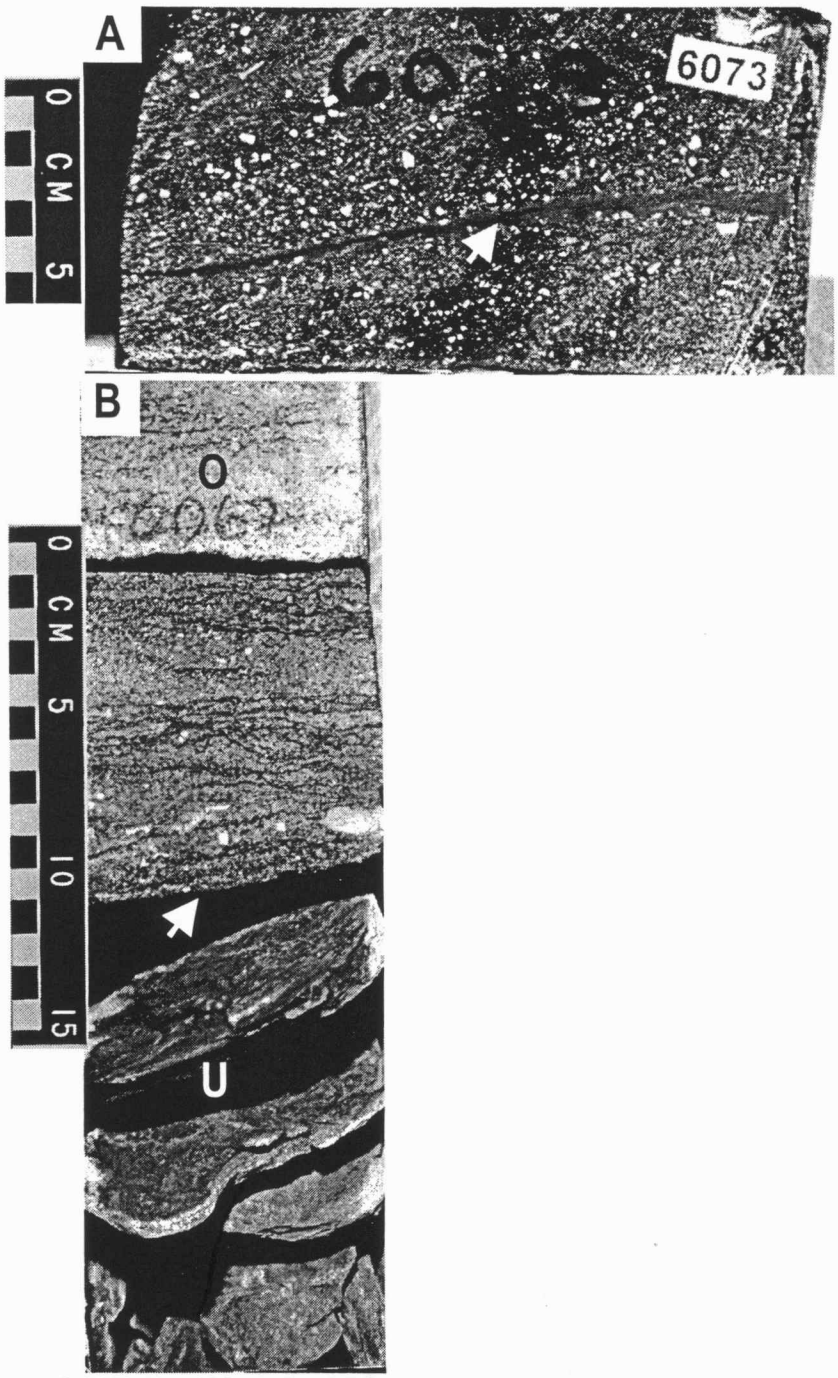

Figure 6.11 Facies U from Gaskill "2A" 10-1. a) A thin mud lamina(arrow) within bioclastic-rich mudstone; b)Erosional contact between facies U and O. Note: the lag deposits at the base of facies O (arrow).

events that disturbed the sea-floor mud and introduced bioclastic fragments. Facies U records a major marine flooding event and a shutting down of siliciclastic sources. The erosional contact that separates Facies U from Facies O records a relative fall in sea-level and indicates surfaces of erosion (Figure 6.13).

Facies U resembles Facies 1, described by Wheeler et al. (1990). Wheeler et al., (1990) interpreted Facies 1 to represent offshore deposits. I concur with Wheeler et al. (1990), and interpret Facies U to have been deposited in an offshore environment.

The depositional model of the lower Morrow at Gentzler Field

The electrofacies model was used to define four laterally continuous surfaces across the Gentzler Field. These surfaces are overlain by onlapping strata and record a basinward shift in facies from electrofacies Ce to electrofacies Be (Appendix B, Figure B.1). Each of the four surfaces correlated across the Gentzler Field were interpreted to represent a sequence boundary (SB) (Weimer et al., 1988). Three of the observed sequence boundaries were found within the Mississippian strata. The lower sequence boundary (labeled SB1 in Appendix B, Figure B.1) separates the St. Genevieve Limestone from the Shore Airport Formation (Chester Formation), which consists of two sequences. The lower sequence is composed of marine sandbodies (electrofacies Be) that were separated by a deep-water marine shale (electrofacies Ce).

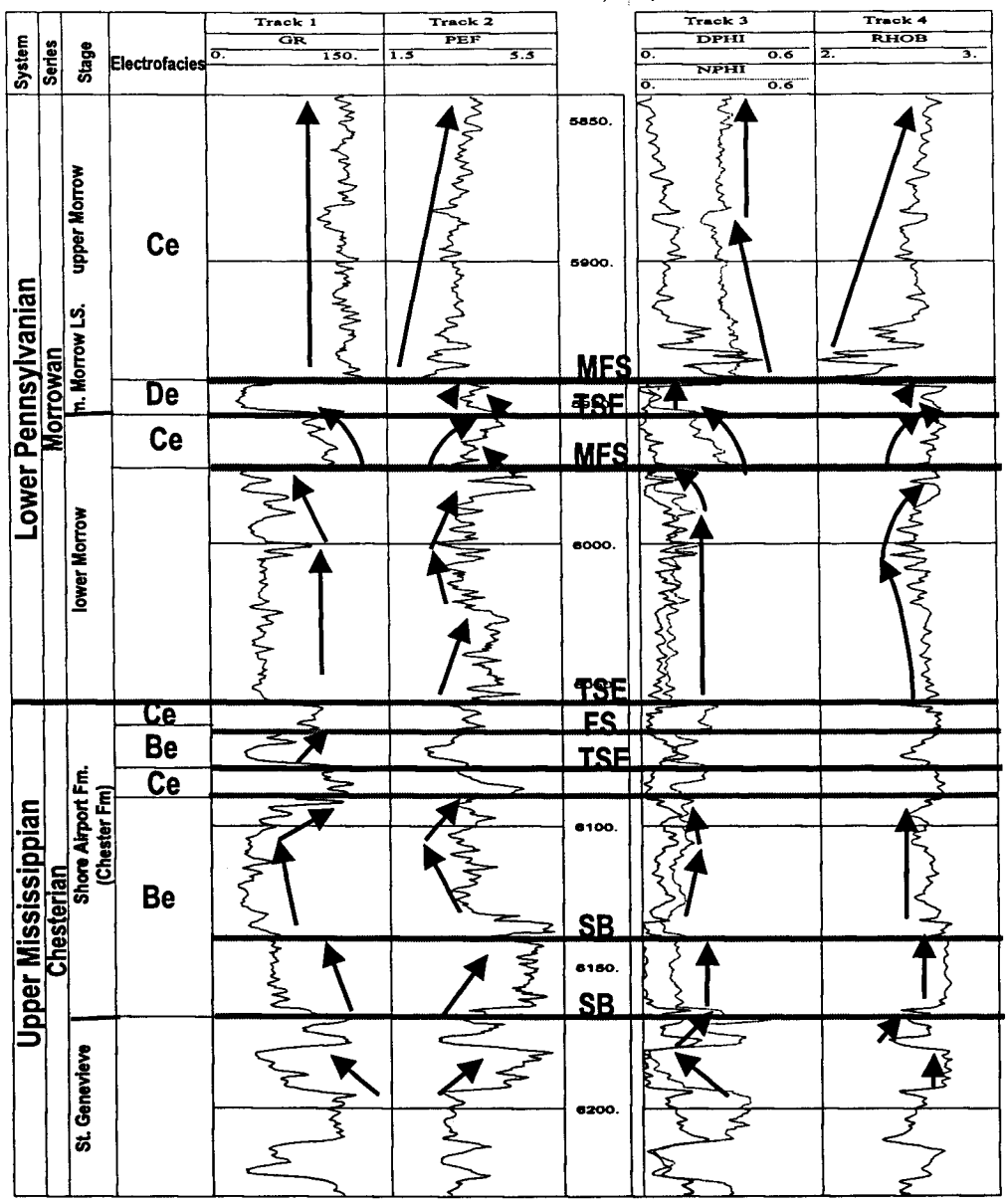

Figure 6.12a Mayberry "B" type log and stratigraphic interpretation. Black arrows show wireline log trend. Note: the stacked parasequence. MFS, maximum flooding surface; TSE, transgressive surface of erosion; FS, flooding surface; TK, thickening units; TN, thinning units.

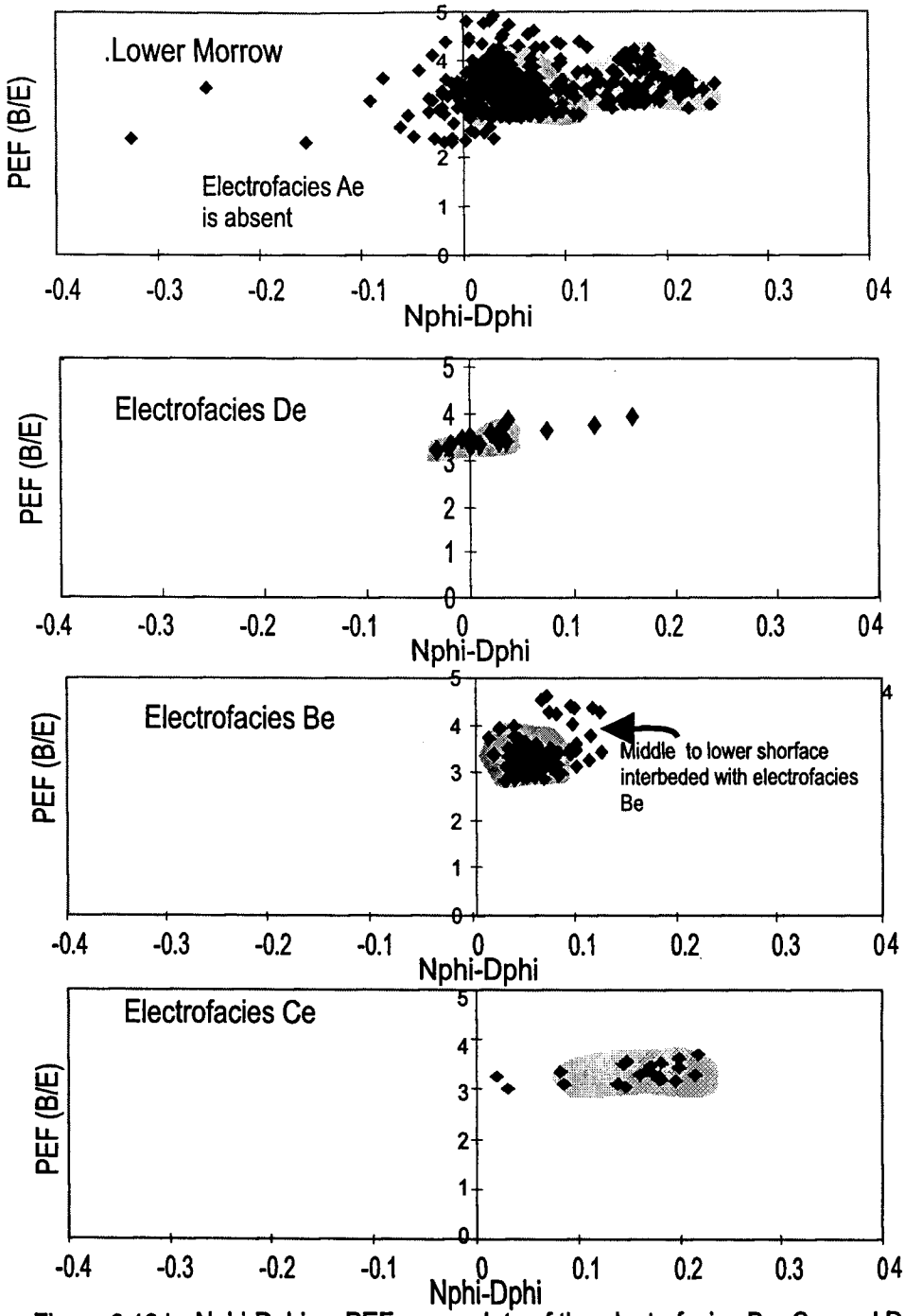

Figure 6.12.b Nphi-Dphi vs PEF cross-plots of the electrofacies Be, Ce, and De, that are found within Mayberry "B" 12-1.

The lower marine sandbodies are separated from the overlying marine shale by a flooding surface (labeled FS in Appendix B, Figure B.1). The upper marine sandbodies (electrofacies Be) are separated from the underlying marine shale by a transgressive surface of erosion (labeled TSE in Appendix B, Figure B.1; Weimer et al., 1988). The upper Chesterian sequence was observed in Mayberry "B" (section 12, T 33 S/R 38 W; figures 6.12a, b). The electrofacies model shows that the upper sequence is bounded by a sequence boundary (labeled SB2 in Appendix B, Figure B.1) that has a valley-like shape. This interpretation is supported by an abrupt truncation of marine shale (electrofacies Ce) across the Mayberry "B" sequence boundary and the different wireline signatures of the sandbodies of Mayberry "B" relative to the observed sandbodies across the field (figures 6.12a, b). The incised-valley fill is represented by clean gamma-ray (30 API), relatively low PEF ($\cong$ 3.5 B/E), moderately low Rhob ($\cong$ 2.6 g/cc) and high porosity (8 %). On the northwestern side of the study area, the Chesterian strata are overlain by another marine shale (electrofacies Ce). This marine shale truncates against the sequence boundary (SB3) southeast of Mayberry "B" and is overlain by younger sandbodies (electrofacies Be). The Chesterian sequences are separated from the lower Morrowan strata by a sequence boundary that is considered to be the pre-Pennsylvanian unconformity (labeled SB3 in Appendix B, Figure B.1).

The electrofacies model shows that the lower Morrowan strata consist of three shallow marine sandbodies (electrofacies Be) (labeled unit 1, 2 and 3 in Appendix B, Figure B.1) that dip towards the southeast (Appendix B, Figure B.1). The lower,

shallow marine sandbodies (electrofacies Be; labeled unit 1 in Appendix B, Figure B.1) were observed only in the southeast of the study area, pinchout towards the northwest of the Mayberry "B, and have an onlap relationship with the pre-Pennsylvanian sequence boundary (labeled SB3 in Appendix B, Figure B.1). An offshore shale (electrofacies Ce) overlies these lower, shallow marine sandbodies (electrofacies Be). This offshore shale also truncates northwest of the Mayberry "B" against the pre-Pennsylvanian unconformity. The offshore shale is separated from the underlying shallow marine sandstone (unit 1) by a flooding surface (labeled FS in Appendix B, Figure B.1) and by a sharp contact with the overlying middle shallow marine sandbodies (unit 2; electrofacies Be).

The middle and upper shallow marine sandbodies (electrofacies Be) cover the entire study area. They are separated by a deep marine shale (electrofacies Ce) that thickens toward the southeast. The offshore shale is separated from the underlying middle shallow marine sandstone (unit 2) by a flooding surface (labeled FS in Appendix B, Figure B.1) and by a sharp contact with the overlying upper shallow marine sandbodies (unit 3). The sharp erosional contacts are interpreted as diastem surfaces (Weimer et al., 1986).

Another relatively thick, widespread deep marine shale (electrofacies Ce) overlies the upper shallow marine sandbodies. This deep marine shale records an extensive flooding event and a shutting down of the siliciclastic sources. This interpretation is supported by the changes in sandstone thicknesses and wireline-log profiles across this deep marine shale. The bounding surface that separates this deep

marine shale from the underlying upper shallow marine sandbodies is interpreted as a maximum flooding surface (labeled MFS in Appendix B, Figure B.1).

A thin, tight, southeast thickening, shallow marine, informally called middle Morrow limestone (electrofacies De) is separated from the underlying thick marine shale by a regionally extensive erosion surface and is overlain by maximum flooding surface (labeled SB.4 and MFS in Appendix B, Figure B.1). This erosion surface is interpreted as sequence boundary (SB.4) separating lower and middl Morrow sequences. An extensive maximum flooding event was inferred from the thick deep marine shale interval that overlies the informally called middle Morrow limestone (electrofacies Ce; Appendix B, Figure B.1).

In the lower Morrow of Gentzler Field, the electrofacies model shows that electrofacies Ae and Ee were absent and only electrofacies Be, De, and Ce were present (Appendix B, Figure B.1). The lithostratigraphic correlation, as displayed in the cross-section, indicates that the pre-Pennsylvanian sequence boundaries did not show valley-like geometries and did not correlate laterally to interfluves. The electrofacies model and correlation indicate that the lower Morrow succession was deposited in an open marine environment that consisted of a series of shoreface deposits (electrofacies Be). Each shoreface succession (electrofacies Be) was overlain by an offshore, fine-grained facies (electrofacies Ce); an example of this shoreface succession is Gaskill "2A" (figures 6.2, 6.13). This interpretation, supported by the geometries and distributions of electrofacies Be and Ce and their onlapping with relationships with sequence boundaries. The backstepping of

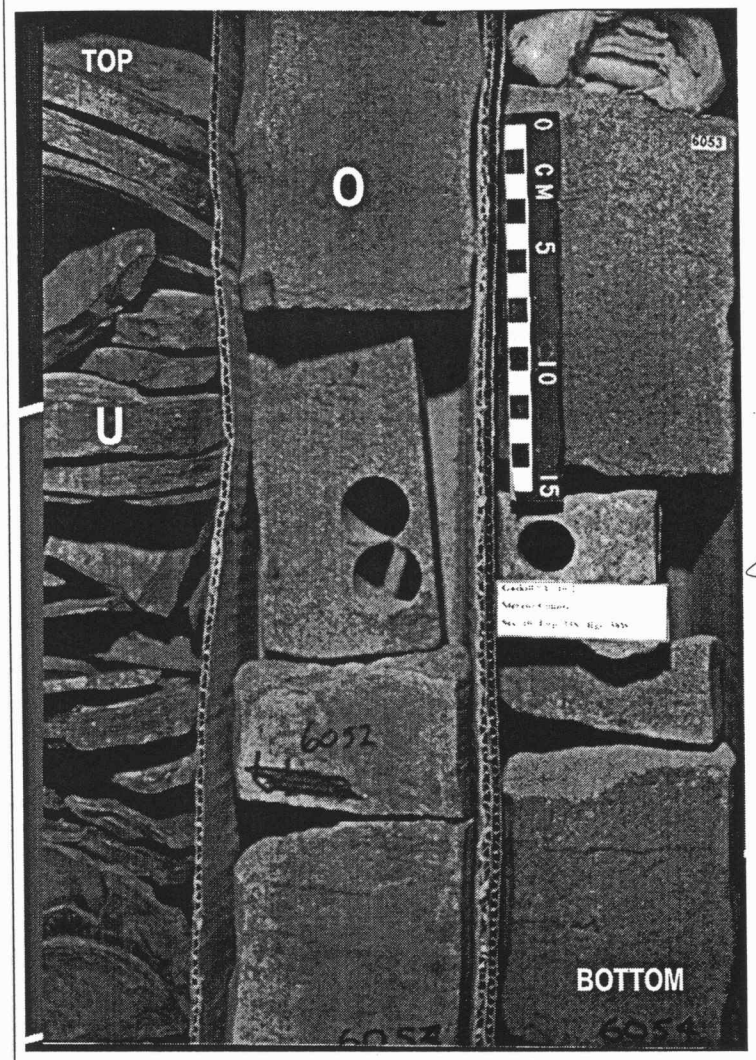

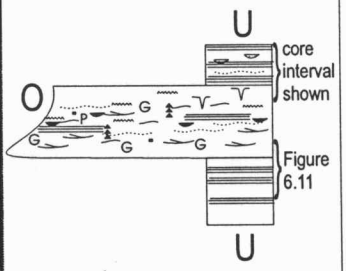

Figure 6.13 Abrupt transition from the upper shoreface (below) into shelf mudstone (above) suggesting an abrupt increase in accommodation spaces (drowning). (Gaskill "2A" 1-10).

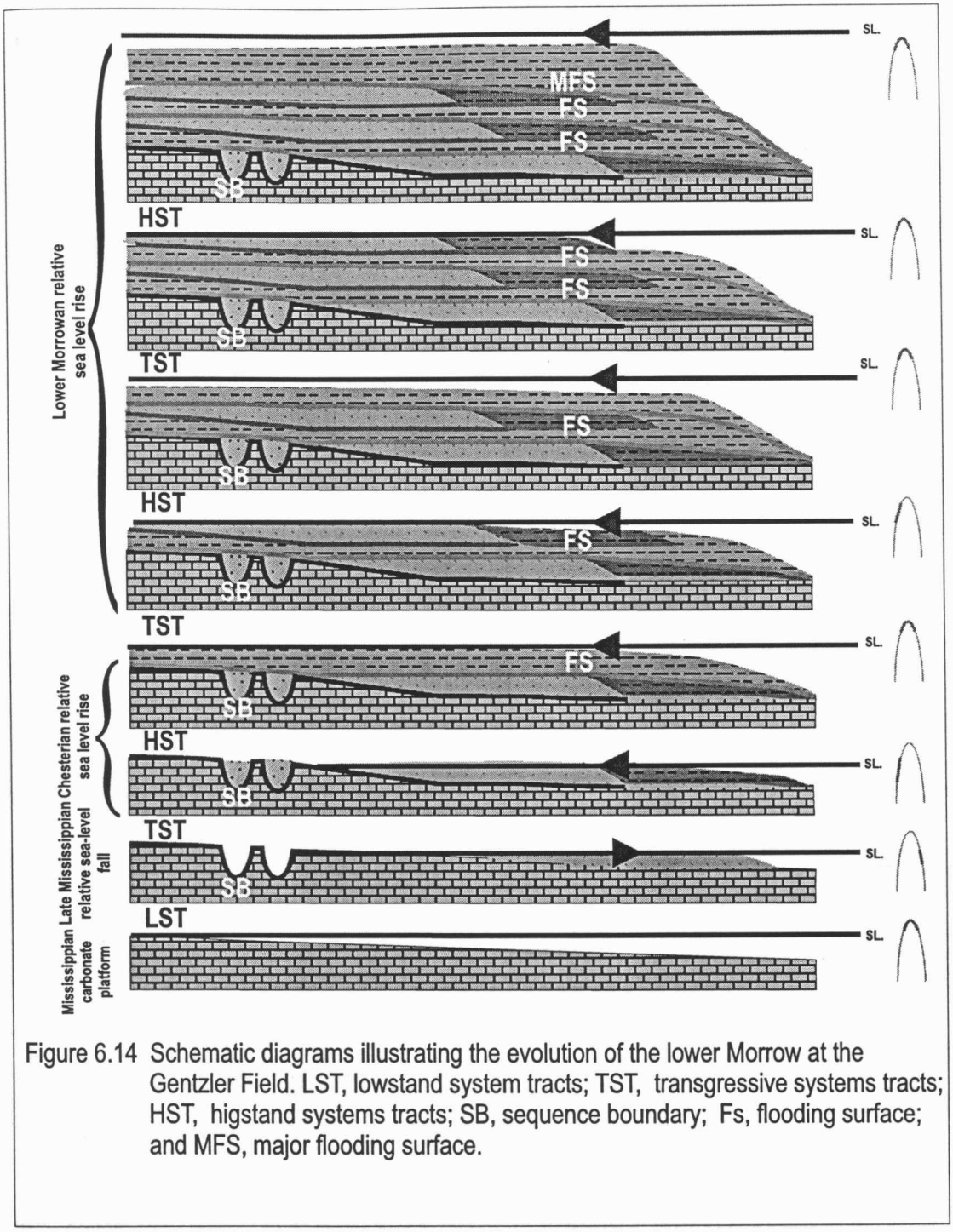

Figure 6.14 Schematic diagrams illustrating the evolution of the lower Morrow at the Gentzler Field. LST, lowstand system tracts; TST, transgressive systems tracts; HST, higstand systems tracts; SB, sequence boundary; Fs, flooding surface; and MFS, major flooding surface.

electrofacies Be suggests rapid relative sea-level rises. (Appendix B, Figure B.1) (Figure 6. 14).

Core descriptions at Gentzler Field show that Facies A, B, and K are not present in the lower Morrow successions (figures 6.2, 6.3). They also show that the lower Morrow sequence in Gentzler Field is composed of coarsening-upward successions that range from fine-grained, low-energy, deep-water facies (Facies U and electrofacies Ce; Figure 6.11b), to coarse-grained, high-energy, shallow-water facies (Facies H and electrofacies Be; figures 6.2, 6.3, 6.14, 6. 15).

Cores from both Gaskill "2A" and Nell "A" show abrupt transitions from low-energy, bioturbated, lower shoreface deposits and offshore mudstone (Facies R, S, T and U) to high-energy, shallow, upper shoreface deposits (Facies O, P and H; Figure 6.5a). The rapid basinward transitions of the facies can be attributed to the rapid change in either accommodation space or in sediment supply during lower Morrow deposition (figures 6.10b, 6. 14). These changes may only be of local extent. Facies as defined by core are consistent with the electrofacies model (Figure 6.13).

Previous studies have attributed the Pennsylvanian sea-level fluctuations to late Paleozoic continental glaciations (Cromwell, 1978; Heckel, 1986; Crowley et al., 1987; Veevers and Powell, 1987). The Pleistocene is the analog of the rapid fluctuations of sea-level attributable to glaciation, the Pleistocene sea-level fluctuated, with a rapid rise in sea-level followed by a slower fall, the result of ice retreating and advancing (Broecker and Van Donk, 1970). Watney (1985) analyzed the upper Pennsylvanian carbonate cycles and estimated each cycle to be about 400 ka in

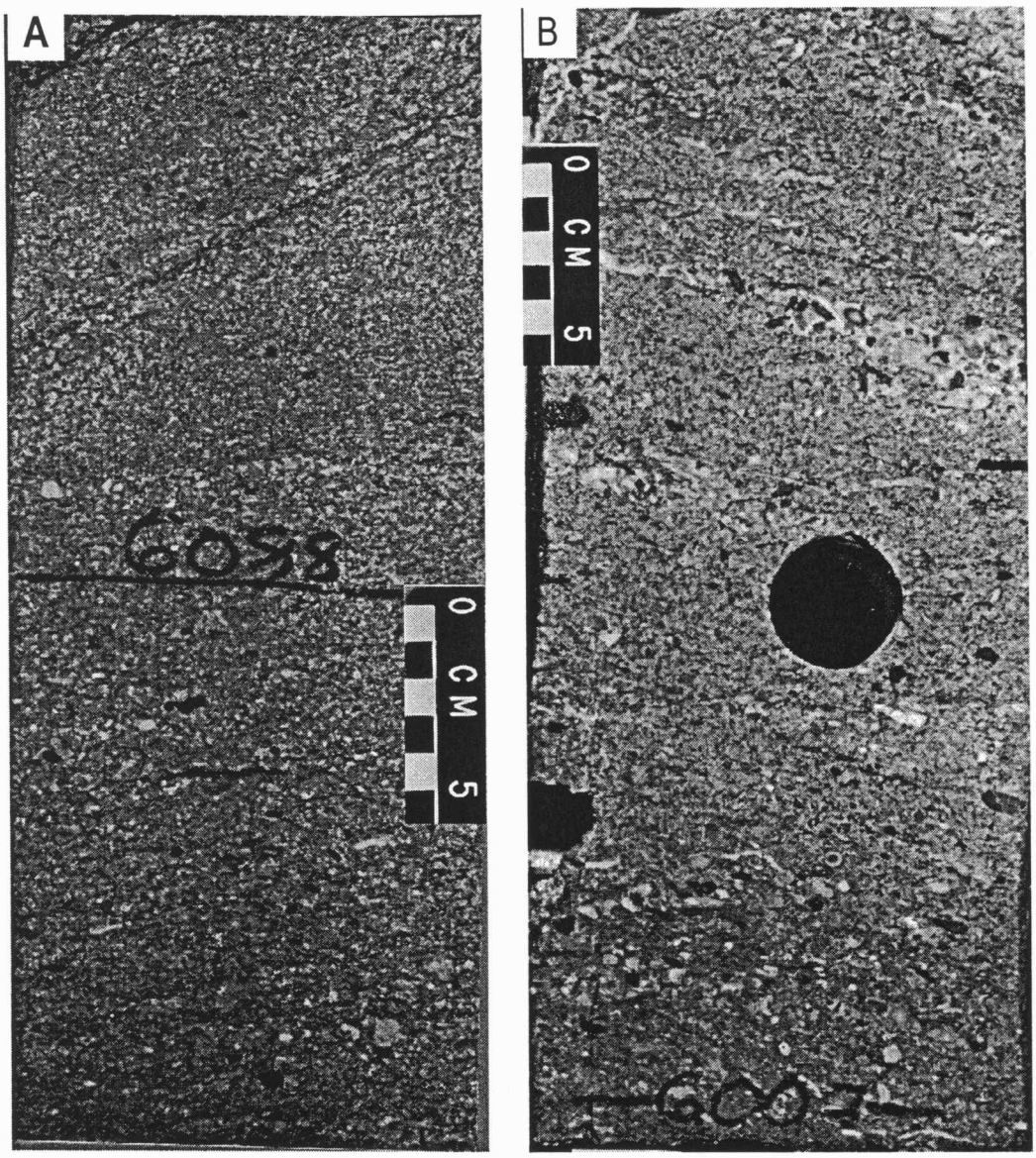

Figure 6.15 Facies H from the Nell "A"19-1. a) and b) show low-angle cross-bedding within pebbly coarse-grained sandstone.

duration and average magnitude of about 25 m. The depositional cycles observed in the middle Pennsylvanian are considered to represent a fourth-order depositional cycle (0.1–1 ma) deposited during the third order of a relatively rapid sea-level cycle (1–10 ma; Youle et al., 1994). In the Hugoton embayment, most of the depositional cycles observed in the Pennsylvanian have been attributed mainly to the glacial-induced sea-level fluctuations (Watney, 1985; Heckel, 1986; Youle et al., 1994).The Chesterian incised valley indicates a period of sea-level fall that resulted in extensive erosion and incision followed by a steady rise in the sea-level and subsequent filling of the incised valley. The distribution and the configuration of lower Morrowan strata across the Gentzler Field reveal a rapid rise (drowning) followed by a steady fall or standstill of the sea-level. Upper shoreface sandstone was deposited on top of deep marine shale (figures 6.5a, 6.13 and 6. 14).

Discussion

The electrofacies model shows that the depositional environments and electrofacies distribution of the lower Morrow strata in the Arroyo Field are different than those encountered in the Gentzler Field (Table 6.2). The electrofacies model illustrated that the lower Morrow strata in the study areas do not represent an open marine, layer cake facies distribution as have been described before this study (Wheeler et al., 1990; Figure 6.16). The electrofacies model indicates that the lower Morrow strata in the Arroyo Field represent an incised valley-fill system, whereas in

Electrofacies	Distribution and thickness of the electrofacies	
	Arroyo Field	Gentzler Field
De	Thick and consists of several units	Thin single unit
Be	Moderately thick	Extremely thick
Ae	Single unit and confined to the paleovalley	Absent
Ee	Present	Absent

Table 6.2 Comparison chart of electrofacies distribution and thickness between the Arroyo and Gentzler fields

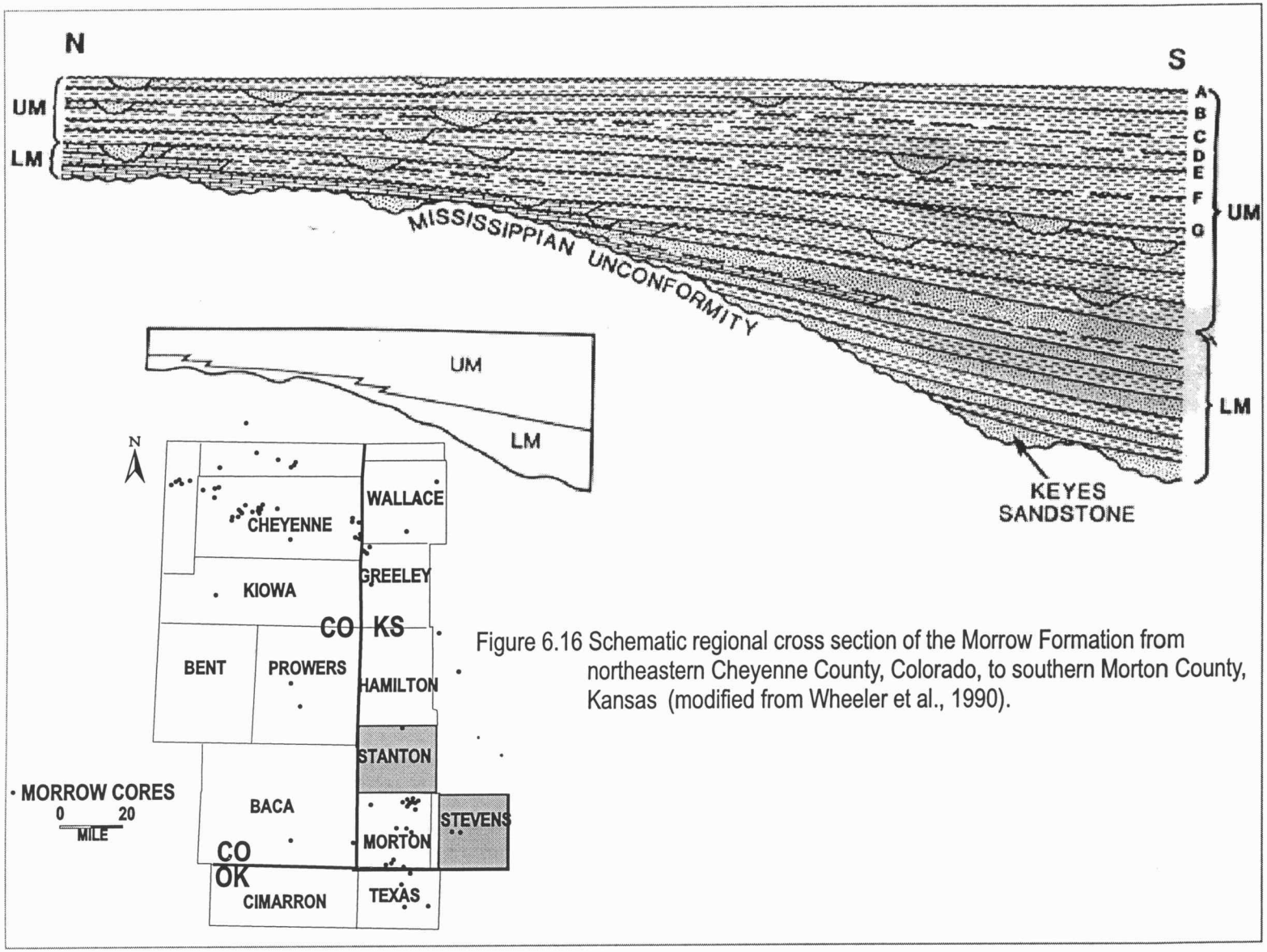

Figure 6.16 Schematic regional cross section of the Morrow Formation from northeastern Cheyenne County, Colorado, to southern Morton County, Kansas (modified from Wheeler et al., 1990).

the Gentzler Field the lower Morrow strata represent an open marine environment where the sea-level did not fall below the shoreline break.

Both case studies represent the same geological time and depositional shelf. In the Gentzler Field area, a Late Mississippian time drop in sea-level resulted in the exposure of the Hugoton Shelf and the development of the Pre-Pennsylvanian sequence boundary. The Hugoton Embayment became a bypass margin that wasmargin that was dominated by southeast-flowing fluvial systems that incised the shelf (Figure 17a and b). During the late Chesterian (?), a gradual rise in relative sea-level was responsible for the filling of the incised valley located in the Gentlzer field. During that time most of the shelf north of the Gentlzer field was still exposed. With the continuous rise in sea-level, the incision at Arroyo Field was filled during the early Morrowan (?) (Figure 6.18). Different magnitudes of sea-level fluctuations were most likely controlled by tectonically induced differential or dissolution subsidence. Variations in the rates of subsidence controlled the configuration of the shelf and the availability of accommodation space. Watney (1985) shows that the Anadarko Shelf subsided at different rates during the upper Pennsylvanian period, causing changes in shelf configuration between a ramp setting and a rimmed platform. Kluth and Coney (1981) indicates that the northern part of the Anadarko shelf subsided more slowly (0.05 m/ky) than the southern part (0.2 m/ky; 0.7 ft/ky). The precise duration and magnitude of subsidence of the Anadarko Shelf are not known in the early Pennsylvanian.

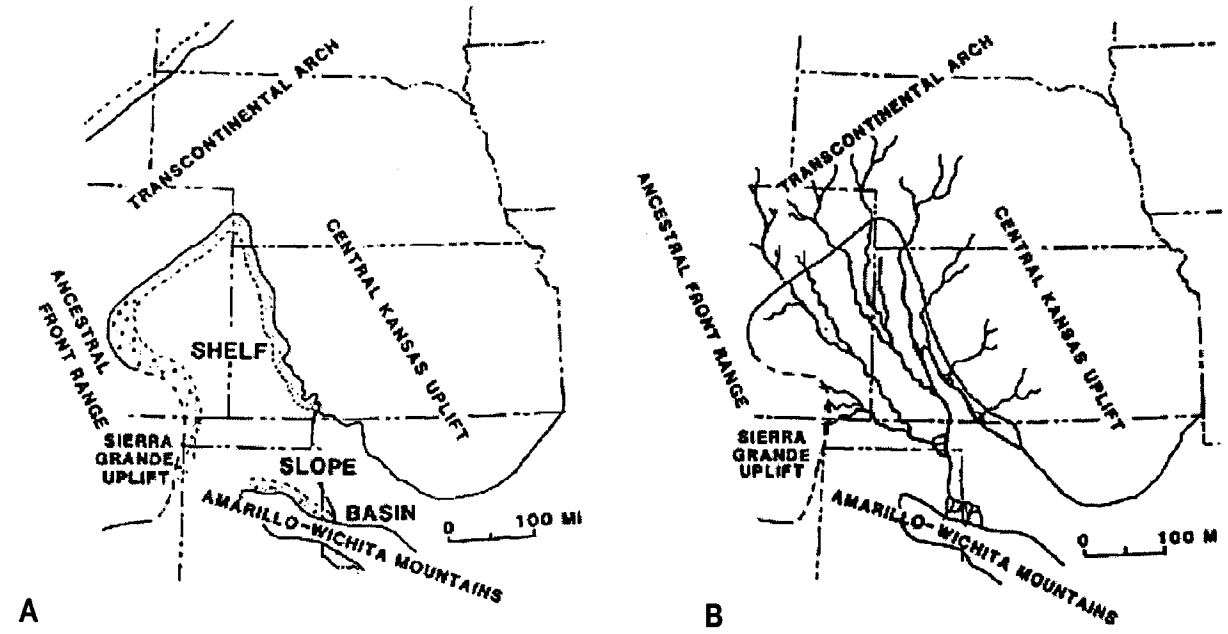

Figure 6.17A) Morrow Paleogeography during high sea level stand, B) Morrow paleogeography with incised drainages during a low sea level stand (modified from Swanson 1979).

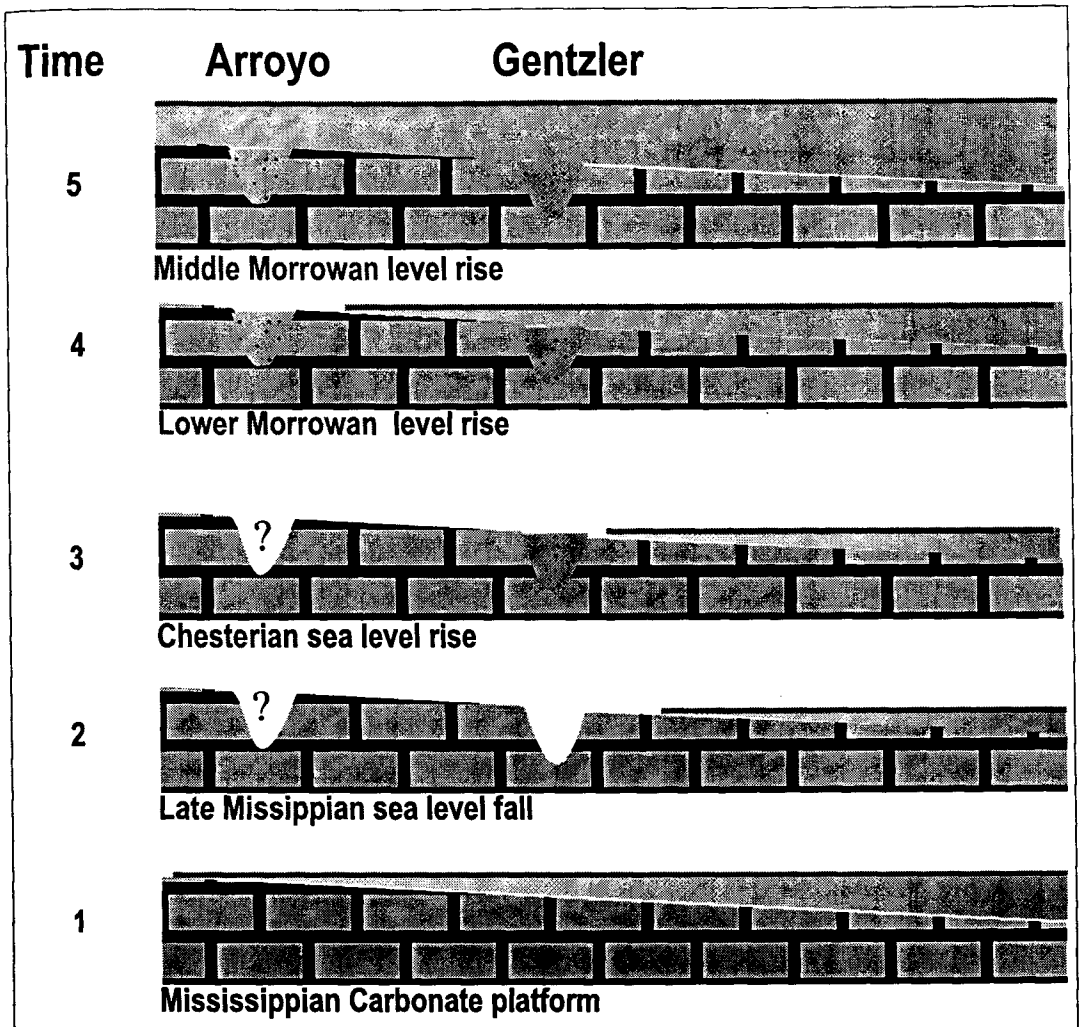

Figure 6.18 Schematic diagram illustration of the evolution of the pre-Penssylvanina incised valley.

Wide spaced wells, absence of two and three dimensional reflection seismic data along with a very low slope gradient of the Hugoton Embayment shelf make it difficult to demonstrate the tectonic influence on the lower Morrow deposition in the study areas. However, tectonically influenced structures and dissolution subsidence have been reported in Morton, Ford, and Clark counties by Merriam (1963), Radar (1987), Clark (1987) Webster (1997) and Hopkins (pers. comm., 1998) that support this tectonic claim.

7. 0 CONCLUSIONS

Integrated analysis of stratigraphic, sedimentologic, and ichnologic information charactrize estuarine and open marine deposites in the Lower Pennsylvanian deposits of southwest Kansas. In the Arroyo Field, the lower Morrow successions were interpreted as a deposits of a wave-dominated estuary. In contrast, lower Morrow rocks at Gentzler Field were interpreted to represent a wave-dominated open marine environment.

Twanty-one lithofacies were identified from core, based on objective criteria (e.g. grain size, sedimentary structures and ichnofauna). Core data and wireline-log responses were integrated to construct an electrofacies model. Distinctive wireline-log responses define five electrofacies, related to depositional environment. Crossplots, RHOmaa-Umaa and Nphi-Dphi versus photoelectric index, were used to determine lithology and distinguish facies in the absence of core data. The electrofacies model was used to establish and map the depositional environments and to construct a sequence-stratigraphic framework for the lower Morrow in the Arroyo and Gentzler fields.

The upper estuarine electrofacies Ae is confined to the deeper part of valleys incised in the pre-Pennsylvanian unconformity. Laterally, the incised valley fill of electrofacies Ae is bounded by electrofacies Ee, which is interpreted as interfluve

deposits. Lower estuarine and upper shoreface facies are represented by electrofacies Be. Electrofacies Ce typifies lower shoreface to offshore facies. The open marine environment of the middle Morrow limestone comprises electrofacies De.

In the Arroyo Field, a surface of subaerial exposure (SB) and a transgressive surface (TS) were identified from core in the Fritz 16-1, and inferred from the spectral gamma ray in the Arnold 1-1. In addition, two maximum flooding surfaces (MFS) and a transgressive surface of erosion (TSE) were inferred. At Arroyo Field, the incised valley-fill deposits (electrofacies Ae, Be and Ee) constitute the initial Pennsylvanian transgressive systems tract (TST). A maximum flooding surface (MFS) separates the TST from the overlying offshore to lower shoreface facies of the highstand system tract (electrofacies Ce). Overlying the offshore and lower shoreface deposits (electrofacies Ce), the middle Morrow limestone (electrofacies De) is separated by a transgressive surface of erosion (TSE). The middle Morrow limestone (electrofacies De) and the overlying upper Morrow offshore facies (electrofacies Ce) represent the transgressive and highstand systems tracts of an overlying sequence. In the Arroyo Field, the lower Morrow successions represent a simple incised-valley fill deposit consisting of one sequence of estuarine and marine deposits.

Facies interpretations and electrofacies model developed at Arroyo Field were used to construct a sequence stratigraphic framework for the lower Morrow at Gentzler Field. Lower Morrow successions at Gentzler Field represent more open-marine environments. Lithofacies and electrofacies are arranged into one sequence

composed of intertidal and upper shoreface (electrofacies Be) and lower shoreface to offshore facies (electrofacies Ce).

The sequence-stratigraphic framework indicates that simple layer-cake open-marine models proposed prior to this study do not accurately represent lower Morrow successions in the Hugoton Embayment (Wheeler at al., 1990). Identification of valley-fill sandstones indicates that the lower Morrow displays complex types of heterogeneity. Heterogeneity is created at different scales by distribution of sequences, facies, facies assemblages and by spatial partitioning within sandstone bodies.

REFERENCES CITED

Abels, A. A., 1962, A subsurface lithofacies study of the Morrowan Series in the northern Anadarko Basin: Shale Shaker Digest, v. 3, p. 93-108.

Abegg F. E., 1994, Lithostratigraphy of the Shore Airport Formation (Chesterian), Southwestern Kansas, , *in*: Bars, D. L, Revision of Stratigraphic Nomenclature in Kansas: Kansas Geological Survey, Bulletin 230, p. 21-38.

Beynon, B. M., Pemberton, S. G., Bell, D. A., and Logan, C. A., 1988, Environmental application of Ichnofossils from the Lower Cretaceous Grand Rapids formation, Cold Lake Oil sands Deposits, *in*: In James, D. P., and Leckie, D. A., eds., Sequence Stratigraphy, sedimentology: surface and subsurface: Canadian Society of Petroleum Geologists, Memoir 15, p. 275-290.

Adams, J. A. S., and C. E. Weaver, 1958, Thorium to uranium ratios as indications of sedimentary processes, Example of concept of geochemical facies: American Association of Petroleum Geologists Bulletin, v. 42, p. 387-430.

Allen, A. W., and F. G. Stephen, 1995, An amazon scale drainage system in the Early Pennsylvanian of central North America: Journal of Geology, v. 103, p. 611-627.

Allen, G. P. and Posamentier H. W., 1993, Sequence Stratigraphy and Facies Model of Incised valley-fill: The Gironde Estuary, France: SEPM Special Publication Vol. 63, No. 3, p. 378-391.

Anderson, J. B., F. P. Siringan, and M. A. Thomas, 1990, Sequence stratigraphy of the late-Pleistocene-Holocene Trinity/Sabine Valley system: relationship to the distribution of sand bodies within the transgressive systems tract (abstract): SEPM Gulf Coast Section Eleventh Annual Research Conference, Sequence Stratigraphy as an Exploration Tool Program with Abstracts, December 2, 1990, p. 15-20.

Bartberger, C. E., Morrison O. J., Leighton V. L., Riggert, V. L., Sanza, G. J. 1996, New field discoveries using 3-d seismic in mature, deeper Paleozoic trends beneath Permian Hugoton gas field, Southwestern Kansas, in American Association of Petroleum Geologist and Society of Economic Paleontologists and Mineralogists , Abstracts with Programs: no. 5, p. 10-11.

Barnes, R. S. K., 1984, Estuarine Biology (second edition): Edward Arnold Ltd., London, p. 76.

Berner, R. A., 1971, Principals of chemical sedimentology: MacGraw Hill, New York, p. 240.

_____, Baldwin, T., and Holdren, G. R. Jr., 1979, Authigenic iron sulfides as paleosalinity indicators: Journal of sedimentary petrology, v. 49, p. 1345-1350.

_____, Raiswell, R., 1984, C/S method for distinguishing fresh from marine sedimentary rocks: Geology, v. 12, p. 365-368.

Beynon, B. M., Pemberton, S. G., Bell, D. A., and Logan, C. A., 1988, Environmental application of Ichnofossils from the Lower Cretaceous Grand Rapids formation, Cold Lake Oil sands Deposits, *in*: In James, D. P., and Leckie, D. A., eds., Sequence Stratigraphy, sedimentology: surface and subsurface: Canadian Society of Petroleum Geologists, Memoir 15, p. 275-290.

Broecker, W. S., and Van Donk, 1970, Insolation changes, ice volume, and the O^{18} record in deep sea cores: Reviews of Geophysics and Space Physics, v. 8, p. 169-198.

Brown, R. L., 1995, Ablative subduction and its structural effects upon the Mid-continent during the Pennsylvanian, *in* K. S. Johnson, ed., Structural styles in the southern Mid-continent: Oklahoma Geological Survey, Norman, Oklahoma, v. 97, p. 83-98.

Carlisle, D., 1983, Concentration of uranium and vanadium in calcretes and gypcretes, in R. C. L. Wilson, ed., Residual Deposits: Geological Society of London Special Publication 11, p. 185-195.

Carr, T. R., and D. A. Budd, 1987, Sequence stratigraphy concepts applied to Early Pennsylvanian shelf carbonates: Geological Society of America, Annual Meeting, Abstracts with Programs, v. 19, p. 612.

_____, and C. E. Lundgren, 1994, Use of gamma ray spectral logs to recognize exposure surfaces at the reservoir scale: Big Bow Field (St. Louis Limestone), Kansas: Rocky Mountain Association of Geologists, unconformity controls symposium, p. 79-88.

Casagrande, D. J., Siefert, K., Berschinski, C., Sutton, N., 1977, Sulfur in peat-forming systems of the Okeefenokee Swamp and Florida Everglades: origins of sulfur in coal: Geochemica et Cosmochimica Acta, v. 41, p. 161-167.

Cheel, R. J., and D. A. Leckie, 1990, A tidal inlet complex in the Cretaceous epeiric sea of North America: Virgelle Member, Milk River Formation, southern Alberta, Canada: Sedimentology, v. 37, p. 67-81.

Chung, G. C., and P. K. Swart, 1990, The concentration of uranium in freshwater vadose and phreatic cements in a Holocene ooid cay: A method of identifying ancient water tables: Journal of Sedimentary Petrology, v. 60, p. 735-746.

Clark, S. L., 1987, Seismic Stratigraphy of Early Pennsylvanian Morrowan Sandstones, Minneola Complex, Ford and Clark Counties, Kansas: American Association of Petroleum Geologists Bulletin v. 71, no.11, p. 1329-1341.

Collins, D. R., and J. H. Doveton, 1989, Applying color information theory to the Display of Lithologic images form wireline logs: Geobyte, February, p. 16-24.

Craig, L. C., and K. L., Varnes, 1979, History of the Mississippian System- an Interpretative summary: USGS Prof. Paper 1010-R, p. 371-406.

Cromwell, J. C., 1978, Gondwanan glaciation, cyclothems, continental positioning and climate change: American Journal of Science, v. 3278, p. 1345-1372.

Crowley, T. J., J. G. Mengel, and D. A. Short, 1987, Gondwanaland's seasonal cycle: Nature, v. 329, p. 803-807.

Dalrymple, R. W _____, 1992, Tidal depositional systems, *in*: R. G. Walker and N. P. James, eds., Facies Models: Response to sea level: Geological Association of Canada, Love Printing Service Ltd., Stittsville, Ontario, p. 195-233.

_____., Zaitlin B. A., Boyd R., 1992, Estuarine Facies Model: Conceptual Basis and stratigraphic Implication: Journal of Sedimentary Petrology, v. 62, p. 1130-1146.

Davis, Jr., R. A., 1983, The Estuarine Depositional System, in R. Henderson, ed., Depositional System: An Introduction to Sedimentology and Stratigraphy: Prentice Hall, Englewood Cliffs, p. 307, 341.

Decker, J and Helmold, K. P., 1985, The effect of grain size on detrital modes: a test of the Gazzi-Dickinson point count method-discussion: Journal of Sedimentary Petrology, v. 55, p. 618-619.

Deer, W. A., R. A. Howie, and J. Zussmand, 1985, An introduction to the rock-forming minerals: Commonwealth Printing, Essex England, p. 281-339.

Demarest, J, M., Kraft, J. C., 1987. Stratigraphic record of the Quaternary sea level: Implication for more ancient strata, *in* Numuedal, D., Pilkey, O. H. and Howard J. D., eds., sea level fluctuation and coastal evolution: Society of Economic Paleontologists and Mineralogists, Special Publication 41, p.41-267.

DeVoto, R. H., 1980, Pennsylvanian Stratigraphy and History: Colorado Geology, Rocky Mountain Association of Geologist. Symposium, p. 71-101.

Digital Petroleum Atlas, 1997, Kansas Geological Survey web site pages, http:\\www.kgs.ukans.edu\DPA.

Doveton, J. H., 1986, Log analysis of subsurface geology—Concepts and computer methods: New York, John Wiley and Sons, 273 p.

_____, 1994, Geological interpretation, SEPM short course, no. 29, p. 169.

Ebbing, J. H., and C. Laban, 1986, Geological history of the area off Walcheren and Zeeuwsch-Vlaanderen (southwestern Netherlands), since the start of the Eemian, *in* D. J. Beets, M. M. Fischer, and W. Gans, eds., Coastal studies of the Holocene of the Netherlands: Mededlingern Rijks Geologishche Dienst, v. 57, p. 251-267.

Ekdale, A. A., Bromley, R. G., and Pemberton, S. G., 1987, Ichnology: Society of Economic Paleontology and Mineralogists, short course no. 15, p. 317.

Emery, D., and K. J. Myers, eds., 1996, Sequence Stratigraphy: Great Britain, Blackwell Science, p. 3-269.

Ettensohn, F. R., Garland, R. D., Jr., and Grow, J. S., 1988, A paleosol interpretation for profiles exhibiting subaerial exposure "crusts" from the Mississippian of the Appalachian Basin, in J. Reinhardt, and W. R. Sigleo, eds., Paleosols and Weathering through Geologic Time: Principles and Applications: Geological Society of America Special Paper 216, p. 49-79.

Franz, R. H., 1985, Lithofacies, Diagenesis, and Petrophysical Properties of Selected Sandstones from the Morrowan Kearny Formation of Southwestern Kansas: Unpublished M. S. thesis, Department of Geology, University of Kansas,

Lawrence, KS, p. 1-177. (Available as Kansas Geological Survey Open-file Report, no. 84-4).

Frey, R. W., and Howard, J. D., 1975, Endobenthic adaptations juvenile thalassinidean shrimp: Bulletin of the Geological Society of Denmark, v. 24, p. 225-301.

_____, and Howard, J. D., 1980, Physical and biogenic processes in Georgia estuaries. II. Intertidal Facies. *in* McCann, S. B., eds., Sedimentary Processes and Animal-sedimentary Relationships in Tidal Environments: Geological Association of Canada, short course notes, v. 1, p. 183-220.

_____, and Howard, J. D., 1985, Trace fossils from the Panther member, Star point Formation (Upper Cretaceous, Coal Creek Canyon, Utah): Journal of Paleontology, v. 59, p 370-404.

Frezon, S. E. and J. H. Dixon, 1975, Texas Panhandle and Oklahoma: Pennsylvanian Systems: USGS, Prof. Paper 853, Part 1, p. 177-194.

Garcia, R., 1981, Depositional system and their relation to gas accumulation in Sacramento Valley, California., American Association Of Petroleum Geologists Bull., 65, p. 653-673.

Geoffrey, A. D., M. Tubmann-Kenneth, D. Cooke, and R. O'Conner, 1996, Geophysical reservoir characterization of Pickerill Field, North Sea, using 3-D seismic and well data, in P. Weimer and D. L. Thomas, eds., Applications of 3-D seismic data to exploration and production: American Association of Petroleum Geologists Studies in Geology, Tulsa, Oklahoma, v. 42, p. 107-121.

Germinario, M. P., 1996, Use of micro-resistivity imaging tools in development Lower Pennsylvanian Morrow channel sandstone reservoir, Cheyenne, Kiowa, and Lincoln, Colorado, in American Association of Petroleum annual convention, Abstracts, no. 5, p. 52.

Goudie, A. S., 1973, Duricrusts in tropical and subtropical landscapes: Clarendon Press, Oxford, p. 174.

Hampson, G.J., E. Trevor, and S. J. Davies, 1997, The application of sequence stratigraphy of Upper Carboniferous fluvio-deltaic strata of the onshore UK and Ireland; implications for the southern North Sea: Journal of the Geological Society of London, v. 154, part 4, p. 719-733.

Hassan, M., A. Hossin, and A. Combaz, A., 1976, Fundamentals of the Differential Gamma Ray Log-Interpretation Technique, Transactions, SPWLA.

Haq, B. U., J. Hardenbol, and P. R. Vail, 1988, Mesozoic and Cenozoic chronostratigraphy and cycles of sea-level changes, *in* C. K. Wilgus, B. S. Hastings, C. G. St. Kendall, H. W. Posamentier, C. A. Ross, and J. C. Van Wagoner, eds., Sea-Level Changes: an Integrated Approach: Special Publication, Society of Economic Paleontologists and Mineralogists, Tulsa, Oklahoma, p. 42, 40-45.

Heckel, P. H., 1986, Sea-level curve for Pennsylvanian eustatic marine transgressive-regressive depositional cycles along midcontinent outcrop belt, North America: Geology, v. 14, p. 330-334.

Herbert, J. R., 1979, Post-Miocene stratigraphy and evolution of northern Core Banks, North Carolina, unpublished masters Thesis, Duke University, p. 166.

Heron, S. D., Jr., T. F. Moslow, W. M., Berelson, J. R. Herbert, G. A. Steele, and K. R. Susman, 1984, Holocene sedimentation of a wave-dominated barrier-island shoreline: Cape Lookout, North Carolina, in B. Greenwood, and R. A. Davis, eds., Hydrodynamics and sedimentation in wave-dominated coastal environments: Marine Geology, v. 60, p. 413-434.

Hopkins, J., 1998, Kansas Geological Survey, University of Kansas, personal communication.

Horne, J. C., Ferm, J. C., Caruccio, F. T., Baganz, B. P., 1978, depositional models in coal exploration and mine planning in the Appalachian Region: American Association of Petroleum Geologist Bulletin, v. 62, p. 2379-2241.

Jopling, A. V., and Walker, R. G., 1968, Morphology and origin of ripple-drift cross lamination, with examples from the Pleistocene of Massachusetts: Journal of Sedimentary Petrology, v. 38, p. 971-984.

Kluth C. G., and P. J. Coney, 1981, Plate tectonics of the ancestral Rocky Mountains: Geology, v. 91, p. 10-15.

Krystinik, L.F., and B. A. Blackeney-DeJarnett, 1990, Sedimentology of the upper Morrow Formation in Eastern Colorado and western Kansas, *in S. A.* Sonnenberg, L. T. Shannon, K. Radar, W. F. Von Drehle and G. W. Martin, eds., Morrow Sandstones of Southeast Colorado and Adjacent Areas: Rocky Mountain Association of Geologists p. 37-50.

Kumar, N. and Sanders, J. E., 1974, Inlet sequence: a vertical succession of sedimentary structures and textures created by the lateral migration of tidal inlets: Sedimentology, v. 21, p. 491-532.

Leckie, D. A., and C. Singh, 1991, Estuarine deposits of the Albian Paddy Member (Peace River Formation) and lowermost Shaftsbury Formation, Alberta, Canada: Journal of Sedimentary Petrography, v. 61, p. 825-849.

Mann, A. W., and R. Horowitz, 1979, Groundwater calcrete deposits in Australia, some observations from western Australia: Journal of Geological Society of Australia, v. 26, p. 293-303.

Martens, C. S., and Goldhaber, M. B., 1978, Early diagenesis in transitional sedimentary environment of the White Oak River estuary, North Carolina: Limnology and Oceanography, v. 32, p.428-441.

McKee, E. D., 1965, Experiment in ripple lamination. *in*: Middleton, G. V. eds., Primary Sedimentary Structures and their Hydrodynamic Interpretation: Society of Economic Mineralogists and Paleontologists, special pub. no. 12, Tulsa, Oklahoma, P66-83.

Merriam, D. F., 1963, The Geologic History of Kansas, Kansas Geological Survey Bulletin 162, p. 135-144, 185-192.

Mitchum, R. M., Jr. and P. R. Vail, 1977, Seismic stratigraphy and global changes of sea-level, part 7: stratigraphic interpretation of seismic reflection patterns in depositional sequences, *in* C. E. Payton, ed., Seismic Stratigraphy-Applications to Hydrocarbon Exploration: Memoir of the American Association of Petroleum Geologist, Tulsa, Oklahoma, p. 26, 135-144.

Montgomery, S. L., and Morrison, E, 1999 South Eubank Field, Haskell County, Kansas: A case of Field Redevelopment Using Subsurface Mapping and 3-dD Seismic Data: American Association of Petroleum Geologists, Bulletin, v. 83, p. 393-410.

Moslow, T. F., and R. S. Tye, 1985, Recognition and characterization of Holocene tidal inlet sequences: Marine Geology, v. 63, p. 129-151.

Nichols, M. M., and R. B. Biggs, 1985, Estuaries, in R. A. Davis Jr., ed., Coastal Sedimentary Environments, 2nd Edition: New York, Springer-Verlag, p. 77-186.

_____, Johnson G. H., and Peebles P. C., 1991, Modern Sediments and Facies Model for a Microtidal Coastal Plain Estuary, James Estuary, Virginia: SEPM Special Pub. v. 61, no. 6, p. 883-889.

Nio, S. D., and Yang, C. S., 1991, Diagnostic attributes of clastic tidal deposits: a review, *in* Smith, D G., Reinson, G. E., Zaitlin, B. A., and Rahmani, R. A., eds., Clastic tidal sedimentology: Canadian Society of Petroleum Geologist, Memoir 16, p.3-28.

Pemberton, S. G., and R. W. Frey, 1982, Trace fossil nomenclature and the *Planolites-Palaeophycus* dilemma: Journal of Paleontology, v. 56, p. 843-881.

_____, and J. A. MacEachern, 1992, Trace Fossil Facies Models: Environmental and Allostratigraphic Significance, *in*: R. G. Walker and N. P. James, eds., Facies Models: Response to sea level: Geological Association of Canada, Love Printing Service Ltd., Stittsville, Ontario, p. 47-72.

Postma, D., 1982, Pyrite and siderite formation in the brackish and fresh water swamp sediments: American Journal of Science, v. 282, p 1151-1183.

Raddysh, H. K., 1988, Sedimentology and "geometry" of the Lower Cretaceous Viking Formation, Gilby A and B Fields, Alberta, *in* D. P. James and D. A. Leckie, eds., Sequences, Stratigraphy, Sedimentology: Surface and Subsurface: Canadian Society of Petroleum Geologists, Memoir 15, p. 417-430.

Rader, K., 1987, Petrographic and subsurface analysis of Pennsylvanian Morrowan sandstones of Southwest Kansas: Unpublished M.S. thesis, Department of Geological Sciences, University of Colorado, Boulder, CO., 106 pages. (Available as Kansas Geological Survey, Open-file report no. 87-131.).

Rader, K., 1990, Petrography of Morrowan Sandstones in Southeast Colorado, Southwest Kansas, and Northwest Oklahoma, *in S. A.* Sonnenberg, L. T. Shannon, K. Radar, W. F. Von Drehle and G. W. Martin, eds., Morrow Sandstones of Southeast Colorado and Adjacent Areas: Rocky Mountain Association of Geologists p. 51-58.

Rahmani, R. A., 1988, Estuarine tidal channel and nearshore sedimentation of a late Cretaceous epicontinental sea, Drumheller, Alberta, Canada, *in* de P. L. Boer, A. Van Gelder, and S. D. Nio, eds., Tide-influenced Sedimentary Environments and Facies: Dordrecht, D. Reidel Publishing Company, p. 433-471.

Rasco, B., 1978, Late Paleozoic Structural evolution of the Las Animas Arch: in J. D. Pruit and P. E. Coffin, eds., Energy Resource of Denver Basin, Rocky Mountain Association of Geologist Guidebook, p. 112-113.

Reading, H. G., and J. D. Collinson, 1996, Clastic Coasts, *in* H. G. Reading, ed., Sedimentary Environments: Processes, Facies and Stratigraphy: Cambridge, Blackwell Science Ltd., p. 213.

Reinson, G. E., 1992, Transgressive Barrier Island and Estuarine Systems. Tidal Depositional Systems, *in*: R. G. Walker and N. P. James, eds., Facies Models: Response to sea level: Geological Association of Canada, Love Printing Service Ltd., Stittsville, Ontario, p. 179-194.

_____, J. E. Clark, and A. E., Foscolos, 1988, Reservoir geology of Crystal Viking Field, Lower Cretaceous estuarine tidal channel-bay complex. South central Alberta: American Association of Petroleum Geologists, Bulletin, v. 72, p. 1270-1294.

Reynolds, A. D., 1994, Sequence stratigraphy from core and wireline log data: Viking Formation, Albian South Central Alberta: Marine Petroleum Geology, 11, 258-282.

Ross, C. A., and J. R. P., Ross, 1985, Late Paleozoic depositional sequences are synchronous and worldwide: Geology, v. 13, p. 194-197.

Rosenthal, L., 1988, Wave-dominated shorelines and incised valley trends: Lower Cretaceous Glauconite Formation, west-central Alberta, *in* D. P. James, and R. Rahmani, eds., Clastic Tidal Sedimentology: Calgary, Canadian Society of Petroleum Geologists Memoir 16, p. 91-106.

Schlumberger, 1989, Log Interpretation Principles/Applications, Schlumberger Educational Surfaces, Houston, Texas, p. 3.1-3.11, 5.1-5.23, 6.1-6.13.

Schopf, J. M., 1975, Pennsylvanian climate in the United State, *in* McKee, E. D., and E. J. Crosby, Coordinators, Paleotectonic Investigations of the Pennsylvanian System in the United States, Part II: USGS Prof. Paper 853, p. 23-31.

Schwartz, R. K., 1982, Bedform and stratification characteristics of some modern small- scale washover sand bodies: Sedimentology, v. 29, p. 835-850.

Serra, O., J. Baldwin, and J. Quirein, 1980, Theory, interpretation and practical applications of natural gamma ray spectroscopy: SPWLA Twenty-First Annual Logging symposium, p. 1-30.

_____, 1985, Sedimentary Environments from Wireline logs, Schlumberger, p. 7-201.

Sonnenberg, S. A., L. T. Shannon, R. Kathleen, W. F. von Drehle, 1990, Regional Structure and Stratigraphy of the Morrowan Series, Southeast Colorado and Adjacent Areas, *in S. A.* Sonnenberg, L. T. Shannon, K. Radar, W. F. Von Drehle and G. W. Martin, eds., Morrow Sandstones of Southeast Colorado and Adjacent Areas: Rocky Mountain Association of Geologists p. 1-8.

_____, 1985, Tectonic and sedimentation model for Morrow sandstone deposition, Sorrento field area, Denver basin, Colorado. Mountain: Geologist, v. 22, p. 180-191.

Strobl, R. S., 1988, The effects of sea level fluctuations on prograding shorelines and estuarine valley-fill sequences in the Glauconitic Member, Medicine River Field and adjacent areas, *in* D. P. James and D. A. Leckie, eds., Sequences, Stratigraphy, Sedimentology: Surface and Subsurface: Canadian Society of Petroleum Geologists, Memoir 15, p. 221-236.

Stumm, W., and Morgan, J. J., 1970, Aquatic chemistry: an introduction emphasizing chemical equilibria in natural water: John Wiley and Sons, New York, p. 583.

Swanson, D. C., 1979, Deltaic deposits in the Pennsylvanian upper Morrow Formation of the Anadarko Basin in Pennsylvanian Sandstones of the Mid-continent, Tulsa Geological Society, pub no. 1, p. 115-168.

Tillman, R. W., and R. M. Martinson, 1984, The Shannon shelf-ridge sandstone complex, Salt Creek Anticline are, Powder River Basin, Wyoming, *in* Tillman, R. W., and Siemers, C. T., eds., Siliciclastic Shelf Sediments: Society of Economic Paleontologists and Mineralogists, Special Pub. no. 34, Tulsa, Oklahoma, p. 85-142.

Vail, P. R., R. M. Mitchum Jr., and S. Thompson III, 1977, Seismic stratigraphy and global changes of sea-level, part 3: relative changes of sea level from coastal onlap, *in* C. E. Payton, ed., Seismic Stratigraphy-Applications to Hydrocarbon Exploration: Memoir of the American Association of Petroleum Geologists, Tulsa, Oklahoma, p. 26, 63-82.

_____, and R. G. Todd, 1981, North Sea Jurassic unconformities, chronostratigraphy and global sea level changes from seismic stratigraphy: Petroleum Geology of the NW Continental Shelf, Proceedings, p. 216-235.

_____, J. Hardenbol, and R. G. Todd, 1984, Jurassic unconformities, chronostratigraphy and sea level changes from seismic stratigraphy, *in* J. S. Schlee, ed., Interregional Unconformities and Hydrocarbon Exploration: Memoir of the American Association of Petroleum Geologists, Tulsa, Oklahoma, p. 33, 129-144.

Van Wagoner, J. C., Mitchum, R. M., Posamentier, J. W., and P. R. Vail, 1987, Key definitions of sequence stratigraphy, *in* A. W. Bally, ed., Atlas of seismic stratigraphy: American Association of Petroleum Geologists Bull, v. 1 p. 11-14.

_____, H. W. Posamentier, R. M. Mitchum, P. R. Vail, J. F. Sarg, T. S. Loutit, and J. Hardenbol, 1988, An overview of sequence stratigraphy and key definitions, *in* C. W Wilgus et al., eds., Sea level changes: An integrated approach: Society of Economic Paleontologists and Mineralogists Special Publication 42, p.39-45.

Veevers, J. J., and C. M. Powell, 1987, Late Paleozoic glacial episodes in Gondwanaland reflected in transgressive-regressive depositional sequences in Euramerica: Geological Society of America Bulletin, v. 98, p. 475-487.

Walker, R. G., 1992, Facies, Facies Models and Modern Stratigraphic Concepts, *in*: R. G. Walker and N. P. James, eds., Facies Models: Response to sea level: Geological Association of Canada, Love Printing Service Ltd., Stittsville, Ontario, p. 1-14.

Watney, W. L., 1985, Resolving controls on epeiric sedimentation using trend surface analysis: Mathematical Geology, v. 71, p. 427-454.

_____, and J. A. French, 1988, Characterization of carbonate reservoirs in the Lansing-Kansas City groups (Upper Pennsylvanian) in Victory Field, Haskell County, Kansa, *in* S.M. Goolsby and M. W. Longman, eds., Occurrence and Petrophysical Properties of Carbonate Reservoirs in the Rocky Mountain Region: Rocky Mountain Association of Geologists Symposium, p. 27-46.

_____, J. H. Doveton, J. A. Jr. French, and D. R. Collins, 1990, Petrophysical characterization of Upper Pennsylvanian depositional sequences in western Kansas, in Geological Society of America, South-Central Section, 24th annual meeting, abstracts, Abstracts with Programs: Geological Society of America 22, no. 1, p. 35.

Webster, R. J., 1997, Stratigraphy, structure, and regional trends of incised valley systems along the north side of the Anadarko Basin, in Clark, Comanche, and

Ford counties, Kansas: American Association of Petroleum Geologists, v. 81, no. 8, p. 1356.

Weimer, R. J., S. A. Sonnenberg, and L. T. Shannon, 1988, Production from valley-fill deposits, Morrow Sandstone, Southeast Colorado: New exploration challenges and rewards (abs): American Association of Petroleum Geologists Bulletin, v. 72, p. 884.

Wheeler, D M., Scott, A. J., Coringrato, V. J., and P. E. Devine, 1990, Stratigraphy and depositional history of the Morrow Formation, Southeast Colorado and Southwest Kansas, *in S. A.* Sonnenberg, L. T. Shannon, K. Radar, W. F. Von Drehle and G. W. Martin, eds., Morrow Sandstones of Southeast Colorado and Adjacent Areas: Rocky Mountain Association of Geologists p. 9-35.

Wightman, M. D., Pemberton, S. G., Singh, C., 1987, Depositional modeling of the upper Mannville (Lower Cretaceous), east central Albert: Implications for the recognition o f brackish water deposits, *in*: Reservoir sedimentology: Society of Economic Mineralogists and Paleontologists, special pub. 40, p. 189-220.

Wood, J. M., and J. C. Hopkins, 1989, Reservoir sandstone bodies in estuarine valley fill Lower Cretaceous Glauconitic Member, Little Bow Field, Alberta, Canada: American Association of Petroleum Geologists Bulletin, v. 73, p. 1361-1382.

Wood, L. J., F. G. Ethridge, and S. A. Schumm, 1993, The effects of rate of base-level fluctuation on coastal-plain, shelf and slope depositional systems, an experimental approach, *in* H. W. Posamentier, C. P. Summerhayes, B. U. Haq, G. P. Allen, eds., Sequence stratigraphy and facies associations: Special Publication of the International Association of Sedimentologists 18, p. 43-53.

Wright, V. P., and M. E. Tucker, 1991, Calcretes: an introduction: *in* V. P. Wright and M. E. Tucker, eds., Calcretes: International Association of Sedimentologist, Reprints Series, v. 2, p. 1-22.

Youle, J. C., 1992, Sequence stratigraphy of the Lower Middle Pennsylvanian and Distribution of Selected Sandstone, Eastern Hugoton Embayment, Southwestern Kansas: Unpublished M.S. thesis, University of Kansas, Lawrence, Kansas. (Available as Kansas Geological Survey open file report number 92-55). p. 157. 166.

_____, W. L. Watney, and L. L. Lambert, 1994, Stratal hierarchy and sequence stratigraphy-Middle Pennsylvanian, southwestern Kansas, U.S.A.: Geological Society of America, Special Paper 288, p. 267-285.

Zaitlin B. A, Dalrymple R. W, Boyd R., 1994, The Stratigraphic Organization of Incised–Valley System Associated with Relative Sea Level Change, *in* Incised Valley Systems Origin and Sedimentary Sequences: SEPM Special Publication No. 51, p. 48-60.

Zeller, D. E. (ed.), 1968, The Stratigraphic Succession in Kansas: Kansas Geological Survey Bulletin, 189, p 17-34.

STRATIGRAPHIC CROSS-SECTION: EQUAL SPACE

Datum = MFS Domain = Depth

Scale = 1: 2400 Vertical Exaggeration = 100 x.

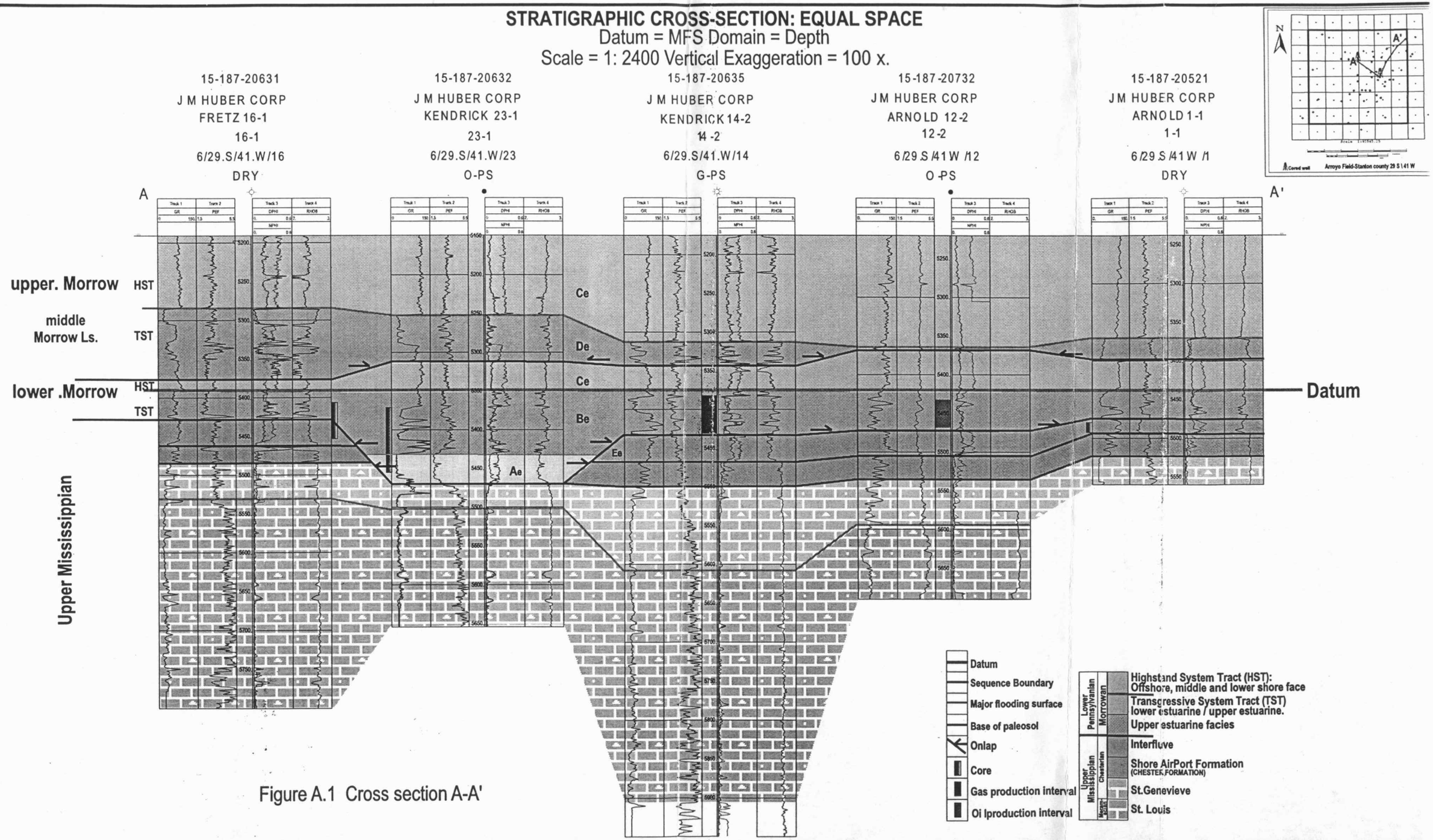

Figure A.1 Cross section A-A'

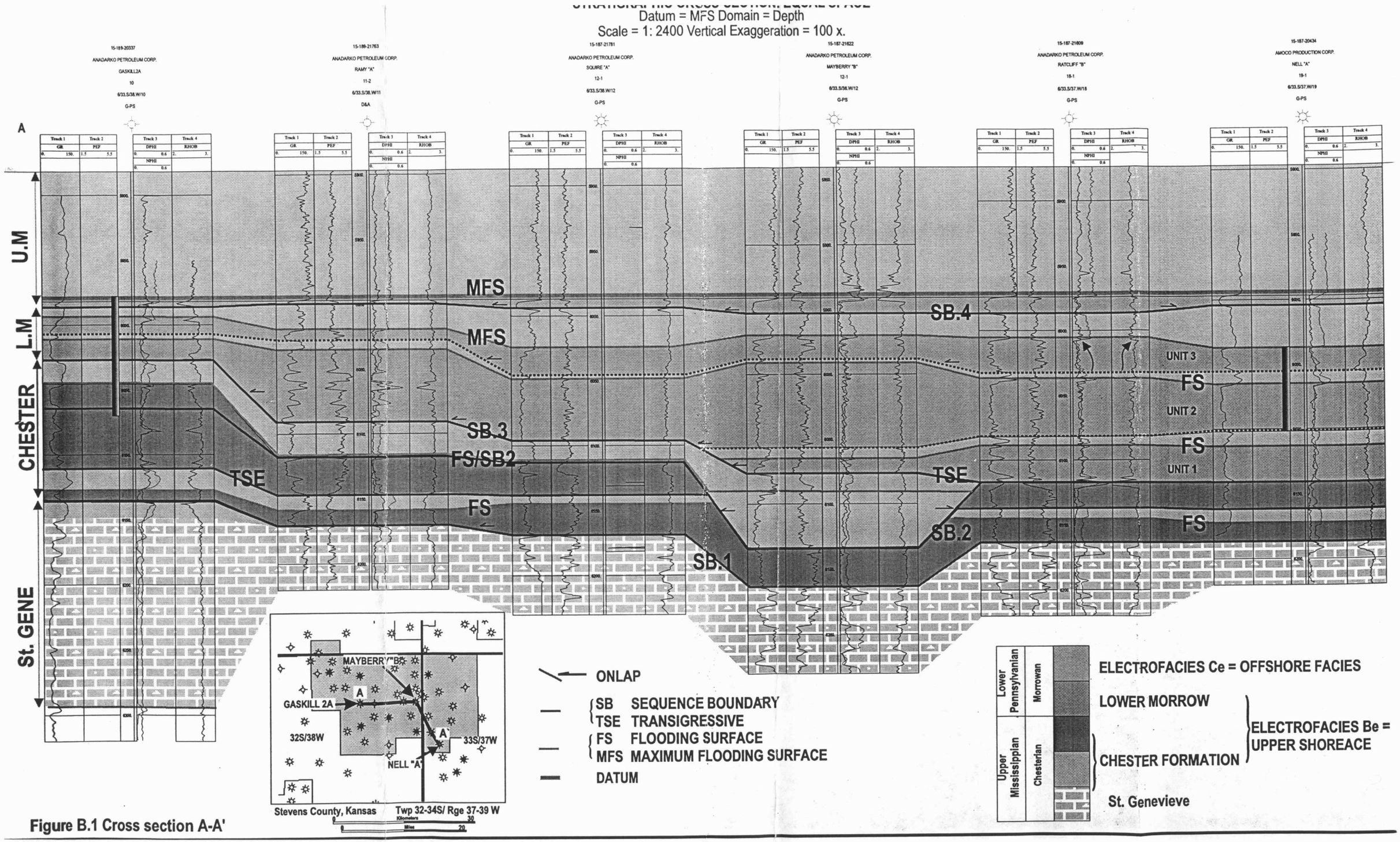

Figure B.1 Cross section A-A'

STRATIGRAPHIC CROSS-SECTION: EQUAL SPACE

Datum = MFS Domain = Depth

Scale = 1: 2400 Vertical Exaggeration = 100 x.

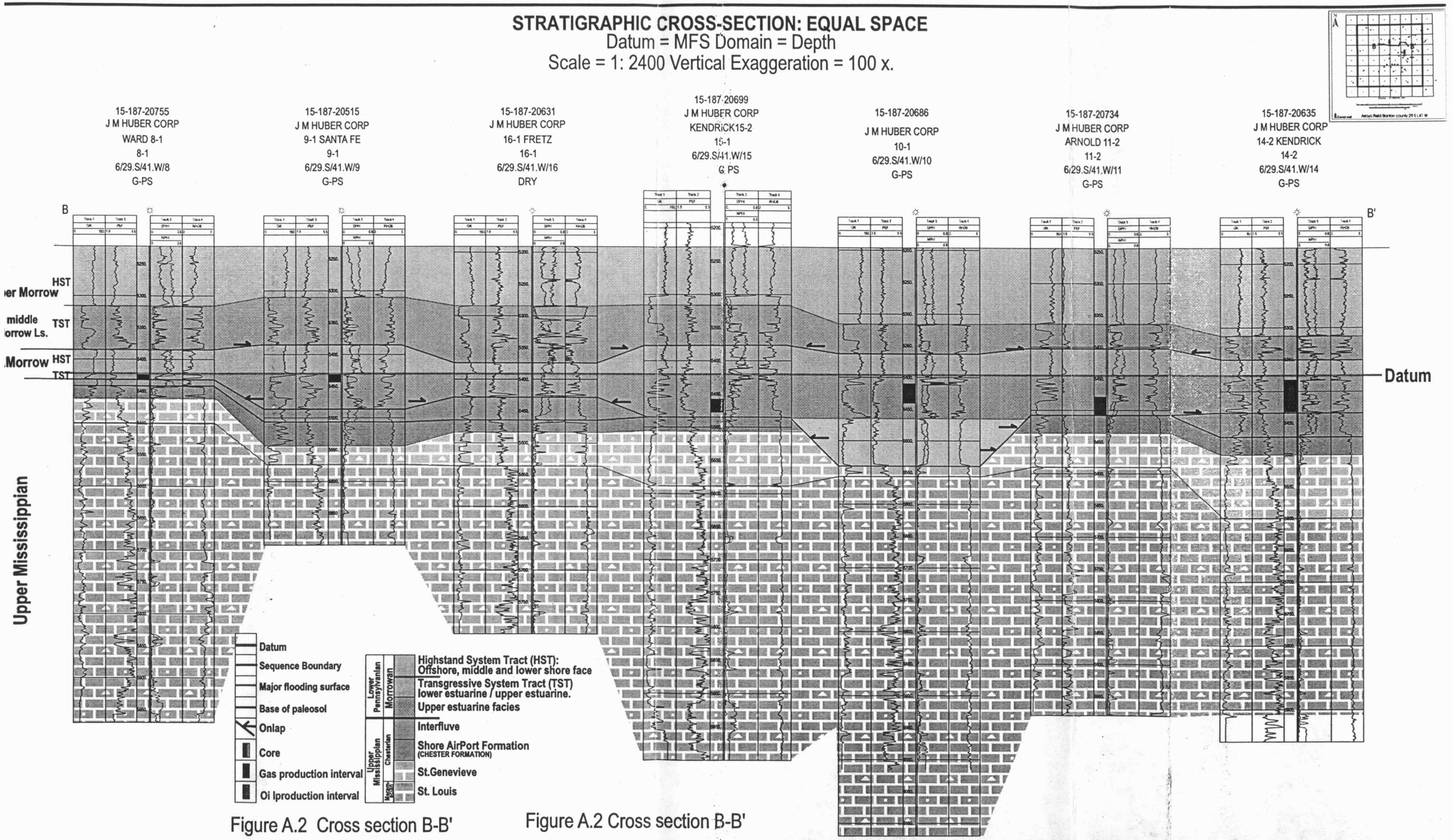

Figure A.2 Cross section B-B'

Figure A.2 Cross section B-B'

STRATIGRAPHIC CROSS-SECTION: EQUAL SPACE

Datum = MFS Domain = Depth

Scale = 1: 2400 Vertical Exaggeration = 100 x.

15-187-20631	15-187-20665	15-187-20632	15-187-20638	15-187-20716	15-187-20689
J M HUBER CORP	J M HUBER CORP	J M HUBER CORP	J M HUBER CORP	J M HUBER CORP.	J M HUBER CORP.
16-1 FRETZ	SMITH TRUST 22-1	23-1 KENDRICK	ARNOLD 23-1	ARNOLD 23-2	UNEY 24-1
16-1	22-1	23-1	23-1	23-2	24-1
6/29.S/41.W/16	6/29.S/41.W/22	6/29.S/41.W/23	6/29.S/41.W/23	6/29.S/41.W/23	6/29.S/41.W/24
DRY	G-PS	O-PS	C-PS	G-PS	O-PS

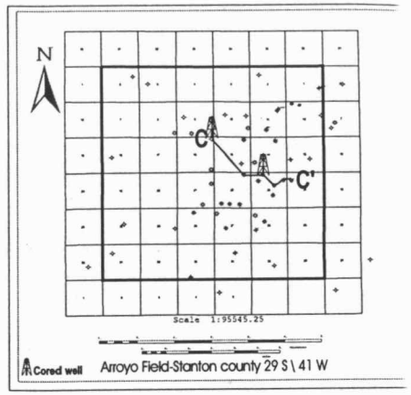

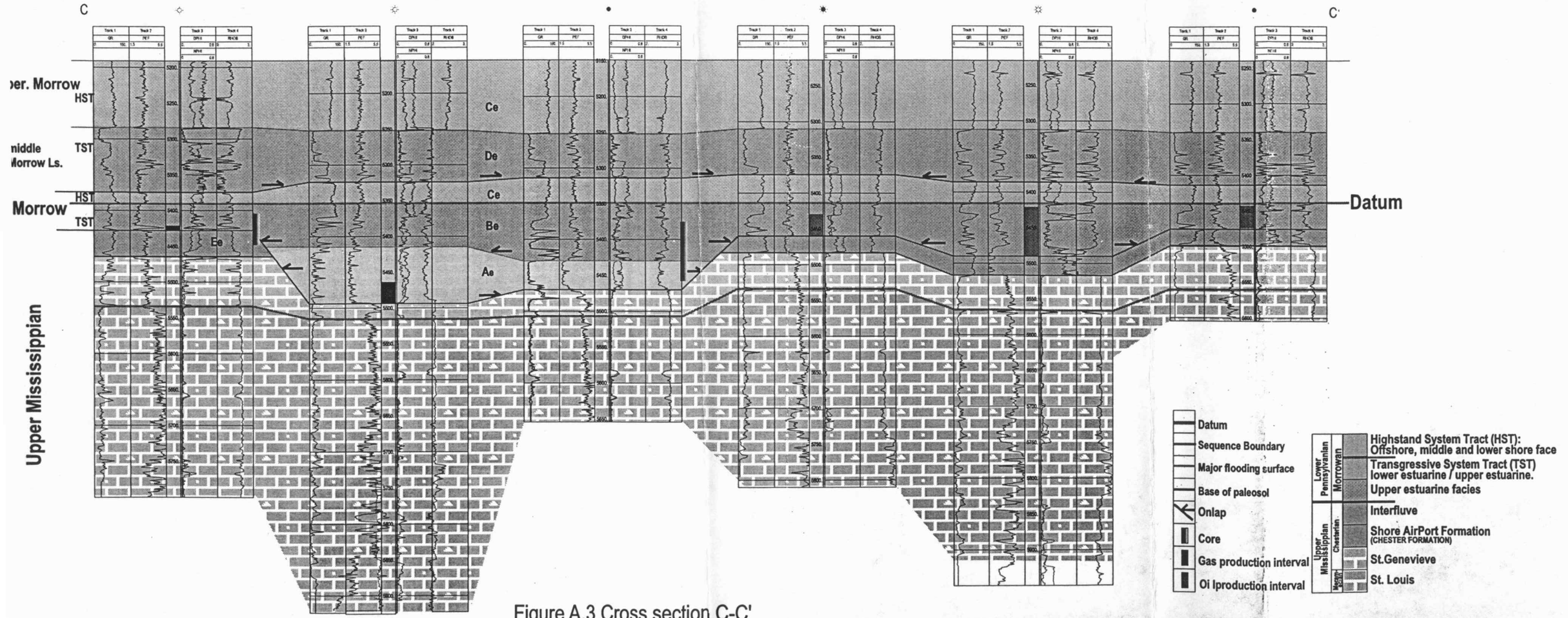

Figure A.3 Cross section C-C'

STRATIGRAPHIC CROSS-SECTION: EQUAL SPACE

Datum = MFS Domain = Depth

Scale = 1: 2400 Vertical Exaggeration = 100 x.

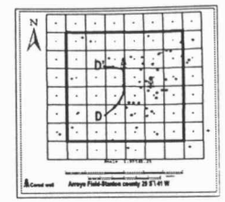

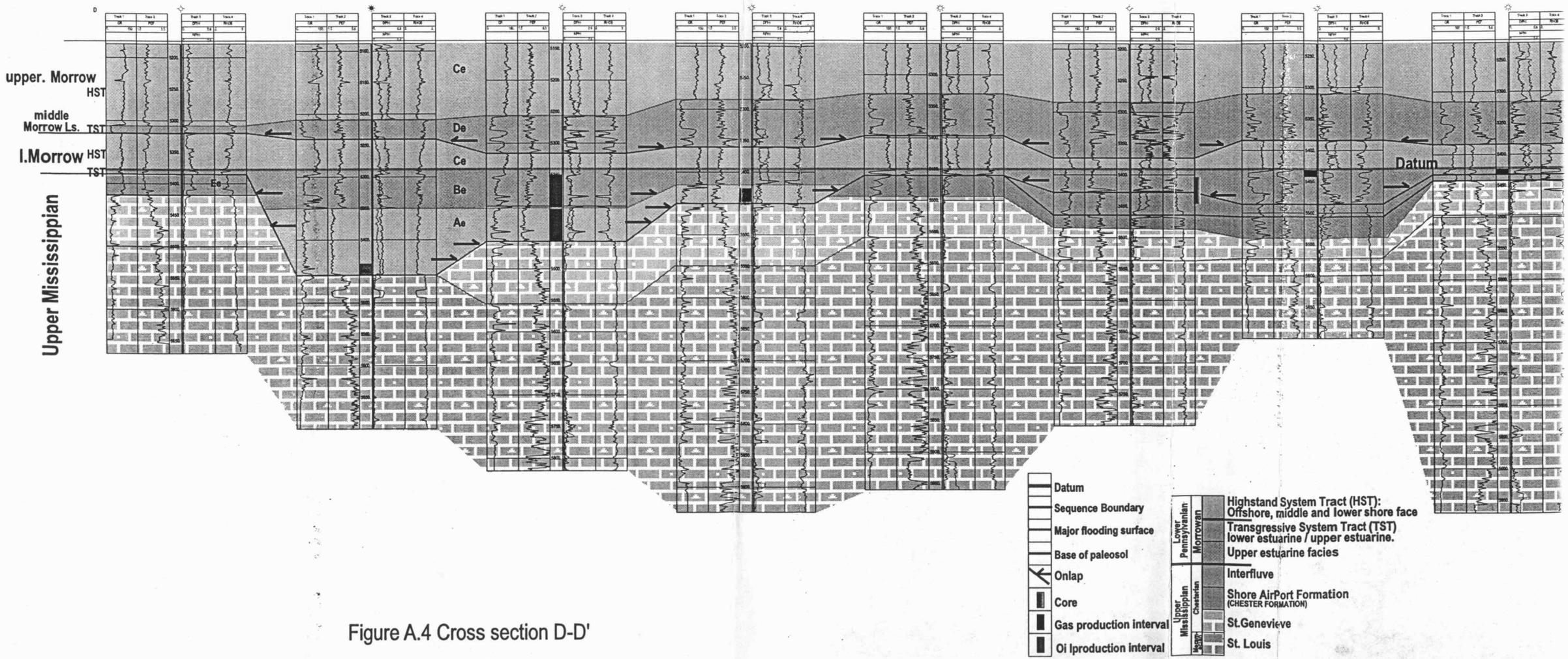

Figure A.4 Cross section D-D'

STRATIGRAPHIC CROSS-SECTION: EQUAL SPACE

Datum = MFS Domain = Depth

Scale = 1: 2400 Vertical Exaggeration = 100 x.

15-187-20692	15-187-20634	15-187-20494	15-187-20466	15-187-20649	15 187 20636
PETROLEUM INC	J M HUBER CORP	J M HUBER CORP	J M HUBER CORP	J M HUBER CORP	J M HUBER CORP
SPIKES 29-1	28-1 LAUMAN	27-2 PRO FARMS	27-1 PRO FARMS	26-2 PRO FARMS	26-1 PRO FARMS
29-1	28-1	27-2	27-1	26-2	26-1
6/29.S/41.W/29	6/29.S/41.W/28	6/29.S/41.W/27	6/29.S/41.W/27	6/29.S/41.W/26	6/29.S/41.W/26
DRY	C-PS	G-PS	C-PS	G-PS	C-PS

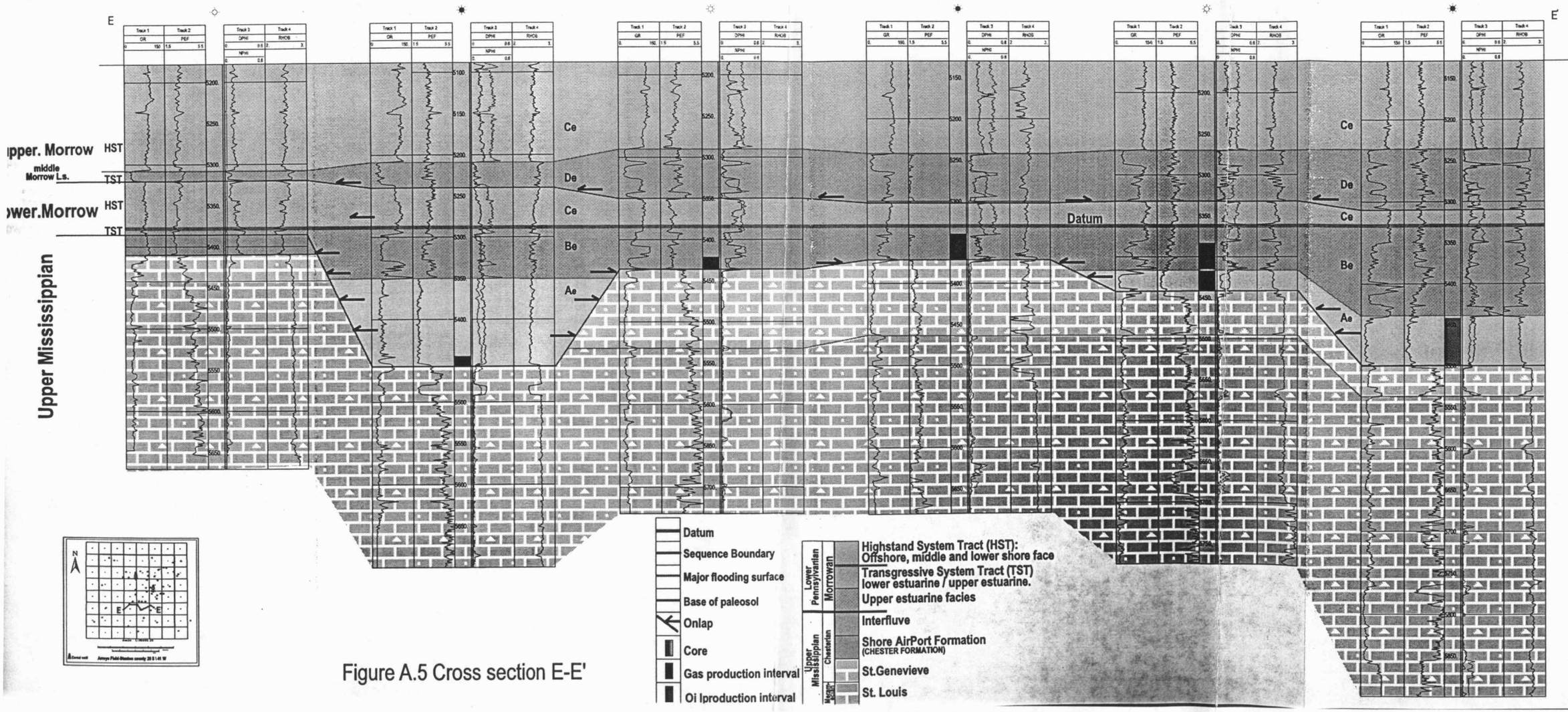

Figure A.5 Cross section E-E'

STRATIGRAPHIC CROSS-SECTION: EQUAL SPACE

Datum = MFS Domain = Depth

Scale = 1: 2400 Vertical Exaggeration = 100 x.

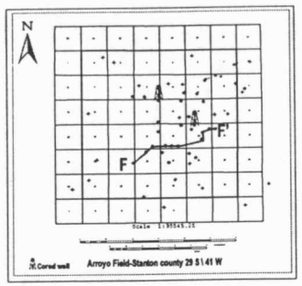

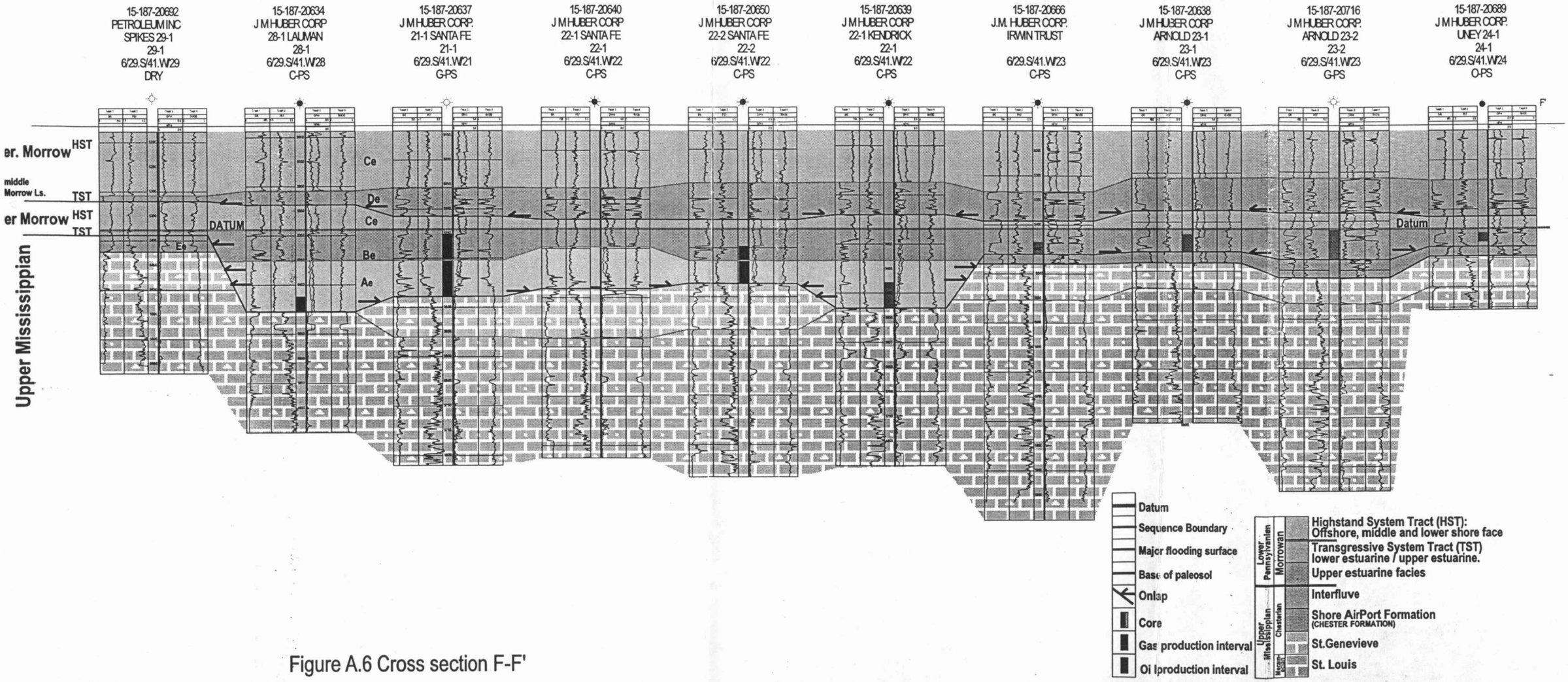

Figure A.6 Cross section F-F'

STRATIGRAPHIC CROSS-SECTION: EQUAL SPACE

Datum = MFS Domain = Depth

Scale = 1: 2400 Vertical Exaggeration = 100 x.

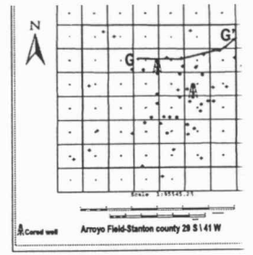

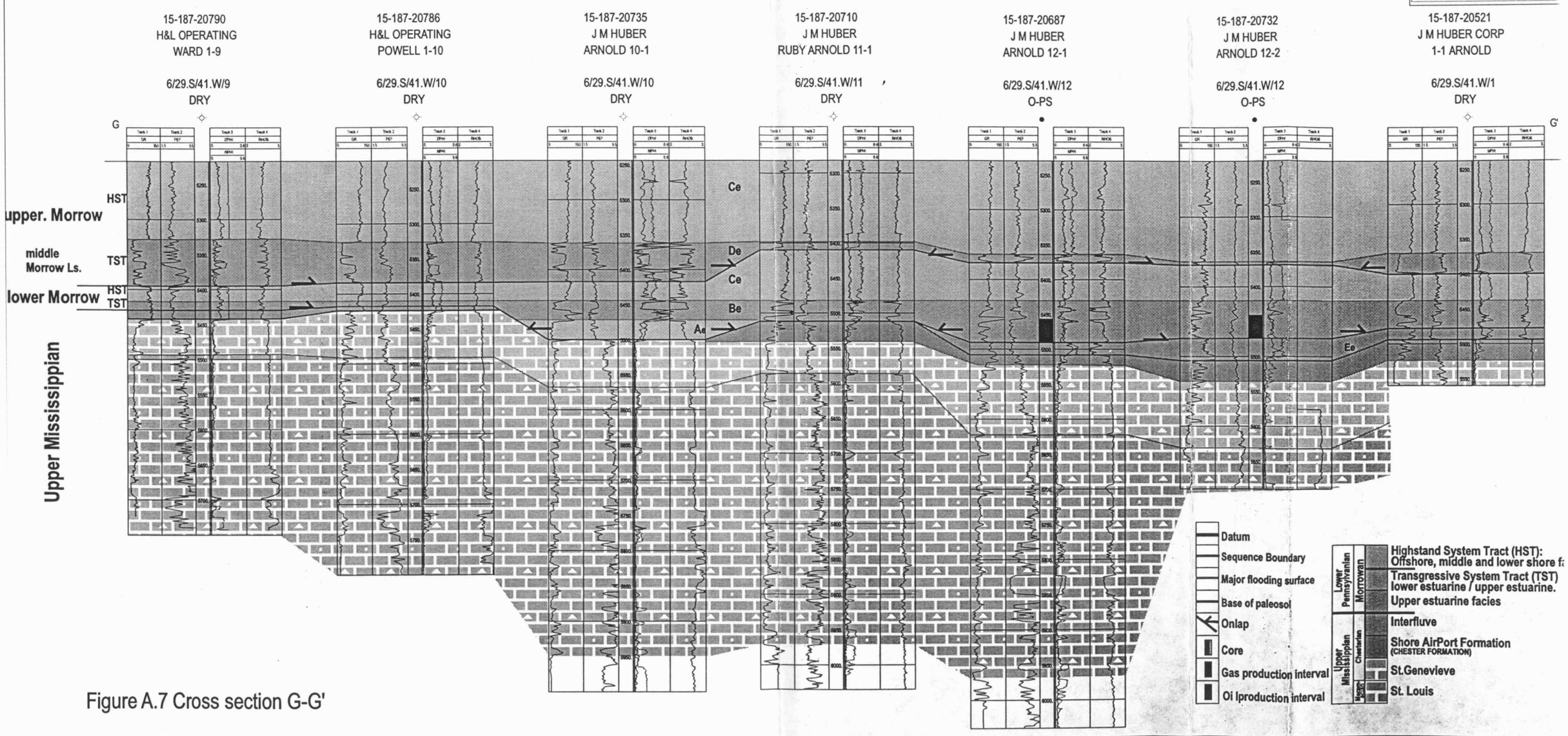

Figure A.7 Cross section G-G'

STRATIGRAPHIC CROSS-SECTION: EQUAL SPACE

Datum = MFS Domain = Depth

Scale = 1: 2400 Vertical Exaggeration = 100 x.

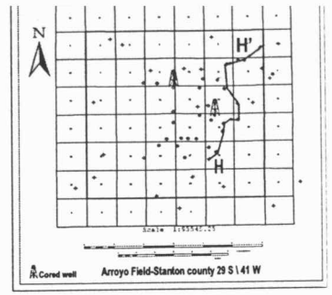

15-187-20458
J.M. HUBER CORP.
SANTA FE 26-1
26-1
6/29.S/41.W/26
DRY

15-187-20636
J.M. HUBER CORP.
PRO FARMS 26-1
26-1
6/29.S/41.W/26
C-PS

15-187-20666
J M HUBER CORP
IRWIN TRUST
6/29.S/41.W/23
C-PS

15-187-20638
J M HUBER CORP
ARNOLD 23-1
23-1
6/29.S/41.W/23
C-PS

15-187-20716
J M HUBER CORP.
ARNOLD 23-2
23-2
6/29.S/41.W/23
G-PS

15-187-20751
J M HUBER CORP
ARNOLD 13-1
13-1
6/29.S/41.W/13
DRY

15-187-20635
J M HUBER CORP
14-2 KENDRICK
41-2
6/29.S/41.W/14
G-PS

15-187-20734
J M HUBER CORP
ARNOLD 11-2
11-2
6/29.S/41.W/11
G-PS

15-187-20710
J M HUBER CORP
RUBY ARNOLD 11-1
11-1
6/29.S/41.W/11
DRY

15-187-20687
J M HUBER CORP
ARNOLD 12-1
12-1
6/29.S/41.W/12
O-PS

15-187-20732
J M HUBER CORP
ARNOLD 12-2
12-2
6/29.S/41.W/12
O-PS

15-187-20
J M HUBER
ARNOL
1-1
6/29.S/41
DR

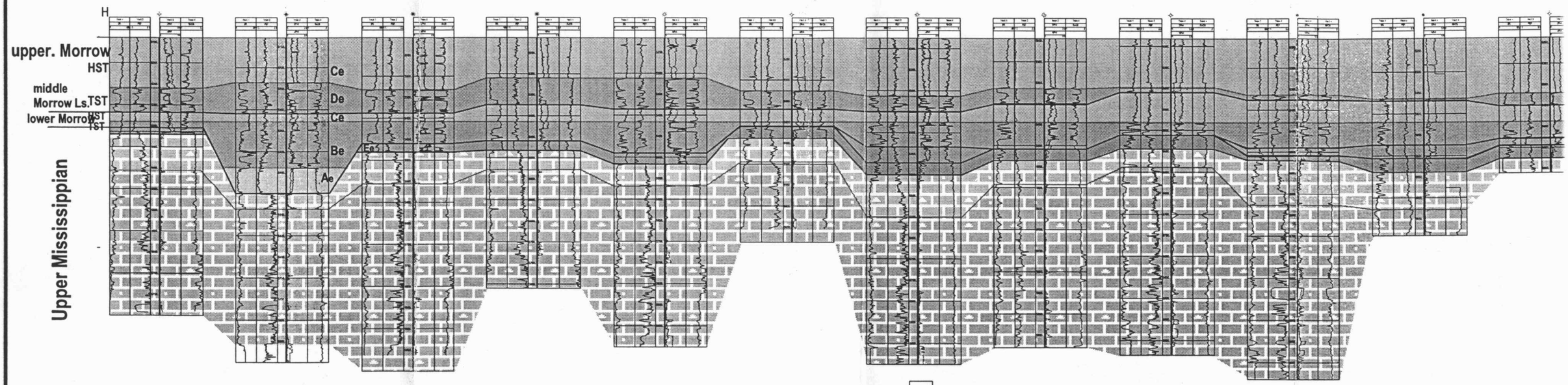

Datum
Sequence Boundary
Major flooding surface
Base of paleosol
Onlap
Core
Gas production interval
Oi lproduction interval

Lower Pennsylvanian
Morrowan
Highstand System Tract (HST):
Offshore, middle and lower shore face
Transgressive System Tract (TST)
lower estuarine / upper estuarine.
Upper estuarine facies

Upper Mississippian
Chesterian
Interfluve
Shore AirPort Formation
(CHESTER FORMATION)
St.Genevieve
Meramec
St. Louis

Figure A.8 Cross section H-H'

STRATIGRAPHIC CROSS-SECTION: EQUAL SPACE

Datum = MFS Domain = Depth

Scale = 1: 2400 Vertical Exaggeration = 100 x.

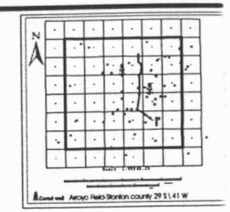

15-187-20735	15-187-20686	15-187-20699	15-187-20665	15-187-20639	15-187-20649	15-187-20636
J M HUBER CORP	J M HUBER CORP	J M HUBER CORP	J M HUBER CORP	J M HUBER CORP	J M HUBER CORP	J M HUBER CORP
ARNOLD 10-1	COCKERHAM 10-1	KENDRICK15-2	SMITH TRUST 22-1	22-1 KENDRICK	26-2 PRO FARMS	26-1 PRO FARMS
10-1	10-1	15-1	22-1	22-1	26-2	26-1
6/29.S/41.W/10	6/29.S/41.W/10	6/29.S/41.W/15	6/29.S/41.W/22	6/29.S/41.W/22	6/29.S/41.W/26	6/29.S/41.W/26
DRY	G-PS	C-PS	G-PS	C-PS	G-PS	C-PS

I

I'

Upper Mississippian

lper. Morrow HST

middle Morrow Ls. TST

HST

wer Morrow

TST

Ce

De

Ce

Be

Ae

Datum

Sequence Boundary

Major flooding surface

Base of paleosol

Onlap

Core

Gas production interval

Lower Pennsylvanian Morrowan

Upper Mississippian Chesterian

Highstand System Tract (HST): Offshore, middle and lower shore face

Transgressive System Tract (TST) lower estuarine / upper estuarine.

Upper estuarine facies

Interfluve

Shore AirPort Formation (CHESTER FORMATION)

St.Genevieve

St. Louis

Figure A.9 Cross section I-I'